HIGHER-LEVEL SIMULATIONS OF TURBULENT FLOWS

by
J. H. Ferziger

Prepared in part from work done under grants
NASA-NgR-2-15 and NSF-ENG-78-17619

Report No. TF-16

Thermosciences Division
Department of Mechanical Engineering
Stanford University
Stanford, California

March 1981

HIGHER-LEVEL SIMULATIONS OF TURBULENT FLOWS

by

J. H. Ferziger
Thermosciences Division
Department of Mechanical Engineering
Stanford University
Stanford, California 94305

Technical Report Number TF-16

Prepared in part from work done under grants
NASA-NgR-2-15 and NSF-ENG-78-17619

March 1981

Table of Contents

Chapter I

BACKGROUND: TURBULENT FLOW COMPUTATION METHODS

1. Methods of Computing Turbulent Flows: Classification

A few years ago, the author and two of his colleagues wrote a paper which attempted to classify methods of dealing with turbulent flows (Kline et al. (1978)). This paper is reviewed and extended here as a means of setting the main subject of this report in context.

There are two sub-areas that need to be dealt with in classifying methods of computing turbulent flows. These are the method by which the fluctuations are treated and the manner in which the geometry of the flow is handled. These are, of course, coupled to some extent, but it is useful to separate them for purposes of this work. We shall take up the problem of dealing with the turbulence first. According to the classification scheme in the paper cited above, there are five broad classes of methods of dealing with the turbulence; there are also subclasses of each. The five major categories are:

i) Correlations. These are the familiar correlations that give the nondimensional skin-friction coefficient as a function of the Reynolds number, Nusselt number as a function of Reynolds and Prandtl numbers, etc. They are extremely useful, but very limited. Their applicability is especially limited in high-technology applications in which the geometry plays an important role in the fluid dynamics (such as airfoils); for such problems, a new set of correlations would be needed each time the geometry of the device is changed.

ii) Integral Methods. In these methods the equations governing the fluid dynamics (which may be the equations used on level (iii) below) are integrated over at least one coordinate direction. This decreases the number of independent variables and greatly simplifies the mathematical problem to be solved. These methods allow considerable use of experimental data and physical insight and have proven quite useful. One of their principal drawbacks is that they need to be reworked when a new type of flow is to be computed.

iii) Reynolds-Averaged Equations. In this approach, one averages the Navier-Stokes equations over either time, homogeneous directions in the flow, or an ensemble of essentially equivalent flows. When averaging of any of these kinds is performed, the equations describing the mean field contain averages of products of fluctuating velocities, and there are fewer equations than unknowns--the well-known closure problem. In fact, the set of equations can never be closed by further averaging; a closure assumption or, what is the same thing, a turbulence model has to be introduced. The closure assumption must represent the unknown higher-order average quantities in terms of the lower-order quantities that are computed explicitly. This subject is undergoing a rapid expansion at the present time. It is also likely that this level should be broken into sublevels or separate levels.

iv) Large Eddy Simulation. In this approach, the equations are averaged over a small spatial region. The object is to remove the small eddies from the flow field so that an equation for the large eddies is derived. The effects of the small eddies on the large ones is then modeled. This is one of the principal subjects of this report and is discussed in considerable detail below.

v) Full Simulation. This is the numerical solution of the exact Navier-Stokes equations. The only errors made are numerical ones which, with care, can be kept as small as desired. By its nature, this approach is limited to low Reynolds numbers. This is the other principal subject of this report and will be covered in detail below.

Currently, computations at levels (iv) and (v) are limited to people with access to very large, fast computers. They are not suitable for engineering design at present and we anticipate that it will be some time before they will be (if ever). We call levels (iv) and (v) together higher-level methods of turbulence computation--hence the title of this report.

A significant point about this classification scheme is that calculations on any levels can be used to generate information that can be used on the lower levels. In applications, engineers commonly use methods at level (ii) or (iii) to produce correlations from which the design is actually done. Large eddy simulation (LES) can be used to produce information that can be used in modeling for Reynolds-averaged calculations. LES could be used in principle at the lower levels as well, but there is little need for this

application. Full simulation can be used to test models for both the Reynolds-averaged equations and large eddy simulation. This will receive considerable attention in this report.

It should be noted that the nomenclature we have used for classifying methods differs from that of Schumann et al. (1980). What we have called higher-level simulations they called direct simulation, and they did not make the distinction between levels (iv) and (v). We believe the distinction important and prefer the nomenclature used in this report.

The second type of classification of methods of computing turbulent flows concerns the treatment of the geometry. This scheme contains just two categories:

a) Full Field Methods. In this approach, the same set of equations is applied everywhere in the flow field. This has the great advantage of not requiring any kind of matching in the interior of the flow and of being easier to program for computer solution. The principal drawback is that fine meshes are needed in some regions of the flow (such as near the boundaries and in shocks), and this can make the cost very high.

b) Zonal Methods. In zonal methods the flow is considered as a collection of "modules," and each module or zone is treated by a separate method. The most common example of this kind of method is the division of flows over bodies into boundary layers and potential flows which are treated by separate methods. In zonal methods, the solutions in the various zones have to be matched at their common boundaries, by an iterative process that may or may not converge well. The modules can be treated by different methods. Thus one can use an integral method for the boundary layer and the full partial differential equations for the outer flow.

The classification scheme given here differs a little from the earlier one of Kline et al. (1978). We believe that the current scheme represents an improvement in clarity. We have found it useful, and it will be one of the ways in which various methods will be compared in the 1980-81 Stanford-AFOSR Symposium on the Computation of Complex Turbulent Flows.

2. Classification of Turbulent Flows

An issue that is quite separate from that of how turbulent flows are computed is that of trying to classify the flows. In a field as complex as this, any classification scheme is inexact, but it is better than having no scheme at all. Thus we shall classify flows according to the phenomena that occur in them. This scheme is not new and contains three categories:

a) Homogeneous Flows. In these flows the state of the fluid is the same at every point in space; they develop in time. There is a limited number of flows of this kind; the experimental data for them have been reviewed recently by the author (Ferziger (1980)). In homogeneous flows without mean strain or shear, the turbulence decays with time; when mean strain or shear are applied, the kinetic energy of the turbulence may increase with time. The mechanism by which the turbulence length scales increase in these flows is not well understood.

b) Free Shear Flows. It is well known that free shear flows are extremely unstable. The laminar mixing layer is unstable with respect to disturbances over a wide range of wavelengths. The instability is of the Kelvin-Helmholtz type in which the perturbation grows rapidly. There is controversy about the precise mechanism of growth of the turbulent free shear layer, but it seems clear that there are large coherent regions of concentrated vorticity in all of these flows. The concentrations of vorticity cause strong large-scale motions within the flow and the vorticity tends to agglomerate further. The controversy centers on the nature of the agglomeration, cf. Roshko (1978) and Chandrsuda et al. (1977).

A subclassification of these flows is necessary. In the mixing layer (the simplest type of free shear layer), the velocity difference across the layer remains fixed as the layer develops. As a result, the layer grows linearly in space or time, indefinitely. In other flows, for example, jets and wakes, the velocity differences are reduced as the flow develops and the turbulence tends to weaken in the downstream direction.

c) Wall-Bounded Flows. The effect of a wall on a shear layer is to prevent (or at least reduce) the large-scale motions described in the previous paragraph and thus inhibit the shear layer from growing so rapidly. Thus, boundary layers and related flows grow less rapidly and have lower turbulence levels than do free shear layers. Another, weaker, mechanism of turbulence production takes over. This mechanism is less well understood than that of the free shear layer and, perhaps for that reason, seems much more complicated. It is known to involve the presence of thin regions of high- and low-speed fluid that exist close to the wall and which are long in streamwise extent (Runstadler et al. (1967), Kim (1969)) and large-scale motions of the outer part of the boundary layer, but several details remain to be filled in.

A further extension of this classification scheme was given by Bradshaw. His view is that the mean turbulent flows can be thought of as a combination of "normal" strains--the mean strains that occur in the "standard" flows--and "extra" rates of strain. There are many extra rates of strain. Some of them are: curvature, rotation, lateral divergence (in axisymmetric flows), buoyancy, blowing or suction, and wall roughness. Although these effects generally appear as small terms in the equations, they have profound effects on the structure of the turbulence and, indirectly, on the behavior of the flow as a whole. Therefore, they are very important, and we shall devote part of this report to investigating their effects on turbulent flows.

Finally, it should be noted that some complex flows may be of one type in one region and another type in another region. In particular, in flows with separation, wall boundary layers may become free shear layers and vice versa.

3. A Short History

There are no known analytical solutions of the Navier-Stokes equations for turbulent flows, and it is unlikely that there ever will be any. This fact, plus the obvious technological importance of turbulent flows, is the reason for the development of computational methods of predicting turbulent flows.

Prior to 1960, computers had too little capacity to do anything more than solve the ordinary differential equations of integral methods or the partial differential equations for simple, two-dimensional potential flows. Progress

in this period was largely restricted to the computerization of methods that had been carried out on desk calculators up to that time.

As computers grew in sophistication, so did the problems for which people sought solutions. The 1960s saw the development of good boundary layer methods based the use of both integral methods and partial differential equations levels (ii and iii of the above scheme). The 1968 Stanford Conference (Kline (1968)) marked a milestone in this development. At that time, people were beginning to solve the Reynolds-averaged Navier-Stokes equations using simple models for relatively simple flows. Through the 1970s, the sophistication of the models grew, as did the complexity of the flows that researchers were willing to try to compute.

The first applications of what we have defined as higher-level methods were made by the meteorologists. That field has needed models for predicting the world's weather patterns for a long time. As soon as computers were large enough, meteorologists tried global weather simulations. The first three-dimensional attempt at this of which the author is aware is that of Smagorinsky (1963); this paper presented a model that will be used extensively later in this report. The grid systems used in these early calculations were necessarily very coarse, and the method used was necessarily what we have called large eddy simulation. Improvements in computers have allowed the use of finer grids, but the grids are still coarse compared to what is desired, this situation, unfortunately, will not change in the foreseeable future. Hence, subgrid-scale modeling will remain an important issue in meteorology (and oceanography) for quite some time.

The first computation of a flow of engineering interest was the simulation of channel flow by Deardorff, a meteorologist, in 1970. In this landmark paper, he laid out many of the foundations of the field. Improvements in his methods were made by Schumann (1973) and Grotzbach (1976). The latter and their group at Karlsruhe have subsequently extended the method to the computation of annular flows, the inclusion of heat transfer, and the inclusion of the effects of buoyancy.

The author's group at Stanford, which is jointly led by W. C. Reynolds, began work in higher-level simulations in 1972. Their objective was to put a sound foundation under the method of large eddy simulation by computing simple flows first. It was felt that in this way the fundamentals of the subject

could slowly be put in order. The first flows chosen for study were the homogeneous turbulent flows, and quite a lot was learned about numerical methods and subgrid-scale modeling (Kwak et al. (1975) and Shaanan et al. (1975)). When the group felt that the techniques for the simulation of homogeneous flows were well developed, it was decided to go on to the study of flows which are inhomogeneous in one coordinate direction. The simplest such flows are the mixing layer and channel. The fully developed mixing layer was computed by Mansour et al. (1978), transition in the mixing layer was studied by Cain et al. (1981), and the channel flow was studied by Moin et al. (1978) and Kim and Moin (1980,1981).

Almost from the beginning it was realized that the effort in computing flows would have to be accompanied by an effort at developing better models for treating the small scales (subgrid scale models) or at least understanding the models that are in use. The method of using direct simulations for this purpose was developed by Clark et al. (1976) and extended by McMillan and Ferziger (1978), McMillan et al. (1980), and Bardina et al. (1980).

It is clear that large eddy simulation will not be a method of direct engineering applicability for some time. For that reason, the major impact the method will have is in the improvement of the understanding of the physics of turbulent flows and in helping to develop, test, evaluate, and improve models that are used in Reynolds-averaged methods. Recently, exact simulations of compressible homogeneous turbulent shear flows and homogeneous turbulent shear flow with a passive scalar were made in order to evaluate these models; cf Feiereisen et.al. (1981, and Shirani et.al. (1981).

A group under Leslie in London has been active in the field since 1975. Their early work centered on the understanding of subgrid scale models (Love and Leslie (1976) and Leslie and Quarini (1979)). Since then they have simulated the mixing of a passive scalar in homogeneous isotropic turbulence (Antonopoulos (1981)).

A number of French groups have studied subgrid scale models from a theoretical point of view and have made several contributions in this area.

Orszag and coworkers have been working since 1970 on the direct simulation of turbulent flows. Their early work centered on the prediction of homogeneous isotropic turbulence (Orszag and Patterson (1971)), and more

recently they have become interested in the study of transition in wall-bounded flows (Kells and Orszag (1979), Orszag and Patera (1980)). The main interest of this group has been in the development of numerical methods (they are responsible for the widespread use of spectral methods in this field), on the study of turbulence theories, and on the prediction of transition.

Riley and Metcalf (1980) have made direct simulations of free shear flows. Their efforts have been directed at the simulation of fully developed wakes at relatively low Reynolds numbers, which may be thought of as the last stages of the decay of a turbulent wake.

Rogallo (1978, 1981) has made extensive direct simulations of all of the homogeneous turbulent flows. His results are an important resource for modelers.

4. Outline of This Report

In Chapter II, we shall consider the fundamentals of large eddy simulation and compare the various approaches to it.

In Chapter III we shall discuss the subgrid scale models required by large eddy simulation. We shall also study the use of large eddy simulation in the development of models for the Reynolds-averaged equations and the application of full simulation to the testing of both subgrid scale and Reynolds-averaged models.

In Chapter IV we shall discuss the numerical methods used in large eddy and full simulation. Since the numerical methods used are almost always somewhat tailored to a particular flow, we shall just touch on some of the special-purpose methods in this chapter. The latter methods will be considered in more detail in the chapters in which the flows are described.

Chapter V will be devoted to the discussion of the simulation of homogeneous flows. The flows will be categorized, and the numerical methods needed for some of the cases will be described, along with physical descriptions of the flows. We shall give the results from both full and large eddy simulations of these flows and show how they can be applied to the testing and development of models. This chapter contains a considerable amount of recent work.

Free shear flows will be considered in Chapter VI. The bulk of the chapter will be devoted to the mixing layer, which has been the principal focus of attention in this area, but we shall also look at wake simulations.

Chapter VII will be concerned with wall-bounded flows. Most of the attention will be given to channel flow, but some discussion of recent work on the boundary layer will also be given. Particular attention will be given to terms which have not been measured in the laboratory.

In Chapter VIII we shall briefly cover applications of large eddy simulation and full simulation that have not been given in the previous chapters. The most important of these applications are in meteorological and other environmental flows. However, a few applications have been made to other laboratory flows, and these will be briefly covered as well.

The concluding chapter, IX, will discuss some directions in which the work is proceeding and what can be expected from higher-level simulations in the next few years.

This report will give greater emphasis to work done in the author's group than to that of other groups. The reader is reminded that this is a consequence of greater familiarity with his own work and that of his colleagues and is in no way intended to imply that work done elsewhere is any less important.

Chapter II

FOUNDATIONS OF LARGE EDDY SIMULATION

1. Rationale

It is generally believed that the largest eddies dominate the physics of any turbulent flow. The differences between the large and small eddies can be summarized as follows:

a) The large eddies interact strongly with the mean flow. The small eddies are created mainly by nonlinear interactions among the large eddies.

b) Most of the transport of mass, momentum, energy, and (in flows containing more than one species) concentration is due to the large eddies. The small eddies dissipate fluctuations of these quantities but affect the mean properties only slightly.

c) The structure of large eddies is very strongly dependent on the geometry and nature of the flow. They are usually vortical, but their shapes and strengths are flow dependent. The small eddies are, on the other hand, much more universal.

d) Due to their dependence on the geometry, the large eddies are highly anisotropic. The small eddies are much more nearly isotropic and, therefore, universal.

e) The time scales of the large eddies approximate the time scales of the mean flow. For flow past a body, the large eddy scale is approximately the dimension of the body divided by the free stream velocity. The small eddies seem to be created and destroyed much more quickly.

An important consequence of these properties is that the large eddies should be harder to model than the small ones. Also, as they vary so much from flow to flow, one should not expect to find a model for the large eddies to be universal. There is hope, however, that one might be able to find a useful model of the small eddies.

This leads to the concept of large eddy simulation. In this approach, the large structures in the flow are computed explicitly and the small ones are modeled. This method should have advantages over methods in which all of the eddies are modeled.

These arguments provide the rationale for large eddy simulation. However, not all of the premises given above hold in all flows. They seem to hold in homogeneous turbulent flows and in free shear flows. In wall-bounded flows, however, the structures responsible for much of the momentum transport (and, presumably, the transport of the other properties as well) may be quite small, especially in the region close to the solid boundary. Special care is necessary in these flows; this will be discussed further in Chapter VII.

If, for now, we accept the statements made above as correct, it follows that large eddy simulation ought to have a number of advantages over Reynolds or time average methods. The most significant advantage is that much of the actual transport of mass, momentum, energy, and species is computed explicitly, and the portions of these fluxes which need to be modeled are much smaller than what is modeled in the Reynolds-averaged equations. Consequently, the overall results are less sensitive to modeling inaccuracy in large eddy simulation than in other approaches. The probability of finding a widely applicable model should be much higher.

The principal disadvantage of large eddy simulation relative to Reynolds-averaged methods is that the computations are necessarily three-dimensional and time-dependent. This means that the cost is much higher. In fact, the cost is currently high enough that, except for the simplest flows, use of the method is restricted to people with access to large amounts of time on very large computers.

The first thing that one needs to do in developing large eddy simulation is to define the large scale component of the flow field--the portion which is to be computed explicitly. There are two common approaches to doing this, they will be described and compared in the next two sections. The remainder of the chapter will present the LES equations and describe the parametr tradeoffs that must be faced in large eddy simulation.

The equations for the large scale field always contain terms which involve the small scale field, which is not computed. These terms play the same role in the large eddy equations as the Reynolds stresses play in the Reynolds-averaged equations. They are therefore called the subgrid scale (SGS) Reynolds stresses, and they must be modeled. A discussion of subgrid scale models and a comparison of them with Reynolds-averaged turbulence models is given in the next chapter.

2. Filtering

The first task in large eddy simulation is that of defining the large scale component of the flow field--the portion which the method will attempt to calculate. There are several ways of doing this mathematically. All are essentially equivalent to averaging the equations over a small region of space or low-pass filtering the equations in Fourier space. The starting point is the incompressible Navier-Stokes equations:

$$\frac{\partial u_i}{\partial t} + \frac{\partial}{\partial x_j} u_i u_j = -\frac{1}{\rho}\frac{\partial p}{\partial x_i} + \nu \frac{\partial^2 u_i}{\partial x_j \partial x_j} \tag{2.1}$$

which must be solved together with the continuity equation:

$$\frac{\partial u_i}{\partial x_i} = 0 \tag{2.2}$$

For homogeneous flows, we prefer to define the large scale field (also called the resolved field) by means of a convolution filter:

$$\overline{u}(\underline{r}) = \int G(|\underline{r} - \underline{r}'|)\, u(\underline{r}')\, d\underline{r}' \tag{2.3}$$

In Fourier space, this has the form:

$$\hat{\overline{u}}(\underline{k}) = \hat{G}(k)\, \hat{u}(\underline{k}) \tag{2.4}$$

Note that for this kind of filter $\hat{G}$ is a function only of the magnitude of $\underline{k}$.

A number of simple filters have been used. These are illustrated in Fig. 2.1. If the equations are simply integrated over a small control volume in space, we have the box filter; most finite-difference and finite-volume methods implicitly use this filter. Its Fourier transform is also shown in the figure. Another common choice is a sharp cutoff filter in Fourier space, this is essentially the Fourier-space version of the first filter. Both of these filters have the difficulty that their Fourier transforms have negative regions, they also are difficult to differentiate. For this reason, we prefer to use the Gaussian filter. Its Fourier transform is also Gaussian, so it is well behaved in both configuration and Fourier space, and it can be differentiated as many times as one likes in both spaces. The Gaussian is

$$G(r) = A\, e^{-6r^2/\Delta^2} \tag{2.5}$$

or, in Fourier space,

$$\hat{G}(k) = e^{-k^2\Delta^2/24} \tag{2.6}$$

The numerical factors have been chosen to make the second moment of this filter the same as that of a box filter of width Δ. $G(r)$ and $\hat{G}(k)$ are Fourier inverses of each other when the variables are continuous, but not in the discrete case; in the latter case, a choice has to be made. The normalization factor, A, has been left unspecified in Eq. (2.5) in order to admit the conservation property that the integral of $G(r)$ over all space be unity whether continuous or discrete quadrature is used.

Use of this type of filter was first suggested by Leonard (1973), he showed how the concept could be generalized. It is sometimes useful to use expansions other than standard Fourier series. For example, Chebychev polynomial expansions have been used (Orszag (1978), Kim and Moin (1980)) as the basis for numerical methods. The filter can be defined in the space of the index of the expansion functions; a sharp cutoff (ignoring all components of the expansion beyond some specified N) is the simplest possibility, but it is easy to construct Gaussian-like filters as well.

When the filter (2.3) is applied to the Navier-Stokes equations (2.1) and the continuity equations (2.2), we have:

$$\frac{\partial \bar{u}_i}{\partial t} + \frac{\partial}{\partial x_j}\overline{u_i u_j} = -\frac{1}{\rho}\frac{\partial \bar{p}}{\partial x_i} + \nu \frac{\partial^2 \bar{u}_i}{\partial x_j \partial x_j} \tag{2.7}$$

and

$$\frac{\partial \bar{u}_i}{\partial x_i} = 0 \tag{2.8}$$

The difficulty comes from the nonlinear term. The approach taken by everyone in the field is to write:

$$u_i = \bar{u}_i + u_i' \tag{2.9}$$

which causes the nonlinear terms to take the form:

$$\overline{u_i u_j} = \overline{\bar{u}_i \bar{u}_j} + \overline{\bar{u}_i u_j'} + \overline{u_i' \bar{u}_j} + \overline{u_i' u_j'} \tag{2.10}$$

The first term is entirely dependent on the large scale component of the field and is computable in LES. The small scale component of the velocity field, u_i', is not computed, so the terms containing it need to be modeled. u_i' is called the subgrid scale component of the velocity field, but this is a misnomer (in this formalism), because the width of the filter (Δ) need not be related to the size of the grid on which the computations will be done. However, it has become standard nomenclature, and the set of terms involving the small scale velocity component,

$$R_{ij} = \overline{u_i' \bar{u}_j} + \overline{\bar{u}_i u_j'} + \overline{u_i' u_j'} \tag{2.11}$$

are commonly called the subgrid scale (SGS) Reynolds streeses. They must be modeled in large eddy simulations--hence the name subgrid modeling. We shall look at models for these terms in the next chapter.

The approach presented above is the one favored by the author and his colleagues at Stanford. It decouples the definition of the large scale field from the numerical solution of equations that result. We favor this method, even though it is more cumbersome than the one given in the next section, because we feel it provides more flexibility. This flexibility will be useful when we discuss methods of testing subgrid scale models in the next chapter.

3. The Deardorff-Schumann Approach

An alternative to the method presented in the previous section is based on the recognition that we shall be solving the equations numerically. The computerprogram will be based on a set of discretized equations. It therefore makes sense to use an approach that arrives at the discretized equations as quickly as possible. The method originally presented by Deardorff (1970) and extended by Schumann (1973) is one which accomplishes this.

The idea is to introduce the grid on which the numerical computations will be done at the outset. Deardorff and Schumann used a staggered grid, which is probably the best choice for solving the incompressible equations, but other grid systems could be used as well. The two-dimensional version of the staggered grid is shown in Fig. 2.2. One integrates each of the equations

over an appropriate control volume; the control volume for the x-momentum equation is shown in Fig. 2.2. The resulting equations have the form (2.7) and (2.8), provided the operation represented by the overbar is interpreted as the volume average. Because the averaging operation is defined relative to the grid, $\overline{u}_i$ is defined only at the grid points. However, it is convenient to think of $\overline{u}_i$ as constant within the control volume. This definition of the large scale velocity differs from the one presented in the previous section. The two definitions are illustrated in Fig. 2.3.

The Deardorff definitions lead to some convenient simplifications. In particular, one can assume that:

$$\overline{\overline{u}_i \overline{u}_j} = \overline{u}_i \overline{u}_j \tag{2.12}$$

and

$$\overline{u}_i' = 0 \tag{2.13}$$

which are properties this approach shares with Reynolds-averaged modeling. The subgrid scale Reynolds stresses then reduce to:

$$R_{ij} = \overline{u_i' u_j'} \tag{2.14}$$

Models are introduced for R_{ij} and the discretized equations are similar to those commonly used on staggered grids.

In Schumann's modification of this approach, the integrals of spatial derivatives are carried out analytically. This results in equations which contain integrals over the surfaces of the control volumes. The difficulty with this approach is that four different types of averages appear: averages over the three types of faces of the grid volume and volume averages. These must be related in some way. Schumann introduced several approximations that relate the surface averages to a single volume average, but the assumptions required are difficult to evaluate and may be questionable, especially at low Reynolds numbers. It is not clear that this method has any significant advantages relative to Deardorff's.

In the Deardorff-Schumann approach, the subgrid scale velocity field is discontinuous at the edges of the control volumes, and the behavior of the subgrid scale Reynolds stress as a function of position is not very smooth. This problem and the increased flexibility in defining the filter are the primary reasons why we prefer the filtering approach to the one presented in this section.

4. The Large Eddy Simulation Equations

The equations of large eddy simulation are essentially (2.7) and (2.8). However, one needs to take into account Eqs. (2.10) and (2.11) as well. Also, one further modification is usually made. The subgrid scale Reynolds stress, defined by Eq. (2.11), can be decomposed into the sum of a trace-free tensor and a diagonal tensor:

$$\begin{aligned} R_{ij} &= (R_{ij} - \tfrac{1}{3}\delta_{ij}R_{kk}) + \tfrac{1}{3}\delta_{ij}R_{kk} \\ &\equiv -\tau_{ij} + \tfrac{1}{3}\delta_{ij}R_{kk} \end{aligned} \tag{2.15}$$

Although the diagonal component of this tensor can be modeled, there is no need to do so. When the decomposition (2.12) is substituted into the filtered Navier-Stokes equations (2.7), the diagonal component produces a term which is equivalent to the gradient of a scalar. It is similar to the pressure gradient term and can be combined with it. It is therefore advantageous to define a modified pressure:

$$P = \frac{p}{\rho} + \frac{1}{3}R_{kk} \tag{2.16}$$

The filtered Navier-Stokes equations can then be written:

$$\frac{\partial \bar{u}_i}{\partial t} + \frac{\partial}{\partial x_j}\overline{\bar{u}_i \bar{u}_j} = -\frac{\partial P}{\partial x_i} + \nu \frac{\partial^2 \bar{u}_i}{\partial x_j \partial x_j} - \frac{\partial \tau_{ij}}{\partial x_j} \tag{2.17}$$

Once a model for τ_{ij} has been introduced, these equations are to be solved numerically along with the filtered continuity equation, which is repeated here for completeness:

$$\frac{\partial \bar{u}_i}{\partial x_j} = 0 \tag{2.18}$$

5. Tradeoffs

In any kind of flow computation, there are tradeoffs. Higher accuracy can always be by reducing the grid size and increasing the number of mesh points. The price is paid in the form of increased computer time.

A similar tradeoff exists in large eddy simulation. Ideally, we would like all the eddies in the large scale field to behave in the manner ascribed to large eddies at the beginning of this chapter and the small eddies to behave as they are supposed to. This separation of large and small eddies is possible only at high Reynolds. At sufficiently high Reynolds numbers, the turbulent energy spectrum contains an inertial subrange in which there is essentially no turbulence production or viscous dissipation. The eddies which are larger than those in the subrange (i.e., lie at lower wavenumbers) behave like "large eddies", and those that lie at wavenumbers below the subrange are "small eddies." Since the width of the filter (Δ) is supposed to mark the boundary between the two classes of eddies, the ideal is to choose the filter width such that the corresponding wavenumber (π/Δ) lies in the subrange. If this is the case, large eddy simulation should be successful.

There are, of course, difficulties that we need to address. The principal of these are:

a) The size of the physical domain considered in the calculation needs to be sufficiently large to hold the largest eddies. We also wish the filter size to be such that all of the "small" eddies lie in or below the subrange. Finally, the computational grid size must be smaller than the filter width (this is discussed in Chapter 4). These requirements set the number of mesh points required in each coordinate direction. It is not unusual to find that the number of mesh points needed to meet these requirements is much greater than the available computer resource will allow. We are then forced to use a filter width which lies outside the subrange.

b) At low Reynolds numbers there is no subrange in the turbulence spectrum.

In either case, we are forced to use a filter width which does not lie within the inertial subrange of the turbulence spectrum. It has been argued by some that one should not do this. We believe that it is reasonable to do large eddy simulation under these circumstances. However, the model may need to be changed to account for the fact that the cutoff is not in an inertial subrange. This problem will be discussed further in the next chapter.

Chapter III

SUBGRID SCALE MODELS

1. The SGS Reynolds Stress

In the preceding chapter we saw that there are terms in the equations of large eddy simulation that involve the small or subgrid scale component of the velocity field, and, as this small-scale velocity field will not be computed, these terms must be modeled. This chapter will be devoted to a discussion of the models used for the so-called subgrid scale (SGS) terms.

To begin, it is well to look at the physical significance of the SGS terms. Equations (2.2) and (2.3) describe the development of the large eddies. In them, the terms containing the small scale velocity represent the interactions between the large and small eddies. On the average, kinetic energy is transferred from the large eddies to the small ones, there is energy flow in both directions, but the net flow is usually toward the small scales. Leslie and Quarini (1979) estimated that the gross transfer to the small scales is about 1.5 times the net transfer. In other words, approximately one-third of the energy transferred to the small scales is returned. We shall see later that the net energy flow may be in the reverse direction in some cases. The subgrid scale terms in Eqs. (2.2) and (2.3) must represent the effect of these transfers on the large scales. In the normal situation, the net energy transfer to the small eddies appears to be a dissipation to the large eddies--energy lost that will not reappear. Thus the model should normally be dissipative.

The terms which need to be modeled were derived in the previous chapter and can be written:

$$R_{ij} = \overline{u_i u_j} - \overline{u}_i \overline{u}_j = \overline{\overline{u}_i u'_j} + \overline{u'_i \overline{u}_j} + \overline{u'_i u'_j} \tag{3.1}$$

As we showed, we prefer to work with the SGS Reynolds stress defined by

$$\tau_{ij} = R_{ij} - \frac{1}{3} R_{kk} \delta_{ij} \tag{3.2}$$

It is also worth mentioning at this point that the terms we have called the Leonard stresses:

$$\lambda_{ij} = \overline{\bar{u}_i \bar{u}_j} - \bar{u}_i \bar{u}_j \tag{3.3}$$

(which were first discussed by Leonard (1973)) may need special treatment. These terms are zero in the Deardorff-Schumann approach but not in the filtering method. Investigation has revealed that they are responsible for only a small amount of energy transfer between the large and small scales. Their major effect seems to be redistribution of energy among the various large scales.

The contents of this chapter are as follows. In the next section, equations governing the SGS Reynolds stresses will be derived and discussed. We shall also compare SGS modeling to Reynolds-averaged modeling. In Section 3, a computational method for validating SGS models will be described and some results given. This will be followed in Section 4 by a discussion of eddy viscosity models, the ones in most common use today. Section 5 will describe some of the contributions that theory has made to the state of the art in SGS modeling. Some new ideas about SGS modeling form the subject of Section 6. Higher-order modeling will be taken up in Section 7. Finally, Section 8 will discuss some effects that arise when there are extra rates of strain (in Bradshaw's sense) in the flow. We shall end the chapter with a short summary of the principal points.

2. The SGS Stress Equations

It is not difficult to derive a set of equations describing the dynamical behavior of the quantities R_{ij} defined by Eq. (3.1). However, the process is somewhat tedious. One takes the Navier-Stokes equations for u_i and also writes them with i replaced by j. The equation for u_i is multiplied by u_j and vice versa. Adding the two resulting equations and filtering the result yields an equation for $\overline{u_i u_j}$. By repeating the same procedure using the dynamical equation for $\bar{u}_i$, one can derive an equation for $\bar{u}_i \bar{u}_j$. Subtracting these two equations, we have the desired equation for R_{ij}:

$$\frac{R_{ij}}{t} + \bar{u}_k \frac{\partial}{\partial x_k} R_{ij} = -\left[\overline{(R_{ik} + \lambda_{ik}) \frac{\partial \bar{u}_j}{\partial x_k}} + \overline{(R_{jk} + \lambda_{jk}) \frac{\partial \bar{u}_i}{\partial x_k}}\right]$$

(Convection) (Production)

$$+ \overline{\frac{p}{\rho}\left(\frac{\partial u_i}{\partial x_j} + \frac{\partial u_j}{\partial x_i}\right)} - \overline{p}\left(\frac{\partial \bar{u}_i}{\partial x_j} + \frac{\partial \bar{u}_j}{\partial x_i}\right) \qquad (3.4)$$

(Redistribution)

$$- 2\left[\overline{\frac{\partial u_i}{\partial x_k}\frac{\partial u_j}{\partial x_k}} - \overline{\frac{\partial \bar{u}_i}{\partial x_k}\frac{\partial \bar{u}_j}{\partial x_k}}\right]$$

(Dissipation)

+ Diffusion terms

There are many diffusion terms, they are not written explicitly, as we shall not need them. Here, λ_{ij} is the Leonard stress defined by Eq. (3.3). An equation for R_{kk}, the subgrid scale turbulent kinetic energy, can be derived by taking the trace of Eq. (3.4). Subtracting δ_{ij} times the resulting equation from Eq. (3.4) gives an equation for τ_{ij}.

All of the terms in Eq. (3.4) are analogous to terms in the familiar Reynolds stress equations of time-average modeling. The interpretations are also similar. However, the differences are quite important. Eqs. (3.4) contain more terms than the equations for the time-average Reynolds stresses because some items that are zero in time-average approach are not zero when filtering is used. In particular, note the appearance of the Leonard stress in the production term and, more importantly, the fact that the production term is filtered. All of the terms in Eq. (3.4) can be computed by the methods described in the next section and models for them studied, but this has not been done to date.

The most common assumption in turbulence modeling is that production and dissipation terms dominate the turbulence budget, and, as a first approximation, we can equate them and ignore the other terms. For the time-average equations, this approximation is reasonable when applied to the turbulent kinetic energy budget far from solid boundaries, but it is less valid for the

component equations because the redistribution terms may be quite large. Near walls, the diffusion terms become quite important and the approximation is even more questionable. The low Reynolds numbers in this region may also affect the structure of the turbulence. Nonetheless, the "production equals dissipation argument" is frequently invoked.

For LES, the situation is somewhat different. It is important to note is that the model is assumed to represent a local spatial average of the local instantaneous small-scale turbulence. This is quite different from what is modeled in time- or ensemble-average modeling and our understanding of subgrid scale turbulence (and consequently, our ability to model it) is more limited. This is compensated for by the fact that a large eddy simulation calculation of a given flow is less sensitive to modeling errors than is a Reynolds-averaged calculation of the same flow.

In particular, because the small scales of turbulence are highly intermittent, we expect gradients of subgrid scale quantities to be relatively large. If this is the case, it is probable that the convection and diffusion terms, which are ignored in many time-averaged models, are more important in SGS modeling. On the other hand, we have recently found evidence that the pressure fluctuations and, more particularly, the pressure-strain correlations reside mainly in the large scales (this will be presented in Chapter 5), and they may be less important in SGS modeling than they are in conventional modeling. Despite these differences, most SGS models to date have relied on ideas developed for time average models.

3. Computational Validation of SGS Models

Two approaches are commonly used for developing and testing time-average models. One method, favored by Lumley, Reynolds and others, uses simple turbulent flows (usually homogeneous flows) to test the validity of the models and to determine the adjustable parameters. The major objection to this approach is that the structure of homogeneous flows differs considerably from the flows one really wishes to simulate, and the constants may not be valid in more complex flows. The other method, used by Spalding, Launder, and others, adjusts the parameters to fit flows similar to the ones that one wishes to calculate. This is difficult because many of the parameters must be adjusted simultaneously and this can be a difficult procedure.

It is even more difficult to develop models for the subgrid scales. Data on the small scales of turbulence are quite scarce, and direct validation of a model using experimental data is nearly impossible. Consequently, the constants have to be found by other methods. One approach is almost completed based on theory and uses the properties of the inertial subrange. Lilly (1967) and others have shown that the constant in the model can be derived on this basis. Unfortunately, it is not always possible to to assure that in a computation the cutoff between the large and small scales will lie in the subrange, so one needs to be cautious about adopting the results of this approach. Indeed, a number of authors found it necessary to modify the SGS model constant to obtain good results.

There is a second approach. With the current generation of computers it is possible to compute homogeneous turbulent flows with no approximations other than those present in any numerical simulation. At present, it is possible to do such calculations with grids as large as $64 \times 64 \times 64$ and, in a limited number of cases, $128 \times 128 \times 128$. This allows simulation at Reynolds numbers based on Taylor microscale up to approximately 40 (80 with the larger grids). The results can be regarded as realizations of physical flow fields and are an interesting and important complement to laboratory results. In particular, the computational results provide all three velocity components and the pressure at a large number of spatial points for a relatively short time span. The laboratory data typically give one or two velocity components over a longer time span at just a few spatial points.

Having a realization of a flow, we proceed in much the same manner an experimentalist would. The computed field can be filtered to give its large scale component; the small scale component is obtained by difference. We can then compute the terms that need to be modeled, and, from the large scale field, we can also compute what the model predicts these terms to be. Direct comparison between the model and the exact value is then possible. This can be done in a couple of ways.

One method is to use a scatter plot. The exact value of the SGS Reynolds stress at each mesh point is plotted against the value predicted by the model. If the model is correct, the results lie on a straight line; a totally invalid model produces a random pattern of points (usually a circle). This is a very graphic test of a model. Some scatter plots will be shown later.

The second method is to compare the model and exact results statistically. In our work we have used the correlation coefficient as a measure of the validity of a model. This is a crude test, but it seems to be sufficient for our purposes. It is important to recall that the square of the correlation coefficient is approximately the fraction of the data that the model is correctly predicting.

These are very severe tests of models--much more severe than the tests usually applied to Reynolds-averaged models. It is possible for a model which performs poorly in these tests to do well in actual simulations. However, failure of a model to do well is a signal for caution.

Use of this kind of testing for Reynolds-averaged models will be taken up in Chapter 5.

4. Eddy Viscosity Models

Eddy viscosity models can be "derived" from the "production equals dissipation" argument discussed earlier. This is done in a number of places and need not be repeated here. For subgrid scale turbulence, the eddy viscosity model amounts to assuming that the subgrid scale Reynolds stress is proportional to the strain in the large scale flow:

$$\tau_{ij} = 2\nu_T \bar{S}_{ij} = \nu_T \left(\frac{\partial \bar{u}_i}{\partial x_j} + \frac{\partial \bar{u}_j}{\partial x_i} \right) \tag{3.5}$$

The eddy viscosity ν_T has the dimensions of a kinematic viscosity. Most work is based on the assumption that the eddy viscosity could be represented by:

$$\nu_T = (C\Delta)^2 |\bar{S}| \tag{3.6}$$

where Δ is the width associated with the filter and $|\bar{S}| = (\bar{S}_{ij}\bar{S}_{ij})^{1/2}$. Recently, a number of authors have shown that this is correct only if the integral scale of the turbulence is smaller than Δ. Since LES is designed for this not to be the case, it is better to assume that:

$$\nu_T = C\, \Delta^{4/3} L^{2/3} |\bar{S}| \tag{3.7}$$

where L is the integral scale of the turbulence. Usually L is estimated from $L = q^3/\varepsilon$, where ε is the dissipation.

Eddy viscosity models have a long record of reasonable success in time-average modeling of simple shear flows, and one might expect them to do well as SGS models. In fact, they have been found to do well in some of the homogeneous flows. In particular, for the homogeneous flows in which there is no mean strain, one is able to predict most of the low-order statistical quantities (for example, the mean square velocity fluctuations and spectra) quite well using eddy viscosity models; that the higher-order statistics, which are sensitive to the small scales, are not well predicted should be no surprise. In the homogeneous flows with strain or shear, there is evidence (McMillan et al. (1980), Shirani et al. (1981)) that the energy transfer can be reversed and flow from the small scales to the large ones. In such cases, the model should no longer dissipate the energy of the large scales. Eddy viscosity models, which are guaranteed to dissipate energy from the large scales, cannot predict this behavior. Despite this, they may not function badly in actual simulations. The reason is that the smallest scales of the resolved field, from which the model normally extracts energy, become relatively weak in these flows, and the model may actually dissipate very little energy. Furthermore, the principal difficulty in computing these flows usually arises from the delivery of a significant amount of energy to scales larger than the computational domain. This makes the normally used periodic boundary conditions incorrect, and the results cannot be relied upon.

Eddy viscosity models are incapable of handling other classes of flows. For example, in transitional flows, we must expect that most of the energy will be in the large scales i.e., the small scales are not in equilibrium with the large scales and the "production equals dissipation" argument is incorrect. Furthermore, although Moin et al. (1978) had reasonable success in simulating channel flow with these models, later extensions by Kim and Moin (1979) and Moin and Kim (1981) clearly show the deficiencies of the model. They found that eddy viscosity models (several were tried) were unable to maintain the energy of the turbulence. The problem is only partially due to the model, as the turbulence tends to decay even when the model is eliminated. This will be discussed in more detail in Chapter 7.

Clark et al. (1979) and McMillan and Ferziger (1979), and McMillan et al. (1980) have applied the model-testing method described above to eddy viscosity SGS models. A typical scatter plot is shown in Fig. 3.1, in which the exact subgrid scale stress is plotted against the Smagorinsky model value. It can be seen that there is a little correlation between the two data sets (the correlation coefficient is approximately .4 for the case shown), but it is even more clear that this is far from an adequate model. This result is fairly typical, although there are variations in the correlation coefficent with many of the significant parameters.

The results show that eddy viscosity models are rather poor and, in fact, they become even poorer when there is mean strain and/or shear in the flow. However, it is not easy to find more accurate models (we shall look at this below), so we may be forced to use eddy viscosity models until something better is developed. Furthermore, as McMillan and Ferziger have shown, the method can be used to predict the effect of Reynolds number on the model parameter. Their results are shown in Fig. 3.2. When these results were applied to channel flow by Moin and Kim (private communication), they did not produce the desired effects, probably for the reasons given above.

In the above, we have used the fact that the natural length scale of the SGS eddies is the width, Δ, associated with the filter. By definition, this is the scale that defines whether an eddy is large or small, and there is little reason to suspect that this is not a correct choice.

However, when the filter is anisotropic, as it should be in computing shear flows, it is not quite so clear what is the correct length scale. Almost everyone has used the cube root of the filter volume:

$$\Delta = (\Delta_1 \Delta_2 \Delta_3)^{1/2} \tag{3.8}$$

However, Bardina et al. (1980) showed that a better choice might be:

$$\Delta = (\Delta_1^2 + \Delta_2^2 + \Delta_3^2)^{1/2} \tag{3.9}$$

It is recommended that Eq. (3.9) be adopted for general use.

5. The Role of Theory

Theoretical insight plays a considerable role in understanding the physics of turbulence and contributes considerably to modeling it. Turbulence is, however, a problem of such complexity that the role of theory in our present state of knowledge is smaller than in most areas of physics or engineering. Progress has been frustratingly slow. A review of recent theories is given by Leslie (1973).

Most theories provide limited information about turbulence. Usually, the theories were developed for homogeneous turbulence and have proved difficult to generalize.

The theories which have attracted the most attention are Kraichnan's direct interaction approximation and others related to it. These theories are statistical in nature i.e., they attempt to make statements about averages of turbulence quantities rather than the detailed dynamics. The question of whether this theory could be extended so as to yield information about the small scales of turbulence and, thus, to provide a SGS model has been investigated by Leslie and his co-workers.

The theory necessarily deals with statistically averaged SGS turbulence. We imagine an ensemble of flows which have the same large-scale motions but different small-scale motions and ask for the average behavior of the small-scale motions. Whether this is adequate for modeling purposes is an open question, but the information generated should be helpful. This theory, like many others, is capable of predicting the existence of an inertial subrange, but, unlike most others, it can predict the Kolomogorov constant as well.

Love and Leslie (1976) extended the theory and showed that a form of the eddy viscosity model could be deduced from it. In particular, they predicted the constant in the model and showed that the large scale strain rate that appears in the eddy viscosity model ought not to be the local one but a spatial average. The constant predicted in this way is in good agreement with that obtained by other theoretical arguments and from empirical fits to experimental data.

With respect to spatial averaging of the strain rate in the eddy viscosity, the evidence is mixed. Love and Leslie (1976) found that it was important in the solution of Burgers' equation, but Mansour et al. (1978) found that it did not matter much.

A number of other issues were investigated by Leslie and Quarini (1979). In particular, they divided the SGS terms into "outscatter" and "backscatter" terms representing, respectively, the energy flows to and from the subgrid scale. They found that eddy viscosity models appear to represent the outscatter fairly well, but they could not say much about the backscatter.

Although limited, these theories are proving useful in choosing and validating models.

6. A Scale Similarity Model

All models, by definition, relate the SGS Reynolds stress to the large scale flow field. Eddy viscosity models view τ_{ij} as a stress and make an analogy between it and the viscous stress. These models are guaranteed to extract energy from the large scale field (i.e., they are dissipative). It is difficult to construct other models with this property. However, as noted above, the desirability of this property is questionable in sheared and strained turbulence.

It is important to observe that the interaction between the large and small scale components of the flow field takes place mainly between the segment of each that is most like the other. The major interaction is thus between the smallest scales of the large scale field and the largest scales of the small scale field (regions 1 and 2 of Fig. 3.3). This is what the SGS term in the filtered equations represents. Since the interacting components are very much alike, it seems natural to have the model reflect this. To do this requires that we find some way of defining the small scale component of the large scale field $\bar{u}_i$. One way to do this was suggested by Bardina et al. (1980). Since $\bar{u}_i$ represents the large scale component of the field, filtering it again produces a field $(\bar{\bar{u}}_i)$ whose content is still richer in the largest scales. Thus,

$$\tilde{u}_i = \bar{u}_i - \bar{\bar{u}}_i \tag{3.10}$$

is a field which contains the smallest scales of the large scale component of the flow field. This suggests that a reasonable model might be

$$\tau_{ij} = c\,\tilde{u}_i\tilde{u}_j \tag{3.11}$$

or, better yet

$$\tau_{ij} = c\left(\bar{u}_i\bar{u}_j - \bar{\bar{u}}_i\bar{\bar{u}}_j\right) \tag{3.12}$$

This modification is suggested by considering the "cross-terms," e.g., $\overline{\bar{u}_i u_j'}$.

Preliminary tests have shown that this model is not dissipative, but it does correlate very well with the exact stress, a scatter plot is given in Fig. 3.4. This suggests that a combination of the two models might be better yet. The correlation is largely due to the fact that, with a Gaussian filter, the two fields in question contain much the same structures. With other filters, particularly one which is a sharp cut-off in Fourier space, the correlation is smaller. These models are currently being investigated.

7. Higher-Order Models

The inadequacies of algebraic eddy viscosity models in Reynolds-averaged modeling have been known for a long time. A number of more complex models have been proposed, and, since they have analogs in SGS modeling, a brief review of them is in order. We shall go into some of these models in more detail later.

Many of the improvements are based on the notion that proportionality between Reynolds stress and mean strain rate is valid, but the eddy viscosity formulation needs improvement. In these models one writes:

$$\nu_T = C_1 q \ell \tag{3.13}$$

where q and ℓ are, respectively, velocity and length scales of the turbulence. In the simplest such models, the length scale is prescribed and a partial differential equation for the turbulence kinetic energy $(q^2/2)$ is solved along with the equations for the mean flow field. These are called one-equation models; their record has not been particularly good, and most people now use still more complex models. In particular, the assumption of a prescribed length scale has been questioned, and methods of predicting the length scale have been proposed. Of these, the most widely used models are those in which an equation for the dissipation of turbulent kinetic energy (which really represents energy transferred to the small, dissipating eddies)

is added to the equations used in one-equation models. The length scale is related to the dissipation ε by:

$$\varepsilon = C_2 q^3 / \ell \tag{3.14}$$

and we have the so-called two-equation models. This is the most popular method of computing time-average flow fields at present.

Finally, the most recent development has been the use of the full Reynolds stress equations. In two dimensions, three PDE's are needed to define the Reynolds stress, while in three dimensions, six are required. Clearly, this is a rather expensive approach.

A way of avoiding the computational cost of full Reynolds stress methods is obtained by noting that the convective and diffusive terms can frequently be neglected. If they are, and approximations are made to the redistribution terms, the equations reduce to algebraic ones. Algebraic models have become popular in recent years. However, there is doubt as to whether the neglect of diffusion is correct near the wall.

All of these models have analogs in SGS modeling, and a number of them have been used. Let us consider them in the order in which they were introduced above.

First, consider one- and two-equation models. They have as their fundamental basis the proportionality of the SGS Reynolds stress and the large-scale stress. We saw earlier that the Smagorinsky model (an algebraic eddy viscosity model) correlates poorly with the exact SGS Reynolds stress. Clark et al. (1979) looked at the behavior of one-equation models as well as an "optimized" eddy viscosity model. In the latter, the eddy viscosity was chosen, at every point in the flow, to give the best local correlation between the SGS Reynolds stress and the large-scale strain. By definition, no eddy viscosity model can do better than this. It was found that the correlation coefficient improved somewhat relative to the Smagorinsky model (from approximately .35 to .50 in a typical case), but this still leaves the model far short of what we would like to have. The lack of correlation seems to be due to the difference between the principal axes of the two tensors. This modeling assumption needs to be changed if further improvement is to be obtained (cf. McMillan and Ferziger (1980)), and more complex models are required.

Schumann (1973) also used one-equation models without finding improvement over algebraic eddy viscosity models.

Next, recall the earlier remark that convection and diffusion are likely to be more important in SGS modeling than they are in time-average modeling. This means that the approximations needed to reduce the full Reynolds stress equations to algebraic model equations are less likely to be valid in the SGS case. However, several authors have used algebraic models. The applications have been almost exclusively to meteorological and environmental flows in which stratification and buoyancy effects are important. These flows are sensitive to small variations in both properties and model, making it difficult to assess the accuracy of a model with precision. To our knowledge, no applications of these models to engineering flows have yet been made.

It is probable that, to obtain a significant improvement over the Smagorinsky eddy viscosity model, we shall need to go to full Reynolds stress models. This, of course, is not something to be looked forward, to as the computing cost is likely to be more than doubled. The only use of these equations to date was in meteorological flows by Deardorff (1972, 1973a,b), who reported a computer time increase of a factor of 2.5. Furthermore, the results were not improved to the degree that he had hoped for. Although this is discouraging, Deardorff's simulation was considerably ahead of its time and had the additional difficulties associated with buoyancy, so it is hard to make definitive conclusions. Thus, we cannot conclude much about these models at present, and quite a bit of work needs to be done on them before they become useful tools of the trade.

8. Other Physical Effects

The author's group has done full simulations of the effects of compressibility on turbulence and the mixing of passive scalars in turbulent flows. To date, the work has concentrated on evaluating time-average models, because it was felt that this is the area in which the work has the most immediate impact.

The effects of compressibility on SGS turbulence are probably quite small. The effect on the turbulence as a whole have been found to be fairly weak, except for effects due to the propagation of acoustic pressure waves. Since the latter are large scale phenomena and the Mach number of the SGS

turbulence is small, we expect that compressibility will have only a weak effect on SGS modeling.

On the other hand, SGS modeling of turbulent mixing is quite important. If we are to simulate combusting flows, it will be necessary to treat the small scales accurately, since that is where the action is in these flows. The effect of the Prandtl/Schmidt number on time-average models is moderately strong, and we expect its effect on SGS models to be even stronger. Furthermore, the specific effects due to combustion are also likely to be important on the small scales. The author intends to look at SGS modeling of mixing and combusting flows in the near future.

Another effect of considerable importance in application is buoyancy, which was mentioned earlier in connection with the meteorological simulations. Flows in which buoyancy is important and, particularly, those which are driven by buoyancy are very difficult flows to measure or simulate, and a great deal of work will need to be done in this area. Important work in this area has been done by the Karlsruhe group (Grotzbach et al. (1979)), and further work is under way in London (Leslie (1980)).

Finally, we should state that meteorologists and environmental engineers have a great interest in both mixing and buoyancy effects, and considerable effort in these areas has been made by these people. In particular, we note again the work of Deardorff cited above and that of Sommeria (1976), Schemm and Lipps (1978), and Findikakis (1981). One of the principal difficulties of these flows is that the Reynolds numbers are so large that eddies of length scale equal to the grid size are quite important. Consequently, the SGS eddies do not behave entirely like "small eddies;" they carry a significant fraction of the total energy and are therefore hard to model.

9. Summary of the State of SGS Modeling

From the arguments given above, we can reach the following conclusions about the current state of the art in SGS modeling.

1. Although they are inadequate in detail, eddy viscosity models can be used in simulating homogeneous turbulent flows. However, they seem to be inadequate for inhomogeneous flows, especially those in which solid boundaries are important.

2. For models in which the length scale is prescribed, the length scale of Eq. (3.9) is preferred.

3. One- and two-equation turbulence models are unlikely to provide significant improvement relative to algebraic eddy viscosity models. An exception to this might be transitional flows.

4. Full Reynolds stress models offer promise as future SGS models. However, the modeling assumptions probably need to be different from those used in time-average modeling.

5. The scale-similarity model is promising, but only when used in conjunction with other, dissipative, models.

6. Full simulations seem to be the best way available at present for testing SGS models and determining the parameters in them. Turbulence theories can also be profitably used in this regard.

7. Full simulations and large eddy simulations can both be used in time-averaged model building. This is the area in which both types of simulations will make their greatest impact in practical engineering calculations in the near future.

Chapter IV

NUMERICAL METHODS

1. Mathematical Preliminaries

This chapter is devoted to setting out the numerical methods used in full and large eddy simulations. To some extent, numerical methods are always tailored to the problem, higher-level simulations of turbulent flows are no exception.

The partial differential equations governing a flow were given in Chapter 2. To complete the methematical setting, it is necessary to specify initial and boundary conditions. This is not easy. Higher-level simulations need details of the initial state, and experimentalists are unable to provide sufficient data about the initial state of their flows; some of the initial data therefore has to be invented. An equally serious problem is that, as the Navier-Stokes equations are nonlinear, it is not always known what boundary conditions should be specified, i.e., we may not know whether a problem is well-posed or not. There are a number of examples of people attempting to solve mathematically ill-posed problems. Another issue is that the partial differential equations have several conservation properties, and it is important that they be preserved in the numerical treatment of the problem. Finally, there are the difficulties inherent in the numerical methods themselves--accuracy, stability, and aliasing, among others. All of these need to be considered.

The equations governing incompressible flows are of mixed type; they contain elements of both parabolic and elliptic partial differential equations. This is a consequence of the momentum equations containing time derivatives, but the continuity equation not having any. As a result, one cannot advance the continuity equation in time. These equations are called incompletely parabolic by mathematicians. Means of dealing with both types of behavior are needed. The compressible equations, which are hyperbolic, are actually easier to deal with from a numerical point of view.

All of these issues will be taken up in the remainder of this chapter. Additionally, we shall need to describe the numerical approximations used in

the computations. Throughout the chapter, it is important to keep in mind the kinds of flows that we are trying to simulate. They are geometrically simple turbulent flows. The fact that they are turbulent means that the high wave-number components of the velocity field are large. Large gradients of the variables can occur in any part of the flow, this has an important influence on the choice of numerical methods. On the other hand, the simplicity of the geometry helps considerably in developing accurate numerical methods.

2. Boundary Conditions

The simplest flows to be simulated are the homogeneous turbulent flows. By definition, these flows are statistically identical at every point in the flow. For these flows, the most convenient and most accurate boundary conditions are periodic ones. The portion of the flow within a rectangular parallelepiped is simulated, and the boundary conditions prescribe that the state of the fluid at a point adjacent to any of the boundaries is identically that on the opposite face of the parallelepiped. These conditions avoid the need for specifying the details of a highly chaotic motion on the surfaces and are the most realistic means of enforcing the idea that any point in the flow is indistinguishable from any other point.

There is one point that requires extra care. In homogeneous turbulent flows on which mean straining or shearing flow is imposed, it is convenient to solve for just the part of the flow containing the turbulent fluctuations; the mean flow is eliminated. When this is done, it is found that there are terms in the equations that do not admit the use of periodic boundary conditions. It is then necessary to do the computation in a coordinate system that deforms with the mean flow, and the ability to use periodic boundary conditions is restored. This will be taken up again in Chapter 5.

The only other flows that we shall consider in any detail in this report are inhomogeneous in one coordinate direction. Of course, this means that they are homogeneous in the other two directions, and these directions can be treated by the periodic conditions described above. There are two types of conditions we must deal with in the inhomogeneous direction; they follow from the nature of the flows we shall be simulating.

For free shear flows, we would like to prescribe the condition that the flow is at rest infinitely far from the shear layer. Dealing with an infinite region is difficult, and two methods have been used for this problem:

i) One can use a finite computational domain. At the top and bottom of the domain one specifies that the vertical derivatives of the horizontal components of the velocity are zero, and the component of the velocity normal to the boundary is set to zero. These are known as no-stress boundary conditions. Unfortunately, no-stress conditions imply the existence of image flows outside the computational domain; the images are reflections of the flow in the boundaries. To assure that the image flows do not interfere with the physical one, there must be no vorticity close to the no-stress boundary. This means that a considerable portion of the computational domain must be wasted in computing the potential part of the flow.

ii) One can use a coordinate transformation that maps the infinite domain onto a finite one. Standard numerical methods can then be used. It is important to choose a mapping that is compatible with the method used for evaluating derivatives. This issue will be dealt with in more detail later.

The second type of inhomogeneous flow that we shall consider is fully developed turbulent channel flow. Two different approaches have been taken for simulating this flow:

i) Deardorff and Schumann decided not to treat the wall directly. The reasons will be stated in detail in Chapter 7. Instead, they decided to compute only the part of the flow within and beyond the region in which the velocity profile is logarithmic. The boundary conditions must then assure that the velocity profile be logarithmic at the edge of the computational domain. In addition, it is necessary to specify something about the nature of the turbulent fluctuations at this boundary. They assume a relationship between the velocity and stress fluctuations at the boundary, this is the simplest assumption one can make, and there is no evidence for any other choice, but it has been called into question.

ii) One can compute the entire flow, including the region near the wall. The wall conditions are then the no-slip conditions that must be imposed at any solid surface. This is a much simpler boundary condition to deal with numerically. The price one pays is that all of the small structures near the

wall must be computed explicitly; this leads to considerable difficulty, as we shall see in Chapter 7.

3. Treatment of the Spatial Derivatives: Conservation Properties

In all flow computations, the spatial derivatives are approximated in terms of the values of the dependent variables at grid points. Higher-level turbulence computations are no different from others in this respect; the methods used in these flows are also used in other types of flow simulation. Again we note that the geometric simplicity of the flows treated by higher-level simulations allows use of methods that might not be easily applied in more complex geometry.

Before giving the specific approximations to be used, it is important to discuss conservation properties. We believe that this issue is not emphasized sufficiently in the literature. The dynamical equations are essentially microscopic conservation equations. The continuity equation expresses conservation of mass. In the compressible case, the Navier-Stokes equations express momentum conservation (or what is the same thing, Newton's second law), and there is a separate energy equation to express the fact that total energy is conserved. In the incompressible case, the Navier-Stokes equations still express momentum conservation, but, in the absence of an explicit energy equation, they are also responsible for conserving the only significant energy in the flow--the kinetic energy. This leads to one of the principal difficulties in the treatment of incompressible flows.

By integration of the microscopic conservation equations over a finite volume, we obtain macroscopic conservation equations. For the incompressible form of the continuity equation we obtain the global conservation of mass relation:

$$\int_S \rho u_i \, dS_i = 0 \tag{4.1}$$

The Navier-Stokes equations give rise to the well-known momentum theorem:

$$\frac{d}{dt}\int_V \rho u_i \, dV = -\int_S \left(\rho u_i u_j + p\delta_{ij} + \mu \left(\frac{\partial u_i}{\partial x_j} + \frac{\partial u_j}{\partial x_i} \right) \right) dS_j \tag{4.2}$$

Finally, multiplying the Navier-Stokes equations by u_i and integrating over a finite volume, we obtain the equation of kinetic energy conservation:

$$\frac{d}{dt}\int_V \rho \frac{u_i u_i}{2}\, dV = -\int_S \left(\rho \frac{u_j u_j}{2} u_i + p u_j + \mu u_j \frac{\partial u_j}{\partial x_i}\right) dS_i - \mu \int_V \frac{\partial u_i}{\partial x_j}\frac{\partial u_i}{\partial x_j}\, dV \tag{4.3}$$

Each of these equations states that the conserved property changes only by flow of the property through the bounding surface, this is a consequence of the fact that there are no sources of any of these properties within the volume. If periodic boundary conditions are applied, the surface terms integrate to zero. In Eqs. (4.1), (4.2) and (4.3), S is the surface of the volume V.

The kinetic energy conservation equation (4.3) is especially interesting. The only non-surface term is the viscous dissipation term, which is usually small. It is essential to note that the kinetic energy within the control volume is not changed by the convection and pressure gradient terms and that the chain rule $(uv)' = u'v + v'u)$ and the continuity equation are used in eliminating the volume integral of the pressure.

It is crucial that the numerical approximations to the equations retain these properties. For the continuity and momentum conservation, this is usually not difficult. It usually turns out that, if the equations are written in the proper form (the so-called conservative form we have used throughout), then almost any approximation will yield these conservation properties. The principal difficulty is with the kinetic energy. Normally, the verification that the numerical approximation guarantees energy conservation has to be done on a case-by-case basis. A means of avoiding this difficulty was found by Mansour et al. (1978). If the Navier-Stokes equations are written in the form:

$$\frac{\partial u_i}{\partial t} + \frac{\partial}{\partial x_j} u_i u_j - \frac{\partial}{\partial x_i} u_j u_j = -\frac{\partial}{\partial x_i}\left(\frac{p}{\rho} + u_j u_j\right) + \nu \frac{\partial^2 u_i}{\partial x_j \partial x_j} \tag{4.4}$$

rather than (2.1), the derivation of the conservation of kinetic energy equation (4.3) can be based on a symmetry property, and the use of the chain rule can be avoided. Since numerical approximations do not always have a chain rule but the symmetry property always holds, using the Navier-Stokes equations

in the form (4.4) can simplify the job of finding well-behaved numerical methods.

Many workers (Deardorff (1970), Schumann (1973), Antonopoulos (1981), Shaanan et al. (1975), among others) have used the staggered-grid mesh system. The grid is shown in Fig. 2.2 for the two-dimensional case, the variables are given at the mesh points shown in the figure. The control volumes for the various equations are different and are displayed in the figure, we shall not give the finite difference equations here, as they appear in several other works. This grid system has the nice property that all of the conservation properties are obtained without difficulty, and, as we shall see in the next section, it gives no problem with the calculation of the pressure. It is the natural grid system for the incompressible equations and has been used more widely than any other. Part of the reason for the success of the staggered mesh system was explained by Shaanan et al. (1975). The approximation $\overline{\bar{u}_i \bar{u}_j} = \bar{u}_i \bar{u}_j$ which has been used by Deardorff and Schumann is valid in the staggered grid system, because the truncation errors represent the difference between these two terms (the Leonard stress) quite well. Stated otherwise, the staggered grid approximates $\bar{u}_i \bar{u}_j$ more accurately than it does $\overline{\bar{u}_i \bar{u}_j}$ and thus leads to great simplification in the finite difference equations.

If a regular grid is used, it is necessary to use a fourth-order finite difference method in order to assure that the Leonard stress is properly computed. This can be done, but the method is cumbersome (Kwak et al. (1975)).

Another popular method of computing derivatives in directions in which a flow is homogeneous is by means of Fourier transforms--the pseudospectral method. In this method one uses the discrete Fourier transform. Any function defined at a set of equally spaced mesh points $x_j = j\Delta x$, $j = 1,2,\ldots,N$, can be represented by the discrete Fourier series:

$$f(x_j) = \sum_{\ell=1}^{N} e^{ik_\ell x_j} \hat{f}(k_\ell) \tag{4.5}$$

where $k_\ell = 2\pi\ell/N\Delta x$. This has the inverse:

$$\hat{f}(k_\ell) = \frac{1}{N} \sum_{j=1}^{N} e^{-ik_\ell x_j} f(x_j) \tag{4.6}$$

which differs from Eq. (4.5) only by the sign of the exponent and the factor $1/N$; thus, bpoth transforms can be computed in the same way. these results can be used in the following way: Given the values of the function $f(x)$ on the grid points $x_j = j\Delta x$, we can compute $\hat{f}(k_\ell)$ from Eq. (4.6). When these are used in Eq. (4.5) and x_j is replaced by the continuous variable x, the result is an interpolation formula. As such, it can be differentiated with respect to x, and this provides a method of computing spatial derivatives. In fact, specializing the result to the grid points, we have:

$$\frac{\partial f}{\partial x}(x_j) = \sum_{\ell=1}^{N} ik_\ell \hat{f}(k_\ell) e^{ik_\ell x_j} \tag{4.7}$$

The derivative df/dx can be computed by using the discrete values $f(x_j)$ to compute $\hat{f}(k_\ell)$, multiplying the result by ik_ℓ, and computing the inverse transform. The result is an extremely accurate estimate of the derivative. This method is especially well adapted to the calculation of the derivatives of periodic functions, which explains its widespread application in the computation of homogeneous turbulent flows.

The practical use of the Fourier transform as a numerical tool is made possible by the existence of an extremely faot algorithm for its computation--the so-called fast Fourier transform (FFT) algorithm.

For later application it is important to note that this method could also be used to compute finite differences. It is not effective to use this as a tool for computing derivatives, but it can play an important role when we come to solving the equation for the pressure. As an example, we take the standard second-order central difference approximation:

$$\left.\frac{\delta y}{\delta x}\right|_j \simeq \frac{y_{j+1} - y_{j-1}}{2\Delta x} \tag{4.8}$$

The derivative obtained from this formula can be put into the form of Eq. (4.7) with ik_ℓ replaced by $ik'_\ell = i(\sin k_\ell \Delta x)/\Delta x$; we call k'_ℓ the effective wavenumber. Effective wavenumbers are a good way to measure the accuracy of finite difference methods that are required to differentiate functions which contain significant high-wavenumber components, and it is not difficult to derive the effective wavenumber for various finite difference approximations. Some effective wavenumbers are plotted in Fig. 4.1.

Next, let us discuss the treatment of directions in which the flow is not homogeneous. For the free shear layer, we noted in the previous section that there are two ways of dealing with the direction normal to the flow (the shear direction). When the no-stress boundary conditions are used, one can generalize the Fourier method described above. The key idea is to expand the functions in terms of sines or cosines (using the set appropriate to the boundary conditions for the particular function) rather than the complex exponentials of Eq. (4.5). The numerical algorithm for computing sine and cosine transforms is equivalent to computing the exponential transform (4.5) using $2N$ rather than N points. Thus the cost of computing the derivatives is approximately doubled when this method is used. We noted earlier that this approach suffers from loss of accuracy due to images.

The alternative to the use of no-stress conditions is the use of a transformation which takes the physical coordinate z into a computational coordinate ζ:

$$z = h(\zeta) \tag{4.9}$$

such that $-\infty < z < \infty$ transforms to $-1 < \zeta < 1$. The derivative becomes:

$$\frac{d}{dz} = \frac{1}{h'} \frac{d}{d\zeta} \tag{4.10}$$

The trick to making this a successful method is to choose the transformation such that $1/h'$ can be expressed in terms of just a few low-order sines and/or cosines. It is then possible to obtain accuracy almost as good as that of the Fourier method for infinite regions. Details of this method are given in the report by Cain et al. (1981).

Finally we come to dealing with directions in which there are solid walls, i.e., a numerical method for treating channel flow. There are two choices that have been commonly used. The first is the use of Chebychev polynomial expansions. This is equivalent to a Fourier method on a nonuniform grid and has been used by Kells and Orszag (1980) and by Orszag and Patera (1980); see also Kim and Moin (1980).

The other method for treating the channel is to use a finite difference method on a nonuniform grid; this is equivalent to using a coordinate trans-

formation in this direction. The choice has generally been adopted (Moin et al. (1978), Moin and Kim (1981)). We shall deal with this further in Chapter 7.

Another important issue is aliasing. Aliasing is the error introduced when two Fourier waves are multiplied; this happens implicitly when the nonlinear convective terms are computed. The waves resulting from the product of two Fourier waves contains the sum and/or difference of the original wavenumbers. These may fall outside the range of wavenumbers $(-\pi/\Delta < k < \pi/\Delta)$ which can be carried in the calculation. When this happens, the wavenumber which falls outside computational range is misinterpreted ("aliased") as one of the wavenumbers which lies inside the band. The result is a numerical error which, in mild cases, adds to the normal truncation error of a finite difference approximation and, in severe cases, can cause the calculation to become totally inaccurate or even unstable.

Aliasing can be controlled in two ways. The simplest way is to assure that the high wavenumbers are relatively unpopulated. Since these are the ones that cause the problem, eliminating them also solves the problem. In large eddy simulation, one can assure that the high wavenumbers are relatively unpopulated by using a filter which cuts off at a moderate wavenumber. In full simulations, the best way to control the problem is to keep the Reynolds number low.

The other method of controlling aliasing is to compute the portion of the field which will be aliased and explicitly eliminate it. This requires extra computation, but it allows one to include more energy in the high wavenumbers and the extra resolution gained may be worth the cost.

4. Time Advancement

We now come to the method of advancing the solution in time. One of the first issues that arises is that of selecting an explicit method or an implicit one. It is important to remember that in higher-level simulations one is looking for time-accurate solutions to the equations of motion. This contrasts strongly with relaxation methods, in which the object is to reach steady state as quickly as possible. The point of view that we adopt is that a well-balanced, time-accurate method is one in which the errors caused by the time advancement method approximately equal those introduced by the spatial

introduced by the spatial differencing method. Once spatial difference approximations and the time-advancement method have been chosen, this criterion selects the time step. The time advancement method must be stable for the time step so chosen. It is usually the case that the time step found in this way is well within the stability bounds of explicit methods, so there is no need to pay the extra cost associated with an implicit method. Thus, with a few exceptions, noted later, the time-advancement methods used in higher-level simulations are explicit. The common choices have been second-order methods such as leapfrog and Adams-Bashforth and the fourth-order Runge-Kutta method. These are standard methods of numerical analysis, so the formulas will not be given here.

For purposes of discussing time-advancement methods, it is convenient to rewrite the Navier-Stokes equations in the form:

$$\frac{\partial u_i}{\partial t} = -\frac{1}{\rho}\frac{\partial p}{\partial x_i} + H_i \tag{4.9}$$

where the viscous and convective terms have been included in H_i. There is no difficulty in time-advancing this equation by an explicit method. Most of the difficulties in solving the incompressible equations come from the lack of a time derivative in the continuity equation; the compressible equations have no such problem. One method of avoiding this difficulty is to treat the flow as if it were compressible and iteratively drive the compressibility effects to zero; the iterative nature of this process makes it inefficient, however.

A more efficient procedure is to note that application of the divergence operator and use of the continuity equation on Eq. (4.9) gives the Poisson equation for the pressure:

$$\frac{\partial^2 p}{\partial x_i \partial x_i} = \rho \frac{\partial H_i}{\partial x_i} \tag{4.10}$$

When one looks at the time-discretized version of Eq. (4.9), it is found that forcing the pressure to satisfy the Poisson equation (4.10) at time step n guarantees that continuity will be maintained at time step $n + 1$. The mixed nature of the equations is brought into clear focus. The Navier-Stokes equations (4.9) are treated as parabolic partial differential equations, but the pressure must be calculated from the Poisson equation (4.10), which is elliptic.

One further important point needs to be made here. Recall that, if the Navier-Stokes equations in the form (2.1) are used, then the derivation of the energy-conservation equation (4.3) requires use of the chain rule and the continuity equation. If we are to have numerical energy conservation, it is necessary to derive the numerical equivalent of Eq. (4.3). Assuming that the required analog to the chain rule exists, the choice made for the numerical approximation to the pressure gradient dictates the numerical approximations used in the continuity equation. Otherwise, one cannot obtain energy conservation; the usual consequence is an unstable calculation. For example, if the central difference approximation is used to estimate $\partial p/\partial x$, it must be used for the continuity equation as well. If a backward difference is used for the pressure gradient, the continuity equation must use the forward difference operator, and vice versa; this is what is done on the staggered grid.

Furthermore, one is not free to finite difference the Poisson equation (4.10) arbitrarily. The correct approximation is derived by applying the numerical divergence operator obtained in the manner described in the preceding paragraph to the finite difference version of the Navier-Stokes equations. Thus, the choice of the finite difference approximation for the pressure gradient dictates the method of differencing the Poisson equation. For example, if the central difference operator is used for $\partial p/\partial x$, it turns out that the difference operator for the Poisson equation must be the second-order central difference operator (as one might expect), but the grid spacing must be $2\Delta x$ and not Δx. We reiterate that the function of the Poisson equation is to maintain continuity in the numerical sense; it is more important to solve the correct equation than to obtain the most accurate solution to the exact partial differential equation.

The most efficient method of solving the Poisson equation is by means of the fast Fourier transform. This is the case whether one uses finite differences or the pseudospectral method, the spatial derivatives. When finite differences are used, one can solve the Poisson equation by using Fourier transforms, but one must be careful to use the effective wavenumber rather than the exact wavenumber.

The staggered grid method accomplishes all of this very efficiently. It does this so well that the need for being careful with finite difference methods is often overlooked.

There is one case in which we cannot use explicit methods. In the computation of flows with solid boundaries, it is necessary to use a very find grid in the direction normal to the wall, close to the wall. A consequence is that the time step allowed by stability is then smaller than the time step allowed by the accuracy criterion. The principal difficulty comes from the viscous term. In this case, it is necessary to treat the viscous terms containing derivatives in the normal direction implicitly. In fact, a special numerical method had to be invented for this problem; it will be sketched in Chapter 7.

5. Initial Conditions

The initial conditions for higher-level simulations cannot be derived directly from experimental results. The data never contain enough information to construct a complete initial field. In fact, the reported results of some experiments are quite incomplete and leave the computor so much freedom that it is always possible to find initial conditions that allow the simulation to match the experiment. From the point of view of one doing higher-level simulations, an ideal experiment reports not only the mean velocity and turbulence intensities, but information about the length scales as well. Ideally, complete spectral information should be provided.

We begin by considering the construction of a velocity field for the simulation of homogeneous isotropic turbulence; the velocity fields required by the other cases are frequently derived from this. The task is to create an initial field that has a specified energy spectrum and is divergence-free. There are several ways to do this; of these, the following is one of the easiest. There are three steps in the process:

1. Each component of the velocity at every grid point is assigned a random value. The resulting field is not divergence-free, nor does it have the desired spectrum.

2. The curl of the field is taken; the resulting field is divergence-free. The numerical operator used to take the curl must be the same as the operator used to define the divergence.

3. The Fourier transform of the velocity field is taken and in each Fourier mode is assigned an amplitude required to give the desired spectrum. The Fourier transform is inverted, and the result is the desired initial field.

This procedure is easily modified to give an initial field which is anisotropic. This can be done by biasing the random numbers used in the first step of the process.

For flows in which there is a mean velocity profile (specifically, the mixing layer and the channel), it is necessary to give the mean velocity profile in addition to the turbulence. The method of producing an initial turbulence field must also be modified. In the case of the mixing layer, we want the fluctuations to be more intense near the central plane of the flow than near the edges. Such a field can be produced in a manner similar to that described above. Insteady of allowing the field created in Step 1 to be uniformly distributed in space, we give it the desired spatial distribution. The steps for removing the divergence and producing the given spectrum are then essentially as described above.

For the channel flow it was found that the subgrid scale model destroyed too much energy and tended to make the flow become laminar if conditions of the kind described above were used. To prevent this, it was necessary to introduce large structures into the flow. These were obtained from solutions of the Orr-Sommerfeld equations. Although these are not the correct large structures for a fully developed channel flow, they are apparently similar enough to them. Randomness was added to the flow by introducing a small amount of more or less isotropic turbulence which is divergence-free and is zero at the walls.

Chapter V

HOMOGENEOUS TURBULENCE

1. Classification

A homogeneous turbulent flow is one in which each point in the flow is, in the statistical sense, equivalent to every other point. Ideally, this requires an infinite medium of fluid, every part of which experiences the same forces. In practice, close approximations to these flows are produced in wind tunnels. The mean flow is designed into the tunnel, while the turbulence is usually created by a grid (or, in a few cases, by a set of jets) and carefully controlled. The time evolution of the flow is simulated by observing its development as it moves downstream in the tunnel and invoking Taylor's hypothesis. If the gradients of mean quantities and other parameters of the flow are carefully chosen, an accurate approximation to a homogeneous flow is produced. It is not difficult to show that homogeneity requires the mean flow to be one in which the mean velocity is a linear function of all of the spatial coordinates. This severely limits the possibilities.

Nearly all turbulent flows of engineering interest are inhomogeneous, the inhomogeneity is usually the result of the shear varying through the flow. When the Reynolds stresses in these flows are modeled, five separate effects are commonly considered. They were mentioned in Chapter 3 and are repeated here:

a. Production. The creation of new Reynolds stresses via the interaction of the Reynolds stresses with the mean flow.

b. Dissipation. The destruction of turbulent energy and Reynolds stresses by the action of viscosity.

c. Redistribution. The conversion of one component of the Reynolds stress into another without change of the total turbulent energy. Much of this effect is mediated by the pressure.

d. Convection. The convection terms usually require no modeling, but their inclusion makes the local Reynolds stresses depend on the mean field in other parts of the flow.

e. Diffusion. The carrying of Reynolds stress from one part of the flow to another via the self-interactions of the turbulence.

By definition, homogeneous flows have no convection or diffusion, so we need to deal with, at most, production, dissipation, and redistribution.

Homogeneous turbulent flows can be grouped into three categories according to the phenomena contained in them. The first group contains the one flow in which the only interesting effect is dissipation. (Inertial energy transfer among the wavenumber components is, of course, an element in all flows but is not counted separately.)

- Homogeneous Isotropic Turbulence. This flow, which at one time was heavily studied because it was thought that it might provide the insight into the nature of all turbulent flows, is the decay back to rest of fluid which has been set into random motion. It is still used as a means of finding turbulence model constants associated with dissipation and is usually the first flow simulated by people doing higher-level simulations.

- The second group of flows contains those in which there is exchange between the various components of the Reynolds stress (redistribution) in addition to dissipation, but there is no direct production of turbulence energy. There are two such flows.

a. Homogeneous Turbulence with Rotation. The effect of rotation on isotropic turbulence is to produce anisotropy. The effect is primarily on the length scale and reduces the rate of decay of the turbulence.

b. Return to Isotropy. Turbulence which has been made anisotropic by the action of strain (see below) tends to return toward isotropy if the additional force is removed.

- The final group contains the flows in which all of the phenomena that are possible in homogeneous flows actually occur. There are two major flows of this type.

a. Strained Homogeneous Turbulence. Turbulence which is initially isotropic (or nearly so) is put through a wind-tunnel section in which a fluid element is stretched in one direction and compressed in either one or two directions. The result is irrotational strain which interacts with the existing

turbulence; there is considerable turbulence energy production, and the flow becomes quite anisotropic.

b. Sheared Homogeneous Turbulence. Nearly isotropic turbulence is produced in a flow which has uniform shear (a straight-line velocity profile). The effects are similar to those observed in the strained turbulence case.

The experimental data for these flows have been reviewed in a paper by the author (Ferziger (1980)).

We shall also consider flows with compressibility and mixing of a passive scalar.

All of the flows described in this chapter are ones which develop in time. It is uncertain that any of them reaches a steady state or even a self-similar state. This issue is controversial; some authors believe that a self-similar state will be reached, while others do not believe so. In any case, these flows are sensitive to the initial conditions. In turn, this means that caution is required in interpreting them and that careful documentation of the initial conditions is necessary.

All of these flows have been calculated by both full and large eddy simulation. The results show that all of the physical phenomena observed in the laboratory have been shown to be a valuable tool in evaluating turbulence models. Much of the work in the area of model validation is recent and unpublished, and we shall give a brief overview of some of the principal results. It is also worth pointing out that a complete compendium of results from full simulations of homogeneous turbulence is being assembled by Dr. R. S. Rogallo of NASA-Ames Research Center and will probably be available in the summer of 1981. His results should be an important resource for people developing turbulence models.

2. Isotropic Turbulence

As we have mentioned earlier, isotropic turbulence is the simplest turbulent flow. It is therefore an obvious first target for any method of simulating or modeling turbulent flows. It has long been used by the developers of Reynolds-averaged models as a basis for choosing the constant(s) associated with the dissipation. It has also been a popular choice as the first flow to be simulated by higher-level methods, and it has been used extensively as a

basis for testing subgrid-scale models. We shall review this work briefly in this section.

To simulate these flows numerically, one begins with an initial condition that has the desired energy spectrum and is divergence-free. Methods of constructing such fields were described in the preceding chapter. In full simulations it is not necessary to begin the calculation with a realistic spectrum; one will develop in time. Of course, if one is trying to match an experiment, the experimental spectrum ought to be specified. In large eddy simulations of this flow, the initial spectrum is obtained by filtering the experimental spectrum.

The initial condition defines the initial Reynolds number. The Reynolds number commonly used to characterize this flow is based on the Taylor microscale λ and the turbulence intensity q. Although these may not be the optimum choices, we shall follow custom and use them. In this flow the turbulence intensity decays and the microscale increases with time, but the microscale Reynolds number decreases.

At the first few time steps, the flow field cannot be regarded as representing true turbulence. The initial field does not contain the proper higher-order statistics or correlations; only after at least some of these have developed can the field be taken as representing physical reality. We have generally taken the behavior of the skewness of the velocity derivative:

$$S = \langle (\partial u/\partial x)^3 \rangle / \langle (\partial u/\partial x)^2 \rangle^{3/2} \qquad (5.1)$$

as the measure of the quality of the flow field. It is nearly zero in the initial field and quickly rises to an asymptotic value at which it tends to remain for a considerable time, except at low Reynolds numbers. The time period in which the skewness is rising is considered a "development" period. This is followed by a period in which the flow is realistically simulated. Finally, the size of the large structures grows to an appreciable fraction of the size of the computational domain, and periodic boundary conditions are no longer valid. At this point, the flow is no longer realistic, unphysical behavior is observed in the results, and the program has to be stopped.

First, let us consider full simulations of this flow. Using $64 \times 64 \times 64$ mesh points in a calculation, one is able to compute at Reynolds numbers

up to $R_\lambda = 50$. This is the practical limit on most present computers, a few cases have been run on a $128 \times 128 \times 128$ grid which allows the Reynolds number doubled. These Reynolds numbers are on the low end of the experimental ones; most experiments have been run with R_λ in the range 30-400. The results of these computations match the experiment very well in terms of the decay of the turbulence intensity, the growth of the length scales, and the value of the skewness. Typical results are shown in Figs. 5.1-5.3.

The principal use to which these results have been put has been in the development and testing of subgrid scale models. Clark et al. (1979) and McMillan and Ferziger (1979,1980) used flow fields generated by full simulation of isotropic turbulence in the way suggested in Section 3.3. Some of the principal results of this work were: that the Smagorinsky model correlates very poorly with the actual SGS Reynolds stress (the actual correlation coefficient is typically .30-.40), that the width of the filter used in large eddy simulation ought to be at least twice the grid size, that changing the shape of the filter matters little, and that the model "constant" (which really ought to be called a parameter) is a function of Reynolds number that can be derived from this type of calculation. Since these results were covered in Chapter 3, we shall not repeat them here.

Full simulation has also been used to study isotropic turbulence at low Reynolds number, a purpose for which it is ideally suited. At low Reynolds numbers ($R_\lambda < 10$), it is possible to do full simulations with only $16 \times 16 \times 16$ mesh points. Interest in these flows centers on the decay rate and the skewness. The decay of isotropic turbulence can be represented by:

$$q^2 = A(t-t_o)^{-n} \tag{5.2}$$

Theory shows that the decay exponent (n) is 2.5 at very low Reynolds number, and both theory and experiment show it to be approximately 1.2 at high Reynolds number. It is therefore of interest to compute the decay exponent as a function of Reynolds number. The results are compared with experiment in Fig. 5.4.

The velocity derivative skewness defined by Eq. (5.1) is approximately .5 at high Reynolds number and can be shown to drop to zero as the Reynolds number goes to zero. The direct simulation and experimental results are shown in Fig. 5.5. Figures 5.4 and 5.5 are from a report by Shirani et al. (1981).

Now let us turn our attention to large eddy simulations of this flow. The major advantage of large eddy simulation is that, since the small eddies are modeled, the computation time is considerably reduced for a given Reynolds number. Alternatively, it is possible to go to higher Reynolds number with LES than with direct simulation.

When large eddy simulations of homogeneous isotropic turbulence were first made, the results of full simulations were not available. Consequently, the constant had to be chosen to fit the decay of the turbulent kinetic energy. It was found that the same constant can be used whether 16^3 or 32^3 mesh points were used; it was later found that the value obtained in this way agreed with those obtained from direct simulation to within 10%. It is also in good agreement with theoretical estimates (Lilly (1967)) despite the fact that these flows are at Reynolds numbers too small to support an inertial subrange. Since the constant needs to be adjusted by this amount to account for changes in numerical method (mainly changes in the spatial differencing method), this was one of the most important early successes or large eddy simulation.

It was found that it made little difference whether the primitive Navier-Stokes equations or the vorticity form of those equations were used; it made very little difference whether the model was based on the strain rate or the vorticity; and it made very little difference which filter was used. However, if pseudospectral differencing is applied to the original Smagorinsky model, the shape of the spectrum at high wavenumbers is distorted. To remedy this problem, it was found necessary to evaluate all of the derivatives that occur in the model by second-order finite-difference approximations. This is similar to the finding by Love and Leslie (1976) that the model ought to be averaged over a finite volume. A typical result obtained by large eddy simulation is shown in Fig. 5.6; other curves are similar and therefore not shown.

Finally, it was found that large eddy simulation is incapable of computing the higher-order statistical quantities such as the skewness and flatness with sufficient accuracy. These quantities are strongly affected by the small scale motions that are filtered out, and there is no way to recover the lost information; all attempts to do so failed.

Most of the results on large eddy simulation are taken from a report by Mansour et al. (1978).

3. Anisotropic Turbulence

Anisotropic turbulence (turbulence in which the fluctuating components are unequal so that $u_1^2 \neq u_2^2 \neq u_3^2$) usually returns to an isotropic state if not strained in any way. However, it is possible for the flow to become even more anisotropic. Thus, if the large scales are such that $\overline{u_1^2} < \overline{u_2^2}$ and the small scales have $\overline{u_1^2} > \overline{u_2^2}$ but the total field is such that $\overline{u_1^2} < \overline{u_2^2}$, it is quite likely that the turbulence will become more anisotropic with time. This is not the case in most flows, however, and the assumption that anisotropic turbulence tends to return to an isotropic state is reasonable in most flows of interest.

In the laboratory, anisotropic turbulence is usually created by straining the flow and then allowing the anisotropic turbulence to relax in the absence of strain. The alternative approach of using the anisotropy of turbulence created by grids has not been successful. The apparent reason is the one mentioned above--the anisotropy resides mainly in the large scales, and the flow may become more rather than less anisotropic. Creating anisotropy by straining an initially isotropic field distributes the anisotropy over the range of scales and is thus better behaved.

Simulations can emulate either of the above methods. One can simply create an initial field in which the components of the velocity fluctuations are unequal, or one can strain an initially isotropic field to produce the anisotropy. Because one has control of the anisotropy as a function of the scale size in the initial conditions in a simulation, there is no important factor favoring one method over the other. The method of creating an anisotropic initial field is preferred, as it is the simpler approach.

Full simulations of homogeneous anisotropic turbulence were made by Schumann and Herring (1976) using the method suggested above. Some of their results are shown in Fig. 5.7. We see that their flow does indeed relax toward isotropy. The tendency of the dissipation and pressure-strain terms toward their values in the isotropic flow is also evident. One should note, however, that the calculation was done on a 32^3 mesh. All of the quantities averaged in Fig. 5.7 fluctuate very strongly in both space and time, and it is likely that nearly all of the contribution to the mean values comes from a few small regions in which the fluctuations are very intense, this statement is based on some of the author's unpublished work. It is therefore likely that

the uncertainty in the reported values is quite large. This is true in some of the other flows that we shall look at as well.

Schumann and Herring used their results to test two versions of Rotta's model for the return to isotropy. This model assumes that the pressure-strain term can be represented by:

$$\langle p' \left(\frac{\partial u_i'}{\partial x_j} + \frac{\partial u_j'}{\partial x_i} \right) \rangle \equiv \Phi_{ij} = -K \langle u_i' u_j' \rangle - \frac{1}{3} \delta_{ij} \langle u_k' u_k' \rangle \qquad (5.3)$$

where one model assumes $K = C\varepsilon/q^2$, and the other assumes $K = C'q/L$, where ε is the dissipation rate and L is the integral scale. The brackets $\langle\ \rangle$ represent an average over the computational field which is assumed equivalent to an experimental time average. As can be seen from the figure, there is considerable variation in the "constant" obtained from the various runs. Clearly, this indicates that something may be wrong with the model. Schumann and Herring were not able to discern any consistent Reynolds number effects in their results.

4. Rotating Turbulence

The effects of rotation on turbulence are subtle and complex. In the equations of motion, the only appearance of the rotation is via the Coriolis force; the centrifugal force can be transformed away. One effect of the Coriolis force is to redistribute the kinetic energy among the components of the turbulence normal to the axis of rotation. The Coriolis force does not appear explicitly in the equation for the turbulent kinetic energy. Nevertheless, rotation has a profound effect on turbulence and, especially, on its rate of production (cf. Ferziger and Shaanan (1976)). In shear flows, rotation may in fact stabilize the flow, there is evidence that it can cause relaminarization of a turbulent boundary layer. It can also destabilize; the well-known Taylor-Görtler instability is a prime example of this.

The effect of rotation on isotropic turbulence is even more subtle. It seems quite likely that the principal effect is the conversion of turbulent energy into inertial waves--waves that propagate principally along the axis of rotation and which are not dissipated except near walls.

Experimentally, the study of the interaction of rotation and turbulence is very difficult. One major difficulty (about which we shall say more later)

is that the fluid must be set into rotation before it passes through a grid that generates turbulence, this is a consequence of the Helmholtz theorem. Three experiments have been performed. Ibbotson and Tritton (1967) found a faster decay of the turbulence when the fluid was rotating, while Traugott (1956) found a decrease in the decay rate. The latest expeirment, and the one that is generally regarded as the best, was done by Wigeland and Nagib (1978). They found cases which went in both directions; however, the predominant effect was a decrease in the decay rate.

Since the source of the effects observed in the experiment was unknown, preliminary calculations using large eddy simulation on a 16^3 grid were made. A series of simulations using the identical initial condition with various rotation rates was made. The results, shown in Fig. 5.9, indicate that the predominant effect of the rotation may be to decrease the rate of decay of the turbulence, but there is unusual behavior, particularly at the early times. This is similar to the behavior observed by Wigeland and Nagib, but a detailed comparison is impossible.

On the basis of these results, it was surmised that rotation decreases the rate of dissipation but that this effect is masked by other effects in the early development of the flow. In order to check this hypothesis, we made full simulations of an experiment that is impossible to do in the laboratory. We allowed the turbulence to develop without rotation for a short time; this is identical to the initial stages of an isotropic turbulence experiment. When the turbulence had developed into a physically realistic field (see the preceding section for details), the rotation was "turned on." Under these conditions, it was found that increasing the rotation rate always decreased the rate of decay of the turbulence. The results are shown in Fig. 5.10.

It appears that the anomalous effects found in the experiments are caused by interactions of the rotation with the thin shear layers produced by the turbulence-producing grid, and similar effects can be produced in the simulation. These are impossible to avoid in the laboratory. In some of the experiments, interactions with the walls also play an important role.

It was also possible to search for the cause of the effect. It was found that the turbulence remains nearly isotropic, so the decrease in the rate of dissipation must be due to an increase in the length scales. Since the length scales are readily computed in these simulations, this was easily checked, and

it was found that there is a large increase in the length scale in the direction of the rotation axis. A theoretical explanation for this (based on the properties of inertial waves), was given and a modification of the model was offered.

5. Strained Turbulence

We now come to flows in which there is turbulence production. In both the strained and sheared turbulence experiments, the turbulence decays for a short time after the start of the flow and then increases with time. The length scales of the turbulence increase more rapidly than in the unstrained decaying isotropic flow. All of this makes these flows interesting objects of study.

In the laboratory, strained turbulence is created by first producing isotropic turbulence with a grid, in the same way as in the experiments described earlier. The turbulence is allowed to develop for a short time and is then made to pass through the test section. In some test sections, the cross-sectional area is kept constant but the aspect ratio in the plane normal to the flow is changed; the effect is to exert plane strain on the turbulence. In other experiments, the test section is a contraction, and the turbulence is compressed in the two directions normal to the flow and stretched in the streamwise direction; the result is axisymmetric strain.

To simulate these flows numerically, an isotropic turbulent flow field is created in the same manner as for the previous flows. The effect of the strain is turned on immediately, and the flow is allowed to develop. In order to simulate this flow correctly, it is necessary to use a straining coordinate system, one which moves with the mean flow that produces the strain. This is necessary because one of the terms due to the applied strain does not permit the application of periodic boundary conditions, the transformation removes this term. For the details of this transformation see Rogallo (1977).

Use of this transformation also introduces a difficulty. After some time, the strained coordinate system becomes quite thin in the direction which is being compressed. When this happens, the length scales in that direction become appreciable compared to the size of the computational domain in that direction. As a result, periodic boundary conditions are no longer valid, and the computation has to be stopped. This happens when the total strain

$\exp(St) \approx 2$, where $S = \partial u/\partial x$. The problem can be partially alleviated by starting with a coordinate system that is distorted in the other direction. Thus the flow contains three periods similar to those found in the flows described above. First there is a development period; this is followed by a period in which the flow is physically realistic, finally, there is a period in which the simulation is invalid, and the calculation must be stopped.

The detailed behavior of strained turbulence is dependent on the initial conditions. However, the trends are the same in all cases. As in the experiments, the turbulent kinetic energy decays until the turbulence becomes organized; then the production of turbulence increases and, somewhat later, so does the kinetic energy of the turbulence. As can be seen in Fig. 5.11, the turbulence becomes highly anisotropic. The fluctuations in the direction being compressed (the x_1-direction for the case shown in Fig. 5.11) increase most rapidly, while the fluctuations in the stretched direction (x_2) continue to decrease. The off-diagonal components of the Reynolds stress tensor are all zero in this flow.

The results of this computation could be used to test Reynolds-averaged models, but they have not been used for this purpose. The reasons are that the majority of engineering flows are shear flows, and sheared homogeneous turbulence seems more appropriate for this purpose and that the experimental data can be used as well. For this reason, Reynolds-averaged models are deferred to the following section.

McMillan and Ferziger (1980) have used strained turbulence simulations for checking subgrid scale models. They found that the Smagorinsky model becomes less accurate as the flow is strained. The correlation between the exact and model results drops from the already low value of 0.3-0.4 to nearly zero. However, the scale similarity model proposed in Chapter 3 is nearly equally valid with or without strain.

In a few cases the correlation between the exact stress and the Smagorinsky model becomes negative. On further investigation, it is found that, if the strain rate is high and maintained for a long time, the energy flow is from the small scales to larger scales, i.e., from the unresolved or subgrid scales to the larger or resolved scales. This seems to be physically correct, although it has not been reported in any of the experimental results of which we are aware. It appears that the smallest scale of the turbulence may be

determined by the strain rate rather than the viscosity. Direct evidence of a similar phenomemon in sheared turbulence will be presented in the following section.

6. Sheared Turbulence

Homogeneous turbulence interacting with mean shear behaves in a manner very similar to strained turbulence. One can regard shear as a combination of strain and rotation; the effect of the rotational component is to weaken the effect of the strain somewhat. The behavior with time is qualitatively similar to that for the strain case; after a period of decay, the turbulent kinetic energy begins to increase. The anisotropy produced is such that the streamwise component of velocity has the largest fluctuations and the normal component has the smallest fluctuations.

Homogeneous sheared turbulence is more difficult to create in the laboratory than strained turbulence. The essential reason is that, because shear has a rotational component, it cannot be suddenly introduced into the flow. It has to be created along with the turbulence. The apparatus used to produce this flow is an array of parallel channels whose flow resistances are arranged so that the velocity distribution at their exits is linear in the direction normal to the channel walls. In this way, a flow with a straight-line mean velocity profile (uniform shear) is created. With careful adjustment, the turbulence can be made to be approximately uniform across the flow. The flow is then followed down the test section, and measurements of the turbulence quantities are made at the midplane of the test section at a number of stations.

Simulation of this flow on a computer is very similar to simulation of strained flow. An initial isotropic velocity field is created in the manner described earlier. It is possible to let the flow relax before the shear is introduced, but this is not done. For this flow it is necessary to use a shearing coordinate system (one that moves with the applied linear mean flow) in order to remove the terms that forbid the use of periodic boundary conditions. The deforming coordinate system is shown in Fig. 5.12. it begins as a Cartesian system at $t = 0$ and deforms as shown until $St = 1/2$. At this point, the computational domain is on the point of becoming too narrow in the normal direction to support the use of periodic boundary conditions. This

flow permits the "remeshing" of the coordinate system in the manner shown in Fig. 5.12. The shear then causes the coordinate system to become Cartesian, and the cycle is begun again. With the aid of this trick, it is possible in principle to carry on for as long as desired. In practice, the length scales in the streamwise direction eventually become too long for the computational domain, and one is forced to stop on this account. Sheared turbulence thus passes through the same three periods as strained turbulence: development, realistic representation of physics, and, finally, breakdown.

The detailed behavior of the flow may depend on the initial conditions, but the trends are essentially independent of how the calculation is started. As one can see from Fig. 5.13, the behavior of the components of the turbulence is very similar to that in the strain case. It also follows the experimental trends very well.

McMillan and Ferziger (1980) used the results of direct simulations of sheared turbulence as the basis of tests of subgrid scale models. The findings differed in no important respect from those found for strained turbulence; for this reason, we shall not give them here. However, we point out that the transfer of energy from the smallest scales to larger scales was noted in this case as well. Further evidence for this will be given below.

Let us look at the results of the simulations in somewhat more detail. Many of the results are those of Feiereisen et al. (1981), Shirani et al. (1981), and Rogallo (1981) which have not yet been published. Only partial results will be given. Three-dimensional spectra of the velocity field are shown in Fig. 5.14. We see that there is a very strong shift of the spectrum of the normal velocity component toward low wavenumbers or large scales. Care is required in dealing with the integral scales. They are the integrals of two-point correlation functions, some of which have regions in which they are negative. The negative regions can cause the integral scales to behave very erratically. The spectra probably show the length-scale behavior more accurately.

The behavior of the pressure spectrum is rather remarkable. The initial condition has a peak at a relatively high wavenumber. The pressure spectrum near the end of the physically realistic period is shown in Fig. 5.15. The spectrum is broken into two components. The decomposition is suggested by the Poisson equation for the pressure; the terms on the right-hand side of that

equation can be classified according to whether or not they contain the mean velocity field. The component P_1 is a consequence of the applied mean field; it develops a k^{-5} spectrum, and the peak in the spectrum moves to the left with advancing time. The component P_2 is due to the self-interactions of the turbulence and is much more broad-band in nature. This has important consequences for pressure-strain modeling.

Finally, we show the time behavior of the terms that contribute to the spectral behavior of the turbulent kinetic energy as a function of wavenumber; these are shown in Fig. 5.16. It is seen that, as expected, the production is mainly in the large scales or low wavenumbers, and the dissipation occurs at higher wavenumbers. Finally, we note that the transfer term, which redistributes energy among the wavenumbers is negative at low wavenumbers (indicating a transfer away from the large scales) and becomes positive at higher wavenumbers. All of this is as anticipated. The surprise is that the transfer again becomes negative at the highest wavenumbers, indicating that the transfer is from both ends of the spectrum to the center. This can be taken to be a confirmation of the finding of McMillan and Ferziger discussed earlier.

Let us now look at some of the applications of these results to Reynolds-averaged modeling. Since this is the first application of this type in this report, we should first look at the possibilities. The time averages can be replaced by averages over the flow field. Although the number of mesh points is large ($64^3 = 262{,}144$), they cannot be regarded as statistically independent. A more realistic measure of statistical reliability is the number of large eddies captured in the computational domain. There are several ways to measure this--none of them exact--but the number of large eddies is small enough that the statistical reliability of the results is not very high. A good test of their validity is to compare results obtained from two simulations which are identical except for the set of random numbers used to initialize them.

From each realization of a shear turbulent flow, we may compute the averaged quantities as a function of time. Since the quantities vary slowly, the values at neighboring times are not independent, and should not be treated as if they are. For this reason, we chose to analyze the flow fields only at those times at which the grid is Cartesian. This is also convenient computationally. The result is that we have the averaged quantities that need

to be modeled at three or four time steps for each of several realizations. The data sets are thus much smaller than those used in subgrid scale model testing, and the kinds of tests performed need to account for this. Furthermore, one needs to consider the effects of changes in the basic parameters of the flow.

These flows contain two independent nondimensional parameters. The first is the Reynolds number. There are several length scales on which a Reynolds number can be based. The integral scale suffers from the difficulties described earlier, and we have used the microscale instead. The two should be related (possibly as a function of Reynolds number), so it does not matter much which length scale is used; however, if we try to apply the results to other flows, the choice of length scale may be very important. The second nondimensional number is the ratio SL/q, where S is the applied mean shear rate and q and L are the velocity and integral length scales. We call this parameter the shear number, and it measures the ratio of an eddy time scale to the time scale imposed on the flow. It can also be shown that the shear number is proportional to the ratio of production to dissipation.

From the results of a simulation, one can compute the Reynolds shear stress $\langle u_1 u_2 \rangle$. This is just a single quantity, and one cannot test eddy viscosity models using it alone. Eddy viscosity models could be tested by asking whether the Reynolds stress tensor, $R_{ij} = \langle u_i u_j \rangle - \frac{1}{3} q^2 \delta_{ij}$, is proportional to the rate of strain tensor

$$R_{ij} = 2\nu_T S_{ij} = \nu_T \left(\frac{\partial u_i}{\partial x_j} + \frac{\partial u_j}{\partial x_i} \right)$$

Since the model could not be tested directly, we computed the "constant" in the model defined by

$$\nu_T = - \frac{\langle u_1 u_2 \rangle}{\partial U_1 / \partial x_2} = CqL \qquad (5.4)$$

and correlatee it as a function of the two nondimensional parameters given above. The result showed that C is nearly inverse to the shear number, which is equivalent to saying that $\langle u_1 u_2 \rangle / \langle q^2 \rangle$ is nearly constant, note that this result is incompatible with C's being a true constant. On further investigation, it was found that all components of the Reynolds stress anisotropy tensor:

$$b_{ij} = \frac{\langle u_i u_j \rangle}{q^2} - \frac{1}{3} \tag{5.5}$$

appear to become constant at long times in homogeneous shear flow. It is impossible to carry the calculation far enough to determine whether this is really the case or whether the b_{ij} simply change very slowly in the later stages of this flow. We are of the opinion that there is asymptotic structural similarity in this flow; this assumption has been the basis of some recent models. In many other shear flows, $\langle u_1 u_2 \rangle / \langle q^2 \rangle$ is approximately constant over a large part of the flow; for example, in the boundary layer this holds except for the region close to the wall.

Another example of model testing with these simulations is provided by the pressure-strain terms. We showed earlier that the pressure can be considered to be composed of two parts, one arising from interaction of the turbulence with the imposed mean field and the other a purely turbulent quantity. The corresponding decomposition of the pressure-strain terms is made by many modelers.

For the part of the pressure strain terms proportional to the mean strain (the "rapid" terms), one can show that, if one allows only terms which are linear in the anisotropy of the Reynolds stress, the model contains only a single constant, which for the 1,1 component can be written (Reynolds (1976)):

$$\left\langle p_1 \frac{\partial u_1}{\partial x_1} \right\rangle = 2 \left(1 + \frac{A_1}{15}\right) \langle u_1 u_2 \rangle \frac{\partial U_1}{\partial x_2} \tag{5.6}$$

There are similar expressions for the other components. Given the computed values of the rapid part of the pressure-strain term, we can calculate a value of the "constant" for each of the four tensor components that are nonzero. If the model is correct, the values obtained should be the same for each tensor index and all realizations. The results showed that the "constant" is nearly independent of the Reynolds and shear numbers, but it varies by a factor of nearly seven among the various components of the tensor. These results show a deficiency in the model and suggest that an improved model should be possible, but we have so far been unable to suggest one.

The part of the pressure-strain term that results from purely turbulent interactions (the "Rotta" term) are usually modeled by:

$$\langle p_2 \left(\frac{\partial u_i}{\partial x_j} + \frac{\partial u_j}{\partial x_i} \right) \rangle = - C \varepsilon b_{ij} \qquad (5.7)$$

This model is based on the notion that the effect of these terms is to return the flow to isotropy. It, too, is easily tested by the method used for the rapid term. It was found that the "constant" displays a great deal of variation with Reynolds number, and many of the values were below the value of 2 required for return of the turbulence to an isotropic state.

Further investigation showed that the anisotropy of the dissipation does not behave as had been expected. It is generally assumed that the dissipation is isotropic at high Reynolds numbers but may be anisotropic at low Reynolds numbers. Thus we expected to find a strong Reynolds number dependence of the anisotropy of the dissipation. In fact, we found almost no variation with microscale Reynolds number in the range from 10 to 100 (see Fig. 5.17). This does not mean that the dissipation cannot become isotropic at still higher Reynolds numbers, but it does suggest that the assumption of isotropy may be questioned.

Since the anisotropic component of the dissipation acts to reduce the isotropy of the Reynolds stress tensor, it should be included with the pressure-strain term. When the combined terms are modeled, it is found that the variation of the "constant" with Reynolds number is greatly reduced (see Fig. 5.18), and the model is fairly good. Modelers who assumed the dissipation to be isotropic have gotten reasonably good results because the anisotropy of the dissipation is implicitly included in their models.

This is a sample of some of the results obtained by Feiereisen et al. (1981) and Shirani et al. (1981). The reader is referred to those reports and forthcoming papers for more complete details.

7. Compressible Turbulence

It is possible to make a compressible version of the homogeneous turbulent shear flow treated in the preceding section. One need only make the velocity gradient large enough that the velocity difference across a large eddy is a significant fraction of the sound speed. It is not possible to

produce this flow in the laboratory, the large velocity differences would make it impossible to maintain homogeneity. This is unfortunate, because it means that we have to believe the results of the calculation without experimental verification. We can, however, check the results at low Mach number against the incompressible experiments.

To compute this flow, the major change we need to make from the incompressible case is that the full set of compressible equations must be used. One can show that a linear velocity profile is a solution to the steady equations, and this solution can serve as the source of the shear imposed on the turbulence. In compressible computations (cf. Ballhaus (1980)), it is customary to use the continuity, momentum, and energy equations in conservation form; the dependent variable in the energy equations is usually the total energy (stagnation enthalpy). However, in the present case, this equation cannot be used without destroying the homogeneity (Feiereisen et al. (1981)), so we are forced to treat the enthalpy as one of the primary dependent variables.

The most popular numerical methods for the compressible equations are designed to relax the solution to a steady state as quickly as possible. They are not time-accurate; that is, they do not produce an accurate picture of the relaxation to steady state, and therefore they cannot be used for the purpose we have in mind. Instead, we have used a standard explicit method. The fourth-order Runge-Kutta method was chosen. The fact that all of the compressible equations contain time derivatives means that one does not need to solve a special equation for the pressure. All variables are advanced in time, the variables which are not explicitly computed from the differential equations are obtained from equations of state.

Morkovin (1963) hypothesized that compressible turbulence behaves very much like incompressible turbulence, and most models are based on this assumption. For most of the quantities in homogeneous turbulent shear flow, this hypothesis turns out to be correct. Most of the differences between the two cases are small, so we shall concentrate on the few cases in which the differences are significant.

The major difference between the incompressible and compressible flows (at least when the turbulence Mach number is not too large) is due to the appearance of acoustic waves in the latter case. The acoustic waves that are

most apparent are those propagating normal to the shear, and we expect the quantities which can be affected by acoustic waves to show the most important differences from the incompressible case. The largest change is in the fluctuating velocity component normal to the shear; it is reduced relative to the incompressible case.

The most striking difference between the two flows is in the pressure and the terms associated with it. In the incompressible case, the pressure was decomposed into two parts: one arising from the mean flow that produces the shear and another that is entirely due to the turbulence. In the compressible case, there is a third term due to the presence of acoustic waves. This term turns out to be significant even at fairly low Mach numbers.

Of course, the pressure-strain terms are also affected in the same way; there are now three of them. It turns out that the third term behaves like the rapid term--the one due to the mean shear--and can therefore be combined with it. However, the "constant" is now a function of the turbulent Mach number in addition to the two dimensionless parameters of the incompressible case--the Reynolds and shear numbers. The resulting constant was fit as a function of these three parameters. The results are shown in Fig. 5.19, and the Mach number dependence is found to be significant.

Further details and results for this flow can be found in the report of Feiereisen et al. (1981).

8. Mixing of a Passive Scalar

By definition, a passive scalar is any quantity that can be convected by a flow and diffuse through it without affecting the velocity field. There are many applications that require knowledge of how a passive scalar behaves, any problem in which heat or mass transfer is important is in this class. Understanding the mixing of a passive scalar is also a preliminary to handling reacting flows, including combustion.

A passive scalar could be introduced into any flow treated in this chapter. In fact, only two of these have been done experimentally, these are isotropic turbulence and sheared homogeneous turbulence, so these are the cases which have been simulated. One also has to decide whether the scalar has a mean component or not. In the experiments, isotropic turbulence has

been measured without a mean gradient of the scalar, and the shear flow has been performed both with and without a mean scalar gradient. To facilitate comparison with these experiments, isotropic turbulence was simulated with an isotropic scalar field, and the shear flow had a mean scalar gradient.

The equation describing the scalar concentration is:

$$\frac{\partial C}{\partial t} + \frac{\partial}{\partial x_j} u_j C = D \frac{\partial^2 C}{\partial x_j \partial x_j} \tag{5.8}$$

If there is a mean scalar field, it is subtracted from the total scalar field to obtain an equation for the fluctuating scalar field. The velocity field is also decomposed into its mean and fluctuating parts. The resulting equation for the scalar fluctuations has the same difficulty as the equation for the velocity field--the mean shear and mean scalar gradient terms do not admit the use of periodic boundary conditions. To remove this problem, the coordinate transformation made for the momentum equations has to be made here as well. It is possible to compute the velocity field prior to the computation of the scalar field, but this would require storing an enormous data set on tape and transferring it back into the machine as needed. For this reason, the velocity and scalar fields were computed simultaneously. The numerical methods used for the scalar field are identical to those used for the velocity field.

In the case of the isotropic field, the most important items to study are the decay rates of the velocity and scalar fields. The scalar field follows a decay law similar to Eq. (5.2):

$$\overline{c'^2} = B(t-t_o)^{-m} \tag{5.9}$$

where c' is the fluctuating part of the scalar field, i.e., $c = \langle C \rangle + c'$. We wish to look at the ratio m/n. The parameters on which this ratio depends are the Reynolds number and the Prandtl or Schmidt number, which is the ratio of kinematic viscosity to diffusivity ($Sc = \nu/D$). It was found that the scalar decays more rapidly than the velocity field when the Schmidt number is less than unity and more slowly than the velocity field when the Schmidt number is greater than unity; this is no surprise. The dependence of the ratio m/n on Reynolds number also depends on whether the Schmidt number is less

than or greater than unity. For $Sc < 1$, it is found that the ratio m/n decreases with increasing Re, and vice versa for $Sc > 1$.

The cases which include shear and a mean gradient of the scalar were analyzed in a manner similar to that used for the homogeneous shear flow. An important result is that the behavior of the scalar field becomes independent of the initial conditions after a short time. Its properties depend almost entirely on the velocity field and the mean gradient of the scalar.

The next quantity studied was the scalar flux $\langle u_i c \rangle$. This quantity is usually modeled by gradient diffusion:

$$\langle u_i c \rangle = D_{ij} \frac{\partial \langle C \rangle}{\partial x_j} \tag{5.10}$$

In the standard case, the concentration gradient is in the same direction as the velocity gradient; the nonzero gradients are $\partial U_1/\partial x_2$ and $\partial C/\partial x_2$ and there are two nonzero eddy diffusivities, D_{12} and D_{22}. The important one in most applications is D_{22}. It was computed for a number of different values of the dimensionless parameters of the flow. One can form the turbulent Prandtl/Schmidt number, Pr_T, by taking the ratio of the eddy viscosity to the eddy diffusivity. A number of models have been proposed for Pr_T, and the ones that were recommended most strongly in the literature were tested. None of them was found to be very accurate. A new model was constructed which gives D_{ij} in terms of b_{ij}, the anisotropy of the Reynolds stress tensor. Although this model models a low-order quantity in terms of a higher-order quantity, it can be made into a useful correlation by using other correlations; this model was found to be a significant improvement over the ones suggested in the literature. A test of the new correlation is shown in Fig. 5.20.

It is also possible to compute the other nonzero elements of D_{ij}. Due to the design of the computer program, this was not done for the full range of cases for which D_{22} was computed. Also, since the elements of the diffusivity tensor depend on the nondimensional parameters and, because it was not possible to match the Reynolds number used in the experiments, a quantitative comparison with experiment is not possible. However, the results are in good qualitative agreement with the data.

We also correlated the mean-square scalar fluctuations as a function of the nondimensional parameters. The principal finding was that, to a good approximation,

$$\frac{\langle c^2 \rangle}{\partial C/\partial x_2} = \frac{\langle q^2 \rangle}{\partial U_1/\partial x_2} \, Sc^{-1} \tag{5.11}$$

One can also construct models for the scalar field based on the ideas used for the velocity field. In particular, one can derive equations for $\langle c^2 \rangle$ and $\langle cu_2 \rangle$, which are similar to the Reynolds stress equations. The terms in them that are most difficult to model are the correlations between the fluctuating pressure field and the gradient of the fluctuating concentration $\langle p \, \partial c/\partial x_i \rangle$. They are analogous to the pressure-strain terms, and models for them can be based on models used for the latter. In particular, the pressure decomposition used in deriving pressure-strain models can be used here as well.

The model for the rapid term (the one containing the pressure derived from the mean shear) contains no adjustable constants. However, we introduced an arbitrary multiplicative constant and found good agreement between the exact and model results. The constant was found to be approximately 0.5, indicating that the arguments made in deriving the model are deficient. Another model suggested by Lumley to overcome some of the undesirable properties of the first model was tested and found to be less accurate than the first model.

The term arising from the component of the pressure that depends entirely on the turbulence was modeled by an analog to Eq. (5.7). The results show this model to be quite good--about as good as the modified Rotta model described earlier.

Chapter VI

FREE SHEAR FLOWS

1. Overview

Free shear flows are one of the classes of flows of major technological interest. They occur in many kinds of devices, and we shall begin this chapter by briefly describing the types of free shear flows.

Free shear flows can be divided into three major categories, there are also more complex cases. The three major types are:

1. Mixing layer. This is the flow that occurs when two parallel flows of different velocity are brought together. In the laboratory this flow is created by having the fluid of different speeds on opposite sides of a dividing plate. At the end of the plate, the two streams come into contact, and the thickness of the layer in which the velocity gradient occurs grows with downstream distance.

2. Jet. A stream of high-velocity fluid issuing from an opening is called a jet. As the high-speed fluid mixes with the surrounding lower-speed fluid, the maximum velocity of the jet decreases, and the rate of growth of its thickness also decreases. The most commonly studied jets are the plane and round ones, but others, such as the rectangular jet, have been studied.

3. Wake. A wake is similar to a jet, but it is a velocity defect in an otherwise uniform stream. Like the jet, the wake has decreasing velocity gradients with downstream distance. Most wakes result from flows around bodies. The wakes form by merging of the boundary layers behind the body or from separation of the boundary layers.

We should also mention:

Complex shear layers. This is not a single type of flow, but a category containing the flows that do not fall into the above categories. Curved jets and wakes are quite common. Another important flow is one in which a laminar boundary layer separates, creating a free shear layer. The free shear layer then undergoes transition to a turbulent free shear layer which grows so rapidly that it soon reattaches to the surface. This is a common mechanism of transition from a laminar to a turbulent boundry layer.

It is also important to distinguish the early phases of free shear flows from the far-downstream flows. The early stages are sensitive to the initial conditions. Fully developed free shear layers are usually self-similar in nearly all of the measured variables and grow according to a power of the downstream distance. A majority of free shear layers occurring in applications are of the early type, but fully developed cases are also of importance.

To date, there have been large eddy and full simulations of mixing layers and full simulations of wakes. The jet has not yet been simulated (although it probably will be in the near future). Complex free shear flows have also not yet been attempted. Thus we shall devote the rest of this chapter to the mixing layer and the wake.

Nearly all laboratory free shear flows develop with downstream distance. It is much easier to simulate a layer that develops in time. One must be very careful in comparing the two cases. Consider the mixing layer. Fluid elements on the two sides of the laboratory shear layer have been in the flow for differing amounts of time. As a result, the development of the flow is not symmetric and the plane on which the mean velocity is the average of the two free stream velocities is inclined. The simulated mixing layer is, however, symmetric. The two flows may be compared if, in the laboratory flow, the velocity difference across the flow is small compared to the average velocity. This experiment requires a long apparatus, but cases exist which meet this criterion fairly well, and these are the ones to which the simulations should be compared.

2. Mixing Layer

As discussed above, this is the simplest of all of the free shear flows. Despite the apparent simplicity of this flow and the large number of experiments that have measured it, there is still controversy about it. Let us consider the fully developed mixing layer first and the transitional case later.

It is generally agreed that the velocity profile of the fully developed mixing layer is self-similar, and so are the components of the Reynolds stress tensor. Another point of general agreement is that the growth of the free shear layer is linear in the fully developed region. The major point of disagreement in this regime of the flow concerns the rate of growth of the

layer. For the mixing layer sketched in Fig. 6.1, the growth rate parameter is conventionally defined as:

$$\frac{d\delta}{dx} = \sigma \frac{u_1 - u_1}{u_1 + u_2} \tag{6.1}$$

The measured values of σ cover the range 0.08-0.16, a much wider range than would be expected for a flow this simple. Birch (1980) recently reviewed the data and believes that there is a single correct value of this parameter, which he believes to be 0.115. However, no reason was given for the spread in the data.

There is less agreement about the early stages of the shear layer. One group, including Roshko and his coworkers and Browand and his coworkers, among others, believes that this part of the flow is essentially two-dimensional. In this view, the initial laminar shear layer rolls up into two-dimensional vortices, which then agglomerate or pair to form larger vortices of the same type (with larger spacing). This process has been observed to continue for several pairings. At this point the flow reaches the end of the apparatus. According to this view, the important process in the growth of the mixing layer is the pairing of the vortices. However, there is evidence that streamwise vortices form in this flow. This is a kind of three-dimensionality, but it is quite regular rather than chaotic.

The other view, held by Bradshaw and others , is that the mixing layer is normally strongly three-dimensional and chaotic. According to this picture, the highly two-dimensional layers that some experimenters have observed are the result of careful arrangement of the initial conditions and design of the experimental apparatus.

Large eddy simulations of the mixing layer were made by Mansour et al. (1978). They used the vorticity equations rather than the primitive equations because the vorticity is confined to a relatively narrow region of the flow. In fact, it appears that it makes little difference which set of equations is used. The subgrid scale model had to be modified to account for this change. At the top and bottom of the computational region, no stress boundary conditions (see Section 4.5) were applied. Fourier sine and cosine transforms were used in the normal direction.

This work showed that it is possible to explain the rapid growth of the mixing layer by vortex pairing. The flow was begun with an initial condition that contained well defined two-dimensional vortices. Although there were only two vortices in the computational domain, the boundary conditions imply that they are part of an infinite array. Various perturbations to a regular vortex array were tried. It was found that small perturbations would cause the vortices to pair. Naturally, the pairing occurred more rapidly when the perturbation was larger. Surprisingly, it was found that the mean velocity profile (defined by averaging the velocity over a plane) was self-similar and that the growth of the momentum thickness of the layer was very nearly linear.

A number of three-dimensional perturbations on this basic flow were also made. First, small, random, three-dimensional disturbances were added to the initial conditions. The three-dimensionality was somewhat amplified by the pairing process, but there were only minor changes in the overall properties of the flow. Another variation was produced by the addition of streamwise vortices to the initial condition. The streamwise vortices were distorted in the pairing process, and they produced slight kinks in the large two-dimensional vortices that result from the pairing. It was conjectured that the kinks would produce larger-scale instability of the mixing layer and would then lead to considerable three-dimensionality, but this could not be demonstrated because the number of grid points was severely limited.

A simulation of the initial stages of the mixing layer was made by Cain et al. (1981). This simulation used numerical methods described in Section 4.5. The transformation of an infinite region to a finite one was used, and the modified Fourier method of taking spatial derivatives in the normal direction was used. The initial profile was a laminar mixing layer with a small random disturbance; the disturbance was strongest on the center plane of the layer.

The results turned out well. Use of the coordinate transformation and the Fourier method allowed the method to be continued until the original layer had grown by nearly a factor of ten in some cases. No effect of image layers was found, and, in most cases, the calculation was stopped only because the layer developed horizontal scales which were too large to permit application of periodic boundary conditions.

Several variations in the computational method were tried. A full simulation was made; this calculation was stopped because the turbulence in the small scales became too strong. The calculation was repeated with filtering, but no subgrid scale model; the problem with the small scales disappeared, and the calculations could be carried almost twice as far in time, at which point the difficulty with the large scales appeared. A final calculation with both filtering and the subgrid scale model was made; it differed only a little from the preceding case. Thus, most of the results were obtained with filtering but no model.

Simulations were made with three levels of initial disturbance. In the low initial turbulence cases, the turbulence intensity was four orders of magnitude smaller than that of a fully developed turbulent layer; this might represent the behavior of a mixing layer produced from laminar boundary layers. The medium initial turbulence level was two orders of magnitude stronger. The high initial turbulence level cases started with turbulence intensities nearly those of the fully developed layer; these might represent a mixing layer produced from turbulent boundary layers. Cases which differed only in the set of random numbers used to generate the initial conditions were also run.

The results show that the low-turbulence cases produced a layer in which the momentum thickness grew very slowly at first but, after a latency period, grew linearly with time at a rate similar to that observed in experiments. The medium-level case gave a shorter latency period and a slightly slower rate of growth at later times. Finally, the high-turbulence level cases gave almost no latency period at all but a still slower growth rate. These results are in qualitative agreement with experimental data. They are shown in Fig. 6.2, 6.3, and 6.4.

All of the cases have mean velocity profiles that are self-similar.

The growth of the turbulence level on the center plane of the mixing layer is shown in Figs. 6.5, 6.6, and 6.7. In the low-turbulence case, the turbulent kinetic energy grows exponentially in the early stages and then levels off; the exponential growth rate is close to that of the most rapidly growing mode according to linear stability theory. The medium initial turbulence cases show similar growth, but the exponential period does not last as long. The high initial turbulence cases grow only slowly as they begin near

the level for a fully developed layer. In all of the cases the kinetic energy of the turbulence overshoots the value for the fully developed layer before settling down. This has been observed in some experiments.

The profile of the turbulent kinetic energy is shown for a typical case in Fig. 6.8. The initial profile is too broad compared to the fully developed profile. This is corrected, but the profile becomes too thin before the final state is reached.

The simulations were also used as the basis for flow visualizations. A grid of "dye lines" was placed on the center plane of the flow at the initial time. The ones in the streamwise direction are essentially vortex lines in the low-intensity cases and remain so by Helmholtz's theorem. The dye lines are moved with the flow, and pictures are drawn at various times. The initial picture is shown in Fig. 6.9, and the final result is shown for two different initial fields in Figs. 6.10 and 6.11. It is clear that the layer has rolled up into vortices, but they are much more two-dimensional in one case than the other. We believe that the three-dimensional shear layer does roll up into vortical structures, but that these structures do not have spanwise uniformity except when precautions are taken to insure that the three-dimensional disturbances are weaker than the two-dimensional ones.

The above results were taken from the report of Cain et al. (1981).

Two-dimensional simulations of the mixing layer were made by Patnaik, Sherman, and Corcos (1976), Acton (1976), Knight (1979), Ashurst (1979), and Riley and Metcalfe (1980), among others. In these simulations, the shear layer rolls up into an array of vortices. The principal object of these studies was the determination of the effect of initial perturbations on the speed and nature of the rollup of the layer. These papers contain interesting results, but, as they are essentially outside the topic of this report, they are not covered here in detail.

Full simulations of the turbulent mixing layer were made by Riley and Metcalfe (1980a,b). These simulations are similar to the work of Cain et al., which they predated. Their calculations are performed at low Reynolds number so that no subgrid scale model is required. Their initial condition is similar to the high initial energy condition of Cain et al., but they also ran a number of cases in which a deterministic perturbation was added to the initial

conditions; this perturbation was the most unstable wave of linear theory. They observed that the layer tended to roll up into vortices and found linear growth of the thickness of the layer, self-similarity of the velocity profile, and, in the case with the largest number of mesh points, constancy of the turbulent energy in the center plane of the layer. All of these observations are in agreement with experiment and the computations described above. An important contribution of this work is the demonstration that the properties of the mixing layer can be reproduced in a simulation which contains no large vortical structures in the initial conditions. They also showed that the addition of the perturbation corresponding to the most unstable wave of linear theory to the initial condition reduced the rate of growth of the layer.

3. Wakes

As stated in the introduction to this chapter, wakes are flows in which there is a defect in the velocity profile. As a wake develops, the velocity profile widens and the velocity gradients decrease. These factors and the fact that the rate of growth of the length scales is not as rapid in wakes as in mixing layers make wakes a little easier to simulate than mixing layers.

There are several types of wakes. The classification plays some role in determining how the flow will be simulated. A self-propelled body (one that drives itself through the fluid) leaves a wake in which the net momentum is zero; the momentum added by the propulsion just equals that due to the drag of the body. On the other hand, the wake of a towed body (or a body in a wind tunnel) has a net momentum deficit. Finally, both types of wakes can occur in plane, axisymmetric, and other geometric arrangements.

The first full simulation of a momentumless wake was made by Orszag and Pao (1974). Their work has been extended to the simulation of towed wakes by Riley and Metcalfe, in a series of papers. They concentrated mainly on the axisymmetric wake, because most of the experimental data is for this case. Despite the axisymmetry of the flow, they used a rectangular grid in their simulations; the axisymmetry is inserted via the initial conditions.

In some respects, their simulations behave very much like the simulations of the preceding section. As in all other flows, a short time period is required for the initial condition to develop into a physically realistic flow. During this period there is relatively little broadening of the wake

and some decay of the turbulence. The higher-order statistics also change from their original values during this period; in particular, the velocity-derivative skewness increases. Finally, the vorticity tends to concentrate during this phase.

Figure 6.12 shows the decay of the maximum mean velocity and the maximum axial component of the turbulence. Several experiments have shown that these quantities decay as $x^{-2/3}$ with downstream distance. Since the simulated wakes are temporally developing, the analogous behavior would have these quantities decay as $t^{-2/3}$. The figure shows that the maximum mean velocity follows the expected similarity behavior quite well. The turbulence decays a little more slowly than expected. Two different realizations of this flow are shown.

Similarity arguments suggest that the radii of the wake and of the turbulence profile should increase as $t^{1/3}$, the spatially decaying wake radius increases in radius as $x^{1/3}$. Figure 6.13 shows that the simulation reproduces this behavior quite well. The decay of the integrated mean and turbulent energies are also well predicted.

The velocity profiles behave in a self-similar manner after the initial period. They agree quite well with the measured profiles except in the wings of the profile; the results are shown in Fig. 6.14. The Reynolds shear stress is also reasonably well predicted, as are some of the higher-order statistics.

To conclude this chapter, we note that full simulations seem to be able to predict free shear flows quite well. The major stumbling block to continuing the simulations further in time is the growth of the length scales with downstram distance or time. This can be partially cured by doing the simulations with larger numbers of grid points. It would be more efficient to rescale the problem after some time, but no way has yet been found to do this without invoking very serious approximations.

Chapter VII

WALL-BOUNDED FLOWS

1. Overview

The last group of flows that we shall consider in detail in this report is the wall-bounded flows. This is the most studied single class of flows because of its many important technological applications. Despite the enormous amount of analytical and experimental attention lavished on these flows, there remains a great deal to be done.

The most important single flow in technological applications is the turbulent boundary layer. The standard case for this flow is the boundary layer in the absence of "extra rates of strain"--no pressure gradient, curvature, rotation, suction, blowing, or roughness, etc. A great deal is known about this flow. In particular, the mean velocity profile has been well measured, and one can "predict" its behavior. (Quotes are used because all of the present prediction schemes rely heavily on experimental data and should be called "postdictive" methods.) However, the mechanism by which momentum is transferred to the wall is only partially understood. Furthermore, the information that is available about the mechanism has not been used in model construction. Thus there is still much to do. It is hoped that higher-level simulations can play a role in this, but it is clear at the outset that the task is not easy.

It is known that the mechanism of momentum transfer to the wall in the boundary layer is connected with the flow structure observed close to the wall. In the near-wall region, the flow consists of alternating "streaks" of high- and low-speed fluid; the streaks are very long in the streamwise direction and thin in the spanwise direction. Their dimensions are believed to scale with the shear stress, which is nearly constant in the vicinity of the wall; however, their size relative to the boundary layer thickness is quite Reynolds number-dependent. The mechanism of momentum transfer involves lifting of the low-speed streaks from the wall. When they are lifted, they are carried a considerable distance into the boundary layer and exchange momentum with the fluid they encounter there. The existence of streaks and their importance in the flow plays a very important role in the simulation of wall-bounded flows.

The boundary layer is made up of at least three sublayers. There is an inner layer in which the viscosity plays an important role (the viscous sublayer), here the length scales are dependent on the shear stress and are small compared to the boundary layer thickness. The outer region of the flow is essentially inviscid and behaves much like a free shear low. In fact, it is frequently called the "wake" region, in the wake region the length scales are approximately 0.1 of the boundary layer thickness. Between these two regions is one in which the shear stress is nearly constant and the viscosity is not important. In this region, the mean velocity has a logarithmic profile, and it is called the logarithmic or buffer region, here the length scales increase linearly with distance from the wall. This knowledge is very important in higher-level simulations of these flows.

The turbulent boundary layer increases in size with downstream distance. This is difficult for higher-level simulations to handle at the present time. One can consider a temporally developing boundary layer, this has been done and will be described in the last section of this chapter. Unfortunately, the velocity profile of the time-developing layer is different from that of the spatially developing layer, and the difference is significant because wall-bounded flows are quite sensitive to small changes in the velocity profile.

Most of the attention to date has been given to turbulent channel flow. It is the ideal choice for simulation, because it is the one true "equilibrium" flow of the class. It reaches a state at which none of its properties changes with downstream distance. Despite this, the physics of the near-wall flow is similar to that of the boundary layer. Thus this flow can be simulated with periodic boundary conditions without making any important assumptions that might affect the results. Of course, one must be careful that the usual criteria needed for the application of periodic boundary conditions be maintained. This flow has been simulated a number of times and will occupy the major part of this chapter.

Another very important issue in wall-bounded flows is that of transition. Laminar boundary layers are much more stable than are laminar free shear flows, but transition takes place when the Reynolds number is high enough. The ability to delay transition would enable us to reduce the drag on bodies, with obvious and important consequences. This is one of the major reasons why transition has received so much attention.

Transition in boundary layers is sensitive to relatively small changes in the velocity profile. Keeping the disturbance level small can delay transition for a long way. On the other hand, minor disturbances, such as a bit of roughness, can trigger transition.

Theory predicts that laminar channel flow is stable with respect to small disturbances at Reynolds numbers below about 5700. One can also show that it is more unstable with respect to large disturbances, but the predicted Reynolds number of transition is smaller than the Reynolds number at which transition is observed to occur. An explanation of this phenomenon will be given later in this chapter.

The next section will take up the computation of fully developed channel flow. There are two approaches to doing this, and we shall discuss them and give results obtained by both approaches. In particular, we shall describe recent results that promise to provide a great deal of interesting information about this flow.

The last section of this chapter will consider transition in wall-bounded flows. This problem has been done recently for both the channel and the time-developing boundary layer. A number of interesting results have been produced, and there is considerable hope that still more will be forthcoming in the near future.

2. Fully Developed Channel Flow

The dynamical behavior of fully developed channel flow is similar in many respects to that of the boundary layer. In particular, the inner layers of the two flows are quite similar. The major differences are that the channel flow requires a pressure gradient to overcome the frictional forces and that the channel flow has no region in which the flow is not completely turbulent, outside the boundary layer, the flow is potential.

Of particular importance in the simulation of the channel flow is the behavior of the length scales. What makes these flows especially hard to simulate is the fact that the spanwise length scales are much smaller near the wall than in the central portion of the flow. This means that a grid that is well adapted to capturing the streaks near the wall will be much finer than necessary near the center. On the other hand, a grid which is scaled for the

central region will not be able to see the streaks at all. The variation in the length scales in the direction normal to the wall is less serious, because a variable grid size can be used in this direction.

Two approaches have been taken to simulate channel flow. In the first method, which was developed by Deardorff and extended by Schumann and co-workers, the wall is not treated explicitly. This avoids much of the difficulty with the small-scale structures that occur near the wall, and reduces the amount of computation considerably. The limit of the computational domain is placed in the logarithmic region of the flow, because this is probably the best understood part of the flow. Another argument put forward for this method is that viscous effects prohibit the existence of an inertial subrange in the inner layers, but one exists in the buffer and wake regions. The difficulty with this method is that the boundary conditions at the top and bottom of the computational domain are not well defined, and assumptions must be made. Also, this approach does not simulate much of the physics of the flow and cannot be used to study its structure and modeling.

Deardorff assumed that the derivative of the streamwise velocity in the normal directin could be written as a sum of two parts, the first guarantees the existence of a logarithmic region, and the second is responsible for the fluctuations. His expression is:

$$\frac{\partial^2 \overline{u}_1}{\partial x_2^2} = -\frac{1}{\kappa(\Delta x_2/2)^2} + \frac{\partial^2 \overline{u}_1}{\partial x_3^2} \tag{7.1}$$

where κ is the von Karman constant (0.41) and Δx_2 is the distance of the first mesh point from the wall. This boundary condition assumes that the fluctuations of the velocity are the same in the normal and spanwise directions. The validity of this assumption is open to question, the reason that Deardorff gave for favoring it is that it produced reasonable results. Kim (private communication) has tested this boundary condition and finds it is not good at all.

Schumann's assumption is that the shear stress and the velocity are in phase at the first mesh point; according to Kim, this assumption is also inaccurate. Mathematically, his assumption is:

$$\tau_{12} = \frac{\langle \tau_w \rangle}{\langle u \rangle} u \tag{7.2}$$

where $\langle u \rangle$ is the mean velocity at the first mesh point, $\langle \tau_w \rangle$ is the mean wall shear stress, and u is the instantaneous velocity.

For the subgrid scale model, Deardorff used the Smagorinsky model. The only modification that he found necessary was the reduction of the magnitude of the constant in the model from the value obtained from theory or the isotropic decay simulations.

Schumann modified the model. He assumed that the subgrid scale model should be composed of two parts. The first is proportional to the time-mean velocity gradient at the particular distance from the wall, the second is proportional to the deviation of the instantaneous velocity from the time-mean. He called these the inhomogeneous and locally isotropic components of the subgrid scale stress. He also used an equation for the subgrid scale turbulent kinetic energy, but found that it gave no significant improvement over an algebraic eddy viscosity model.

For the mean velocity profile, Schumann obtained very good results. The results for the components of the Reynolds stress are also quite good. Schumann also used his results for testing the Rotta model for the pressure-strain term. These results are shown in Figs. 7.1 and 7.2. It is interesting to note that the "constant" is different for the various components. However, one should be cautious about accepting these rsults, because the pressure is very sensitive to changes in the way in which the flow is computed, and we believe that large uncertainties must be assigned to these results. In fact, the results near the boundary seem to be due to the boundary conditions used. We shall have more to say about this below.

Moin et al. (1978) made the first attempt to solve the channel flow problem while treating the wall boundary conditions exactly. Doing this means that a nonuniform grid has to be used in the direction normal to the wall, the use of Chebychev polynomials is an alternative.

One of the major difficulties with this method is that the length scales of the flow become very small near the wall, the local turbulence Reynolds number also becomes very small, and it is not clear that the Smagorinsky model can be used any longer. In fact, it is possible that the overall length scales of the turbulence will be smaller than the size of the grid in this

region. It is then improper to use the grid or filter size in the subgrid scale model. Instead, Moin et al. used the minimum of the Prandtl mixing length and the grid size. This modification is arbitrary but is a simple method that appears to work.

Another difficulty is that the smallness of the grid tends to make numerical methods unstable. There are two nondimensional numbers that determine the stability of a numerical method. They are the Courant number $u_2\Delta x_2/\Delta t$ and the viscous parameter $\nu\Delta t/\Delta x_2^2$. Roughly speaking, stability requires that both of these numbers be smaller than some constant of the order of unity. It turns out that the viscous condition is more stringent near the wall, and if an explicit method were used, it would be necessary to use an extremely small time step. Consequently, a method which treats the viscous terms containing derivatives with respect to the normal coordinate implicitly was devised and used. Doing this meant that the normal method of solving for the pressure via the Poisson equation had to be abandoned. We shall briefly describe the revised numerical method.

Most of the terms in the momentum equations are time-differenced using the second-order Adams-Bashforth explicit method. The exceptions are the pressure gradients and the viscous terms containing derivatives with respect to the normal coordinate, which are treated by the implicit Crank-Nicolson method. The continuity equation, which contains no time derivatives, is evaluated at the new time step. The resulting set of equations if Fourier-transformed in both horizontal directions to produce a set of equations which are essentially ordinary differential equations with respect to the normal coordinate. These are finite-differenced by a second-order method, and the resulting set of equations is block-tridiagonal with 4×4 blocks. This system is easily solved by a standard block-tridiagonal algorithm, and, when the resulting functions are inverse Fourier-transformed, we have the velocity and pressure fields at the new time step. Kim and Moin (1979) made improvements on this method.

The initial conditions were described in Chapter 3; they consist of a mean profile, solutions obtained from stability theory, and random fluctuations. The program was required to run for some time to ascertain that the turbulence would not decay and to develop the proper statistics. When this was done, it was found that the resulting velocity field contained many of the

features observed in the laboratory. In particular, the mean velocity profile was very close to the experimental one, and the fluctuating components were also quite close to the experimental ones. The most interesting observation about the results was the tendency of the fluid near the boundaries to form high- and low-speed streaks and for the Reynolds stress to be highly intermittent in both time and space. All of this suggests that much of the physics is captured. However, the grid was not fine enough to resolve the small structures near the wall adequately (the "streaks" are too wide), and the quantitative results have to be treated cautiously. Moin et al. (1978) showed that this approach to simulating wall-bounded flows can succeed and indicates that better resolution would probably produce still better results. The pressure-strain correlations calculated by Moin et al. (1978) differ considerably from those of Schumann (1973). One should be very careful about accepting any of these results without further confirmation. The pressure-strain results are very sensitive to small changes in the flow, we believe that the trends (and the "splat" effect in particular) are correct, but the quantitative values are somewhat uncertain.

Over the last three years, Kim and Moin have improved the channel flow calculation in a number of ways. The principal improvement has been in the ability to use more grid points the original $64 \times 64 \times 64$ grid and, in some recent calculations 128 grid points have been used in one or two of the directions. They have also made improvements in the subgrid scale model and in the numerical method.

Kim and Moin (1979) reported the results of $64 \times 64 \times 64$ simulations with a model which damped the subgrid scale viscosity near the wall more strongly than the previous model. We shall look at some of their results. The mean velocity profile they obtained is compared with several experiments in Fig. 7.3. The existence of a logarithmic region in the flow with the correct slope is one of the major achievements of the whole of higher-level simulations. The profile near the wall lies below the expected profile (indicated by $u^+ = y^+$ in the figure), and this is probably due to a weakness of the model in the region near the wall. The components of the turbulence are shown in Fig. 7.4; although the experimental data are not shown, the agreement is quite good--the experimental data show quite a bit of scatter. The pressure-strain terms are shown in Fig. 7.5. In the center of the channel,

these terms drain energy from the fluctuations of the streamwise velocity and transfer it to the other components; this accords with expectation. However, near the wall there is a large transfer from the normal fluctuations to the spanwise ones. This had also been found by Moin et al. (1978) and was unexpected. It is apparently due to fluid moving toward the wall being stopped by the wall. The vertical motions are converted into horizontal motions, and the result of this "splat" effect and the normal energy transfers is shown in the figure. Again, the quantitative results may be incorrect, but it is unlikely that the qualitative result is incorrect. More recent (and more accurate) results by Moin and Kim (1981) show a smaller, but still significant, "splat" effect.

Contours of the fluctuating velocity on a plane parallel to and close to the wall are shown in Fig. 7.6, the presence of long streaks is obvious. A similar plot for a plane close to the center of the channel is shown in Fig. 7.7; there is no evidonce of streaky behavior at this plane. A number of other plots of this kind are given in their paper.

In a more recent paper, Kim and Moin (1981) have done calculations with still greater resolution and further improvements in both models and numerical methods. The results are qualitatively similar to those presented above but differ quantitatively. They have also produced a simulated flow-visualization motion picture that duplicates most of the phenomena observed in laboratory motion pictures. This application of the results should play a very important role in the future.

The splat effect is also seen in the shear-free wall layer. This is simply a turbulence near a wall which is moving at the same mean velocity as the wall. The precise nature of this flow depends on the Reynolds number. A simulation by Biringen and Reynolds (1981) captured most of the effects observed in the experiments. However, we shall not review these results in detail here.

3. Transition

As stated in the introduction, transition in boundary layers is a subject of great technological importance. However, transition is very sensitive to a number of factors, including the precise velocity profile, the level of the disturbance, wall roughness, etc. As a result, transition experiments are

very difficult to perform reproduceably, and there is considerable scatter in the data. Naturally, simulations of these flows will be very sensitive to similar factors. Thus, a great deal of care will be necessary to simulate these flows.

Linear stability theory predicts that the laminar boundary layer profile is unstable with respect to disturbances that result in Tollmien-Schlichting waves. This instability is much less explosive than that of the free shear layer. It is generally believed that the Tollmien-Schlichting waves grow until nonlinear effects take over and complex interactions lead to the fully turbulent boundary layer. However, the late stages of transition are poorly understood.

The first direct simulation of transition in wall-bounded flows was made by Kells and Orszag (1979) and Orszag and Patera (1980,1981). They chose to study channel flow at Reynolds numbers for which the flow is linearly stable. However, transition does take place at the Reynolds numbers studied. In their simulation, Orszag and Patera took a fully developed laminar channel profile (Poiseuille profile) and added finite-amplitude two-dimensional Tollmien-Schlichting waves to it, these waves are different in the channel than in the boundary layer. They found that the waves decayed slowly and that the rate of decay decreases as the Reynolds number increases, this is expected. However, they found that, when a small three-dimensional disturbance is introduced into the flow, it grows very rapidly. The growth of the three-dimensional wave is rapid enough to enter the nonlinear regime before the two-dimensional wave has decayed. At this point the simulation develops considerable energy at high wavenumbers and has to be stopped; as there is no model in the simulation, there is no way to continue. However, this simulation has provided an explanation of the instability of this flow; it is apparently due to the three-dimensional instability of stable two-dimensional waves. Orszag and Patera (1981) have done similar simulations for Couette and cylindrical tube flows.

Some of their results are shown in Fig. 7.8. The decay of the two-dimensional wave and the growth of the three-dimensional wave are quite apparent.

A simulation of the instability of the boundary layer has been made by Wray (unpublished). In order to avoid the difficulty that arises from the spatially developing boundary layer, he chose a time-developing boundary

layer; physically, this corresponds to the boundary layer that develops on a suddenly started plate. Although the velocity profile of the time-developing boundary layer is different from that of the spatial layer, the calculation was started with the Blasius profile appropriate to the spatial layer. To this profile, a weak Tollmien-Schlichting wave and a weak three-dimensional random disturbance was added.

The disturbance grows very slowly at first (as expected) until it builds up to a level at which nonlinear effects become important. At this point, the rate of change of the layer becomes spectacular. The contours of the various velocity components and the vorticity develop more and more structure. Comparisons with experimental results for the parameters reveal a considerable similarity; the comparison is necessarily qualitative, but it is remarkably good.

Eventually, this simulation developed a considerable amount of energy at high wavenumbers, and it had to be stopped. There is no way to continue this simulation beyond this point without more resolution. Unfortunately, it may be that the small scales play an important role in the development of this flow, and it is not known whether the addition of a model will cure the problem.

Chapter VIII

OTHER APPLICATIONS

As we have stated earlier, higher-level simulation began in meteorology and oceanography. These fields have maintained an active interest in the simulation of the global circulation of the Earth's atmosphere and oceans. The methods used are similar to the ones described in this report, but there are additional difficulties. The principal of these is that thermal energy and the transport of water vapor (in the atmosphere) and salt (in the ocean) are very important in these flows, and one must deal with the effects of stratification, evaporation, and condensation. When coupled with the limitation to very coarse grids (200 km is typical in these simulations today), we see that the problems are considerably more difficult than the ones dealt with in this report. They are, however, of great importance, and considerable effort is being devoted to them. The author has only a passing knowledge of the work in these areas, and this is the reason why the subject is not covered in this report.

Methods similar to the ones given in this report have also been applied to smaller-scale environmental problems. For example, simulations have been made of local parts of the atmosphere by these methods; these are called mesoscale simulations. The author is familiar only with a few papers by Deardorff in this area, in these papers, he used a complete Reynolds stress model for the subgrid scale Reynolds stresses. Others have applied these methods to the prediction of the flow in lakes, harbors, and other small bodies of water. Of the work in this field, the author is familiar only with some of what has been done at his institution. Findikakis (1980) has recently developed a finite-element method for computing such flows.

On a still smaller scale, there have been a number of extensions of the work covered in the earlier sections of this report. Schumann and his coworkers have used the method that was described for channel flow for the simulation of flows in annuli and made other extensions. In particular, they have computed the channel and the annulus with heat transfer, in the simulations, the temperature is treated as a passive scalar. We have not dealt with this work at length in this paper for several reasons. It is covered in detail in the report of Schumann et al. (1980). Also, since the results produced by

Schumann's method differ considerably from those of Kim and Moin (1979) and Moin and Kim (1981) for the channel flow, we are unsure about the accuracy of the method when applied to heat transfer. For similar reasons we have not covered their work on the effect of roughness.

Schumann, Grötzbach, and Kleiser have applied their method to natural convection flow between parallel horizontal plates. They covered a very large range of Rayleigh number and were able to predict the observed transitions from one flow regime to another. This is an excellent piece of work and was not covered because it did not fit any of the subject headings used in this paper. Grötzbach (1979) has also investigated simulated flows in vertical channels with the influence of buoyancy.

Finally, we shall mention a method that competes with the grid-based methods that are the primary subject of this report. These are methods in which the motions of vortices are followed (vortex-tracking methods). A number of interesting features of transitional and turbulent flows have been computed by this method, including flows with separation. The full capabilities of this approach and a comparison of it with the methods discussed in this report are given in a review paper by Leonard (1981). Hybrid methods which use some ideas from vortex-tracking and some from grid-based methods are also being investigated at the present time, the interested reader is referred to the paper by Couet, Leonard, and Buneman (1980).

There are undoubtedly areas that have been overlooked in this report. The author has tried his best to be complete, but in any subject area that has become this large something is likely to be missed. There is no intent to minimize any contributions that have been missed.

Chapter IX

CONCLUSIONS AND FUTURE DIRECTIONS

1. Where Are We Now?

We hope that this report has shown that higher-level simulations of turbulent flow have reached a point in their development which allows them to play an important role in turbulent fluid mechanics. Let us now sum up where the field stands today. We start with the positive points.

a) The basic ideas of large eddy simulation seem sound. Specifically, they seem to be able to handle homogeneous turbulent flows and free shear flows quite well. For wall-bounded flows, the importance of small structures near the wall is a problem, and these flows are difficult to deal with, but good progress has been made.

b) Direct simulation of many interesting flows are now feasible. We are limited to low Reynolds numbers, but this restriction may not be important in some flows, as the large scales may be nearly Reynolds number independent. Alternatively, one can regard the viscosity as a simple subgrid scale model and pretend that a higher Reynolds number flow is being simulated. Both of these approaches have been taken. Orszag has used the concept of "Reynolds number similarity" with considerable success. Rubesin (1979) regarded direct simulations as large eddy simulations, also with considerable success.

c) Higher-level simulations have come to the point at which they are able to provide information on quantities that are difficult to measure in the laboratory. In this role, they are able to evaluate turbulence models in a way that is very difficult to do by any other method.

d) Higher-level simulations are able, in some cases, to simulate flows that are very difficult or impossible to perform in the laboratory. Some examples are flows with rotation and/or compressibility.

e) It is now possible to do flow visualizations using full and/or large eddy simulations. These visualizations reproduce much of what is seen in the laboratory. They also offer flexibility that is difficult to match in the laboratory. They can be used to look in detail at specific regions, and can even be used backwards in time.

Now let us consider some of the difficulties.

a) The most obvious problem is that these methods require large amounts of computer time. Although some of the simpler flows can be done in a few minutes on large machines, running times of the order of hours are not unusual for the more difficult flows. Use of these methods must be restricted to individuals with access to the machines that can do these simulations. Some means of assuring that the problems of greatest interest are done is necessary.

b) Although some flows are amenable to full simulation, Reynolds number similarity does not hold for all flows, so it is not possible to treat low Reynolds number flows as models of a high Reynolds number flow in all cases. Better subgrid scale models will be necessary if high Reynolds number flows are to be simulated, but it may be very difficult to find models with wide applicability.

On balance, the contribution of higher level simulations seems to be more than worth the cost, and the approach is just beginning to reach its potential. With new generations of computers, it should be possible to do much more with these methods.

2. Where Are We Going?

It is clear that a great deal remains to be done in turbulence simulation. There are many directions which can be taken in the future, and, with more groups beginning to do these types of simulations, we expect the area to broaden rapidly. Of course, it is difficult to predict the future with any precision, but it is always interesting to try. Let us look at what can be expected in the next few years.

a) One obvious direction in which higher-level simulations will be extended is toward the simulation of a larger number and greater variety of flows. There are many possibilities, so the following list cannot be all-inclusive.

i) The flows which have already been simulated can be done with additional effects. Thus, to any of the flows treated in this report we can add rotation, curvature, heat transfer, passive scalars, and/or pressure gradients alone or in combination. In the wall-bounded flows we can also add

wall roughness and blowing or suction. Many of these effects are quite important in engineering flows and should be considered at an early date.

ii) To date, no method has been found for dealing with inflow or outflow boundaries. The outflow boundary can probably be handled by the usual method of requiring the streamwise derivatives to be zero at the outlet. The inflow condition is much more difficult, because it is necessary to prescribe a realistic representation of the turbulence in order not to require too much of the computation; to do this would waste a very large part of the computational resource. Being able to handle inflow and outflow boundaries is central to the computation of many flows of interest.

iii) There are some fairly simple flows which have not been done. Included among these are the jet and the wall jet.

b) Simulation of wall-bounded flows is much simpler if the kinds of boundary conditions used by Deardorff and Schumann can be applied. Chapman (1980) estimated that the savings to be realized in this way could make the difference between practical use of the higher-level simulations and their continuing to be confined to research. Accurate boundary conditions of that type need to be searched for.

c) Use of higher-level simulations in conjunction with flow visualization and statistical methods should become a very powerful tool for investigating the structure of turbulent flows. It is possible that such an approach may be able to tie the structure of turbulent flows to the modeling. This is highly speculative, but, if it can be done, it could be an important step forward. We may become "computational experimentalists."

d) The interaction of higher-level simulations and conventional models should become stronger. We can envision a time when people developing new models will routinely validate them using higher-level simulations. Certainly, we can expect higher-level simulations to be helpful in determining the constants in the models. It is worthwhile to set up a facility which is available for this purpose.

e) We expect that there will be considerable work on the improvement of subgrid scale models, but the direction this work will take is not obvious.

f) Higher-level simulations will be extended to include a number of phenomena that are not currently treated. Sound generation should be relatively

easy, as it seems to depend mainly on the large scales. Combustion should be very challenging, because the chemical reaction depends on intimate mixing at the small scales.

g) Something has to be left to the reader's imagination.

Acknowledgements

A work of this kind can never be done by one person. The author is indebted to a great many people for making this work possible. I shall try to thank everybody, but it is possible that someone may be left out, if this is the case, I take this opportunity to apologize.

Let me begin with my colleagues. Prof. W. C. Reynolds has been the co-leader of the effort in higher-level simulations at Stanford since the beginning, when I knew essentially nothing about turbulence; he has taught me a very large part of what I now know. Prof. S. J. Kline has also taught me a great deal about turbulent flows and has been a very important friend when I have needed one. Profs. J. P. Johnston and R. J. Moffat have also played important roles in this work; from them I have learned a lot about the art of experimenting in turbulence. Dr. S. Schechter of SRI and Profs. J. Oliger and G. H. Golub of the Computer Science Department have taught me a great deal about numerical methods. Dr. S. Biringen was a one-year visitor who contributed an important piece to this work. Prof. D. C. Leslie and his group were outstanding hosts during a sabbatical stay at Queen Mary College, London, I learned much about turbulence theory from them.

Next I must thank my students, who have done most of the actual work and all of the really hard work. Drs. D. Kwak and S. Shaanan provided the early basis of the method; Dr. R. A. Clark developed the method of computational model validation; Dr. N. N. Mansour pioneered the free shear layer work, Dr. P. Moin did the same on the channel flow. More recently, Drs. W. J. Feiereisen, A. B. Cain, and E. Shirani and Mr. J. Bardina have made important contributions; their work figures very prominently in this report, and I am indebted to them for allowing me to use some of their unpublished results.

A number of colleagues at NASA-Ames Research Center have played important roles in this work. In particular, I want to thank Drs. D. R. Chapman, M. Rubesin, V. Peterson, and H. Mark for the constant attention they gave this work. Drs. A. Leonard, R. S. Rogallo, P. Moin, J. Kim, and A. Wray, among others, have provided many useful ideas and many of the results contained in this report.

I also wish to thank Drs. J. N. Nielsen and O. J. McMillan of Nielsen Engineering and Research for allowing us to extend the area of work and for important contributions.

Lastly, and perhaps most importantly, I must thank the organizations who provided the support for this work. NASA-Ames Research Center has supported this work financially since its inception; their generosity in allowing us to use their computers has been even more important than their direct assistance. The National Science Foundation has supported the work on the mixing of a passive scalar over the last two years and has allowed us to broaden the base of our activity. The Office of Naval Research supported work at Nielsen Engineering and Research on model validation.

Mrs. Ruth Korb typed this manuscript in record time under a great deal of pressure and without complaint. Her work over many years has never been sufficiently appreciated.

This work was originally written as a set of notes for lectures given at the Von Kármán Institute of Fluid Dynamics in Brussels in March, 1981. I wish to thank the Institute and Professors W. Kollmann and J. Essers in particular for the invitation that compelled me to tackle a job that might not have been done otherwise, and for their kind hospitality at the Institute.

References

Acton, E., "The Modeling [illegible]ge Eddies in a Two-Dimensional Shear Layer," J. Fluid Mech., 76, 561-592 (1976).

Antonopoulos-Domis, M., "Large Eddy Simulation of the Decay of a Passive Scalar in Isotropic Turbulence," J. Fluid Mech. , 104, 55 (1981).

Ashurst, W. T., "Calculation of Plane Sudden Expansion Flow via Vortex Dynamics," Proc. 2nd. Conf. on Turbulent Shear Flows, London, 1979.

Ballhaus, W., "Prediction of Transonic Flows," in Numerical Fluid Dynamics, W. Kollman, ed., Hemisphere, Washington, 1979.

Bardina, J., J. H. Ferziger, and W. C. Reynolds, "Improved Subgrid Scale Models for Large Eddy Simultion," AIAA paper 80-1357, 1980.

Browand, F. K., and T. R. Troutt, "Vortices in the Turbulent Mixing Layer: The Asymptotic Limit," Presented at 32nd Meeting of APS, Division of Fluid Dynamics, Univ. of Notre Dame, Nov. 18-20, 1979.

Brown, G. L., and A. Roshko, "On Density Effects and Large Structures in Turbulent Mixing Layers," J. Fluid Mech., 64, 775 (1974).

Cain, A. B., W. C. Reynolds, and J. H. Ferziger, "Simulation of the Transition and Early Turbulence Regions of a Mixing Layer," Report TF-14, Dept. of Mech. Engrg., Stanford Univ., Stanford, CA., 1981.

Chandrsuda, C., and P. Bradshaw, "An Assessment of the Evidence for Orderly Structure in Turbulent Mixing Layers," Report 75-03, Aeronautics Dept., Imperial Coll., London (1975).

Chapman, D. R., "Computational Aerodynamics Development and Outlook," AIAA J., 17, 1293 (1979).

Chapman, D. R., and G. D. Kuhn, "Simulation of the Wall Region of a Turbulent Boundary Layer," AIAA paper 81-1024, 1981.

Clark, R. A., J. H. Ferziger, and W. C. Reynolds, "Evaluation of Subgrid Scale Turbulence Models Using a Fully Simulated Turbulent Flow," J. Fluid Mech. 91, 92 (1979).

Coles, D. E., and E. Hirst, eds., Computation of Turbulent Boundary Layers--1968 AFOSR-IFP-Stanford Conference, Vol. II, Dept. of Mech. Engrg., Stanford Univ., 1968.

Cooley, J. W., and J. W. Tukey, "An Algorithm for the Machine Calculation of Complex Fourier Series," Math Comput., 19, 297-301 (1965).

Couet, B., O. Buneman, and A. Leonard, "Three-Dimensional Simulation of the Free Shear Layer Using the Vortex in Cell Method," Proc. 2nd Conf. on Turbulent Shear Flows, London, 1979.

C-2

Deardorff, J. W., and G. E. Willis, "The Effect of Two-Dimensionality on the Suppression of Thermal Turbulence," J. Fluid Mech., 23, 337-353 (1965).

Deardorff, J. W., and G. E. Willis, "Investigation of Turbulent Thermal Convection between Horizontal Plates," J. Fluid Mech., 28, 675-704 (1967).

Deardorff, J. W., and G. E. Willis, "Investigation of Thermal Convection between Horizontal Plates," J. Fluid Mech., 28, 675 (1968).

Deardorff, J. W., "A Numerical Study of Three-Dimensional Turbulent Channel Flow at Large Reynolds Number," J. Fluid Mech., 41, 452-480 (1970).

Deardorff, J. W., "On the Magnitude of the Subgrid Scale Eddy Coefficient," J. Comp. Phys., 7, 120-133 (1971).

Deardorff, J. W., "Three-Dimensional Numerical Study of Turbulence in an Entrained Mixed Layer," Boundary Layer Meteorology, 1, 199-226 (1974).

Deardorff, J. W., "Three-Dimensional Numerical Modeling of the Planetary Boundary Layer," Workshop in Micrometeorology, A.M.S., 271-311 (1973).

Deardorff, J. W., "Simulation of Turbulent Channel Flow," J. Fluids Engrg., 95, 429 (1973).

Deardorff, J. W., "Three-Dimensional Numerical Study of Turbulence in an Entraining Mixed Layer," Boundary Layer Meteorology, 1, 199 (1974).

Feiereisen, W. J., W. C. Reynolds and J. H. Ferziger, "Simulation of Compressible Turbulence," Report TF-13, Dept. of Mech. Engrg., Stanford University (1981).

Ferziger, J. H., "Large Eddy Numerical Simulation of Turbulent Flow," AIAA Journal, 15, 1261 (1977).

Ferziger, J. H., and D. C. Leslie, "Large Eddy Simulation--A Predictive Approach to Turbulent Flow Computation," AIAA paper 79-1441, 1979.

Ferziger, J. H., "Homogeneous Turbulent Flows: A Review and Evaluation," prepared for the 1980-81 Stanford-AFOSR-HTTM Conf. on Complex Turbulent Flows, Dept. of Mech. Engrg., Stanford Univ. (1980).

Findikakis, A., "Large Eddy Simulations of Stratified Flows," Dissertation, Dept. of Civil Engrg., Stanford University, Stanford, CA., 1981.

Fox, D. G., and J. W. Deardorff, "Computer Methods for Simulation of Multidimensional, Nonlinear, Subsonic, Incompressible Flow," J. Heat Transfer, 45, 337-346 (1972).

Fox, D. G., and D. K. Lilly, "Numerical Simulation of Turbulent Flows," Rev. of Geophys. and Space Phys., 10, 51-72 (1972).

Fox, D. G., and S. A. Orszag, "Pseudospectral Approximation to Two-Dimensional Turbulence," J. Comp. Phys., 11, 612-619 (1973).

Gottlieb, D., and S. A. Orszag, "Numerical Analysis of Spectral Methods: Theory and Applications," NSF-CBMS Monograph 16, SIAM, Philadelphia (1977).

Grötzbach, G., G. Lörcher, and U. Schumann, "Anwendung und experimentelle Absicherung der direkten numerischen Simulation turbulenter Stromungen," Reaktortagung, Nürnberg, 8.43-11.4, 145-148 (1975).

Grötzbach, G., "Direkte numerische Simulation turbulenter Geschwindigkeits-, Druck-, und Temperaturfelder bei Kanalstromungen, Dissertation, Univ. of Karlsruhe (1977).

Grötzbach, G., "Numerische Experimente zur Untersuchung des Wärmtetransports in turbulenter Flüssigmetallströmung," Reaktortagung, Mannheim, 29.3-1.4, 7-10 (1977).

Grötzbach, G., "Numerische Untersuchung der Quervermischung bei auftreibsbeinflusster turbulenter Konvektion in einem vertikalen Kanal," KFK 2648 (1978).

Grötzbach, G., Direct Numerical Simulation of Secondary Currents in Turbulent Channel Flows," Lect. Notes in Phys., 76, 308-319, Springer Verlag (1978).

Grötzbach, G., Convective Velocities of Wall Pressure Fluctuations in a Turbulent Channel Flow Deduced from a Computer-Generated Movie," Lect. Notes in Phys., 76, 320-324, Springer Verlag (1978).

Grötzbach, G., Numerical Investigation of the Influence of Secondary Flows on Characteristic Turbulence Data, KFK 2553 Kernforschungszentrum Karlsruhe (1978).

Grötzbach, G., "Direct Numerical Simulation of Laminar and Turbulent Benard Convection," Report, Kernforschungszentrum Karlsruhe (1979).

Grötzbach, G., and U. Schumann, "Direct Numerical Simulation of Turbulent Velocity-, Pressure-, and Temperature-Fields in Channel Flows," Proc. of the Symp. on Turbulent Shear Flows, Penn. State Univ., Apr. 18-20, 1979.

Grötzbach, G., "Numerical Investigation of Radial Mixing Capabilities in Strongly Buoyancy-Influenced Vertical Turbulent Channel Flows," Nucl. Engr. and Design, 54, 49 (1979).

Grötzbach, G., "Numerical Simulation of Turbulent Liquid Metal Flows in Plane Channels and Annuli," Report KFK 2968, Kernforschungszentrum, Karlsruhe (1980).

Ibbetson, A., and D. J. Tritton, "Experiments on Turbulence in a Rotating Fluid," J. Fluid Mech., 68, 639 (1975).

Kim, H. T., S. J. Kline, and W. C. Reynolds, "The Production of Turbulence Near a Smooth Wall in a Turbulent Boundary Layer," J. Fluid Mech., 50, 133 (1971).

Kim, J., and P. Moin, "Large Eddy Simulation of Turbulent Channel Flow," AGARD Symposium on Turbulent Boundary Layers, The Hague, 1979.

Kleiser, L., and U. Schumann, "Simulation of 3-D Incompressible Flows between Parallel Plates with a Fourier-Chebyshev Spectral Method," EUROVISC Working Party on Transition in Boundary Layers, Univ. Stuttgart, Oct. 2-3, 1978.

Kline, S. J., M. V. Morkovin, G. Sovran, and D. J. Cockrell, eds., Computation of Turbulent Boundary Layers--1968 AFOSR-IFP-Stanford Conference, Vol. 1. Dept. of Mech. Engrg., Stanford University, 1968.

Kline, S. J., J. H. Ferziger, and J. P. Johnston, "Calculation of Turbulent Shear Flows: Status and Ten-Year Outlook," ASME J. Fluids Engrg., 100, 3 (1978).

Kline, S. J., and B. J. Cantwell, eds., Proc. of the 1980-1981 Stanford-AFOSR-HTTM Conf. on Complex Turbulent Flows, Dept. of Mech. Engrg., Stanford Univ. (1981).

Knight, D. D., "Numerical Investigation of Large Scale Structures in the Turbulent Mixing Layer," Proc. 6th Biennial Symp. on Turbulence, U. of Missouri, Rolla, Oct. 8-10, 1979.

Launder, B. E., G. J. Reece, and W. Rodi, "Progress in the Development of a Reynolds Stress Turbulence Closure," J. Fluid Mech., 68, 537 (1975).

Leonard, A., "Energy Cascade in Large Eddy Simulations of Turbulent Fluid Flows," Adv. in Geophysics, 18A, 237 (1974).

Leonard, A., "Vortex Methods for Flow Simulation, J. Comp. Phys. (to be published).

Leslie, D. C., "Developments in the Theory of Turbulence," Oxford U.P., 1973.

Leslie, D. C., and G. L. Quarini, "The Application of Turbulence Theory to the Formulation of Subgrid Modeling Procedures," J. Fluid Mech., 91, 65 (1979).

Lilly, D. K., "On the Computational Stability of Numerical Solutions of Time-Dependent, Nonlinear, Geophysical Fluid Dynamic Problems," Mon. Wea. Rev., 93, 11 (1965).

Lilly, D. K., "The Representation of Small Scale Turbulence in Numerical Simulation Experiments," Proc. IBM Sci. Comp. Symp. on Env. Sci., IBM-Form No. 320-1951, 195-210 (1967).

Love, M. D., and D. C. Leslie, "Studies of Subgrid Modeling with Classical Closures and Burgers' Equation," Proc. Symp. on Turbulent Shear Flows," Penn. State Univ., 1976.

Mansour, N. N., P. Moin, W. C. Reynolds, and J. H. Ferziger, "Improved Methods for Large Eddy Simulations of Turbulence," Proc. 1st Int'l. Symp. on Turbulent Shear Flows, Penn. State Univ., 1977.

McMillan, O. J., and J. H. Ferziger, "Direct Testing of Subgrid Scale Models," AIAA Journal, 17, 1340 (1979).

McMillan, O. J., J. H. Ferziger, and R. S. Rogallo, "Tests of New Subgrid Scale Models in Strained Turbulence," AIAA paper 80-1339, 1980.

Metcalfe, R. W., and J. J. Riley, "Direct Numerical Simulations of Turbulent Shear Flows," Proc. 7th Int'l. Conf. on Numerical Methods in Fluid Dynamics, Stanford University, 1980.

Moin, P., and J. Kim, "Improved Simulation of Turbulent Channel Flow," submitted to J. Fluid Mech., 1981.

Moin, P., W. C. Reynolds, and J. H. Ferziger, "Large Eddy Simulation of an Incompressible Turbulent Channel Flow," Report TF-12, Dept. of Mech. Engrg., Stanford University, Stanford, CA., 1978.

Morkovin, H. V., "Effects of Compressibility on Turbulence," in Mechanique de la Turbulence," CNRS, Paris, 1962.

Orszag, S. A., "Numerical Methods for the Simulation of Turbulence," Phys. Fluid, Suppl. II, 250-257 (1969).

Orszag, S. A., "Numerical Simulation of Incompressible Flow within Simple Boundaries. I. Galerkin (Spectral) Representations," Stud. Appl. Math. 50, 293-327 (1971).

Orszag, S. A., "Numerical Simulation of Incompressible Flows within Simple Boundaries," J. Fluid Mech., 49, 75-112 (1971).

Orszag, S. A., "Galerkin Approximations to Flows within Slabs, Spheres, and Cylinders," Phys. Rev. Let. 26, 1100-1103 (1971).

Orszag, S. A., and G. S. Patterson, Jr., "Numerical Simulation of Turbulence," in Statistical Models and Turbulence, 127-147, Springer-Verlag, Berlin (1972).

Orszag, S. A., and M. Israeli, "Numerical Flow Simulation by Spectral Methods," in Numerical Models of Ocean Circulation, 284-300, Washington (1973).

Orszag, S. A., "Numerical Simulation of Turbulent Flows," Flow Research Rept. No. 52, M.I.T., Cambridge (1974).

Orszag, S. A., and Y. H. Pao, "Numerical Computation of Turbulent Shear Flow," Adv. Geophys., 18A, 225-236 (1974).

Orszag, S. A., and M. Israeli, "Numerical Simulation of Viscous Incompressible Flows," Ann. Rev. of Fluid Mech., 6, 281-318 (1974).

Orszag, S. A., "Comparison of Pseudospectral and Spectral Approximation," Stud. in Appl. Math., 51, 253-259 (1975).

Orszag, S. A., "Turbulence and Transition: A Progress Report," Lect. Notes in Phys., 59, 32-51 (1976).

Orszag, S. A., and L. C. Kells, "Transition to Turbulence in Plane Poiseuille and Plane Couette Flow" (to be published).

Patnaik, P. C., F. S. Sherman, and G. M. Corcos, "A Numerical Simulation of Kelvin-Helmholtz Waves of Finite Amplitude," J. Fluid Mech., 73, 215-240 (1976).

Patterson, G. S., Jr., and S. A. Orszag, "Spectral Calculations of Isotropic Turbulence: Efficient Removal of Aliasing Interactions," Phys. Fluids, 14, 1538-1541 (1971).

Reynolds, W. C., "Computation of Turbulent Flows," Ann. Rev. Fluid Mech., 8, 183-208 (1976).

Riley, J. J., and G. S. Patterson, "Diffusion Experiments with Numerically Integrated Isotropic Turbulence," Phys. Fluids, 17, 292-297 (1974).

Riley, J. J., and Metcalfe, R. W., "The Direct Numerical Simulations of the Turbulent Wakes of Axisymmetric Bodies--An Interim Report," Report No. 135, Flow Research Corp., Kent, Wash., 1978. Also available as NASA CR-152282.

Riley, J. J., and R. W. Metcalfe, "Direct Numerical Simulations of the Turbulent Wake of an Axisymmetric Body," in Turbulent Shear Flows. II (L. Bradbury et al., eds.), Springer, 1980.

Riley, J. J., and R. W. Metcalfe, "Direct Numerical Simulation of a Perturbed Turbulent Mixing Layer," AIAA paper 80-0274, 1980.

Rogallo, R. S., "An ILLIAC Program for the Numerical Simulation of Homogeneous Incompressible Turbulence," NASA TM-73, 1978.

Rose, H. A., "Eddy Diffusivity, Eddy Noise, and Subgrid Scale Modeling," J. Fluid Mech., 81, 719-734 (1977).

Rose, H. A., and P. L. Sulem, "Fully Developed Turbulence and Statistical Mechanics," J. de Physique, 39, 441-484 (1978).

Roshko, A., "Structure of Turbulent Shear Flows: A New Look," AIAA Journal, 14, 1249-1357 (1976).

Rubesin, M. W., "Subgrid- or Reynolds Stress Modeling for Three-Dimensional Turbulence Computations," Proc. AGARD Meeting on Turbulent Flows, The Hague, 1979.

Runstadler, P. W., S. J. Kline, and W. C. Reynolds, "An Investigation of the Flow Structure of the Turbulent Boundary Layer," Report MD-8, Dept. of Mech. Engrg., Stanford Univ. (1963).

Schemm, C. E., and F. B. Lipps, J. Atmos. Sci., 33, 1021 (1976).

Schumann, U., "Ein Verfahren zur direkten numerischen Simulation turbulenter Stromungen in Platten- und Ringspaltkanalen und uber seine Anwendung zur Untersuchung von Turbulenzmodellen," dissertation, Univ. of Karlsruhe, 1973.

Schumann, U., "Results of a Numerical Simulation of Turbulent Channel Flows," in Int'l. Meeting on Reactor Heat Transfer (M. Dalle-Donne, ed.), 250-251 (1973).

Schumann, U., "Subgrid Scale Modeling for Finite Difference Simulations of Turbulent Flows in Plane Channels and Annuli," J. Comp. Phys., 18, 376 (1975).

Schumann, U., "Experiences with the Spectral Method for Three-Dimensional Turbulence Simulations," GAMM-Conf. on Numerical Methods in Fluid Mech., DFVLR, 209-216, Koln, Oct. 8-10, 1975.

Schumann, U., and J. R. Herring, "Axisymmetric Homogeneous Turbulence: A Comparison of Direct Spectral Simulations with the Direct Interaction Approximation," J. Fluid Mech., 76, 755-782 (1976).

Schumann, U., and G. S. Patterson, "Numerical Study of Pressure and Velocity Fluctuations in Nearly Isotropic Turbulence," J. Fluid Mech., 88, 685-709 (1978).

Schumann, U., and G. S. Patterson, "Numerical Study of the Return of Axisymmetric Turbulence to Isotropy," J. Fluid Mech., 88, 711-735 (1978).

Schumann, U., G. Grötzbach, and L. Kleiser, "Direct Numerical Simulation of Turbulence," in Prediction Methods for Turbulent Flows (W. Kollmann, ed.), Hemisphere, New York (1980).

Sicilian, J. M., and A. Leonard, "The Use of Fourier Expansions in Turbulent Flow Simulations," Report No. TF-2, Thermosciences Div., Stanford Univ., (1974).

Siggia, E. D., and G. S. Patterson, Jr., "Intermittency Effects in a Numerical Simulation of Stationary Three-Dimensional Turbulence," J. Fluid Mech., 86, 567-592 (1978).

Smagorinsky, J., "General Circulation Experiments with the Primitive Equations. I. The Basic Experiment," Mon. Wea. Rev., 91, 99 (1963).

Sommeria, G., J. Atmos. Sci., 33, 216 (1976).

Traugott, S. C., "Influence of Solid-Body Rotation on Screen-Produced Turbulence," Quart. J. Mech. Appl. Math., 104 (1954).

Tennekes, H., and J. L. Lumley, A First Course in Turbulence, MIT Press, 1972.

Wigeland, R., and H. M. Nagib, "Grid-Generated Turbulence With and Without Rotation," Fluids and Heat Transfer Report R78-1, Ill. Inst. of Tech., 1978.

Winant, C. D., and F. K. Browand, "Vortex Pairing: The Mechanism of Mixing Layer Growth at Moderate Reynolds Number," J. Fluid Mech., 63, 237-255 (1974).

Wray, A. A., M. Y. Hussaini, and D. Degani, "Numerical Simulation of Transition to Turbulence," 2nd. GAMM-Conf. on Numerical Methods in Fluid Mechanics (E. H. Hirschel & W. Geller, eds.), DFVLR, Koln, 247-254 (1977).

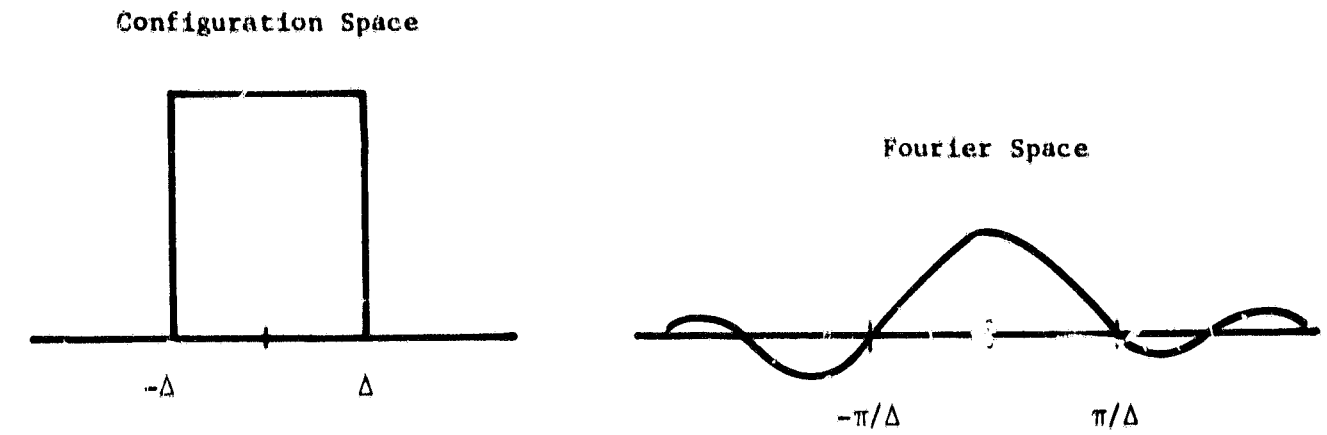

a) Box Filter

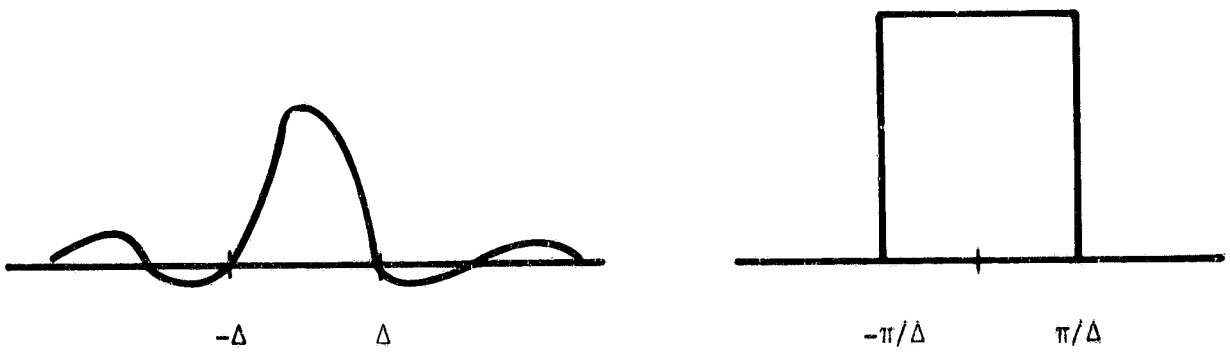

b) Fourier Space Sharp-cutoff

c) Gaussian

Figure 2.1 Some Filters Commonly Used in Large Eddy Simulation

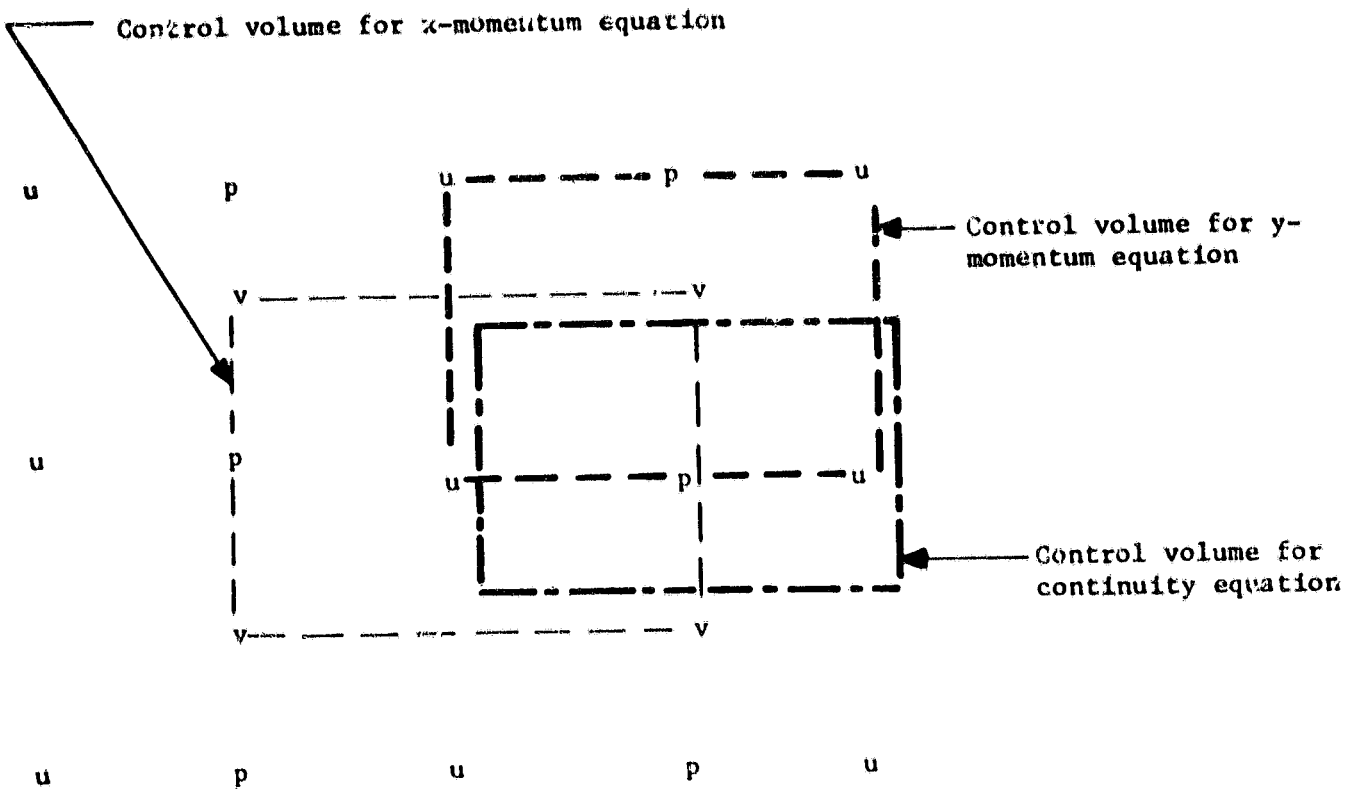

Figure 2.2 The Staggered Grid and the Control Volumes.

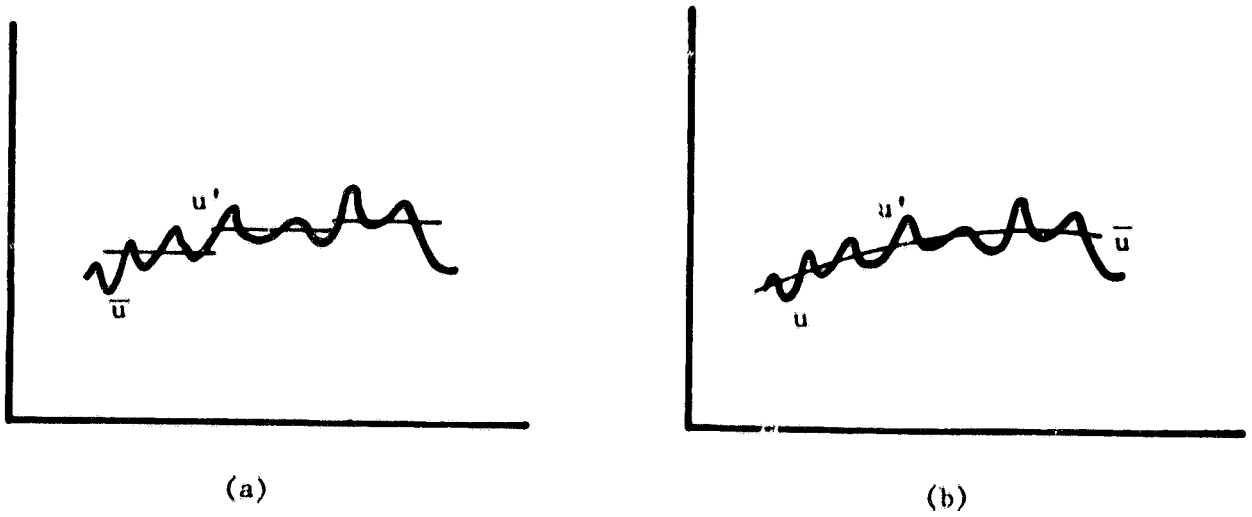

Figure 2.3 Definition of the large scale field by
(a) the Deardorff averaging method
(b) filtering

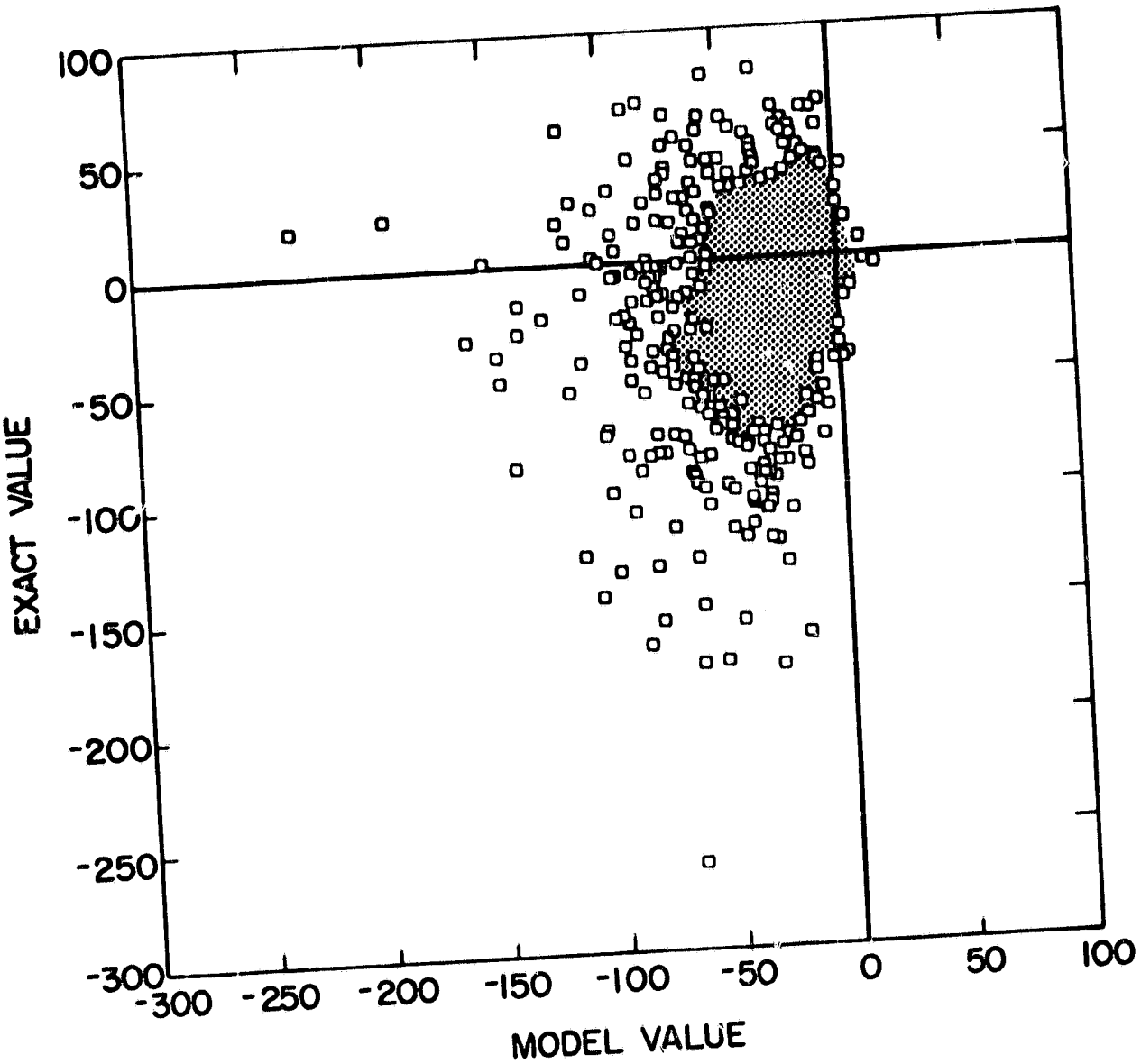

Figure 3.1 Scatter plot of $u_i \partial \tau_{ij} / \partial x_j$ (the dissipation due to the subgrid scale model) for the Smagorinsky model in weakly strained turbulence. The correlation coefficient is 0.4 for this case. From McMillan et al. (1980).

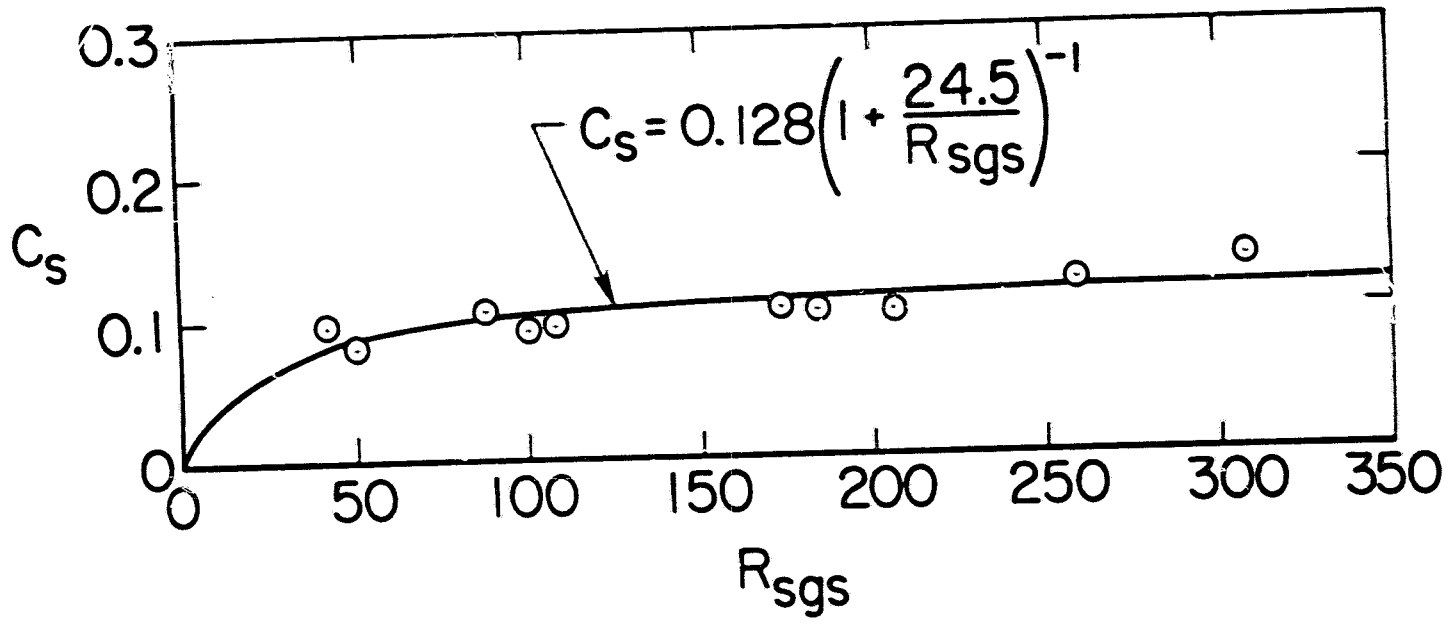

Figure 3.2 The constant in the Smagorinsky model as a function of the subgrid scale Reynolds number $R_{SGS} = |\bar{S}|\Delta^2/\nu$ where $|\bar{S}|$ is the r.m.s. large scale strain. From McMillan and Ferziger (1978).

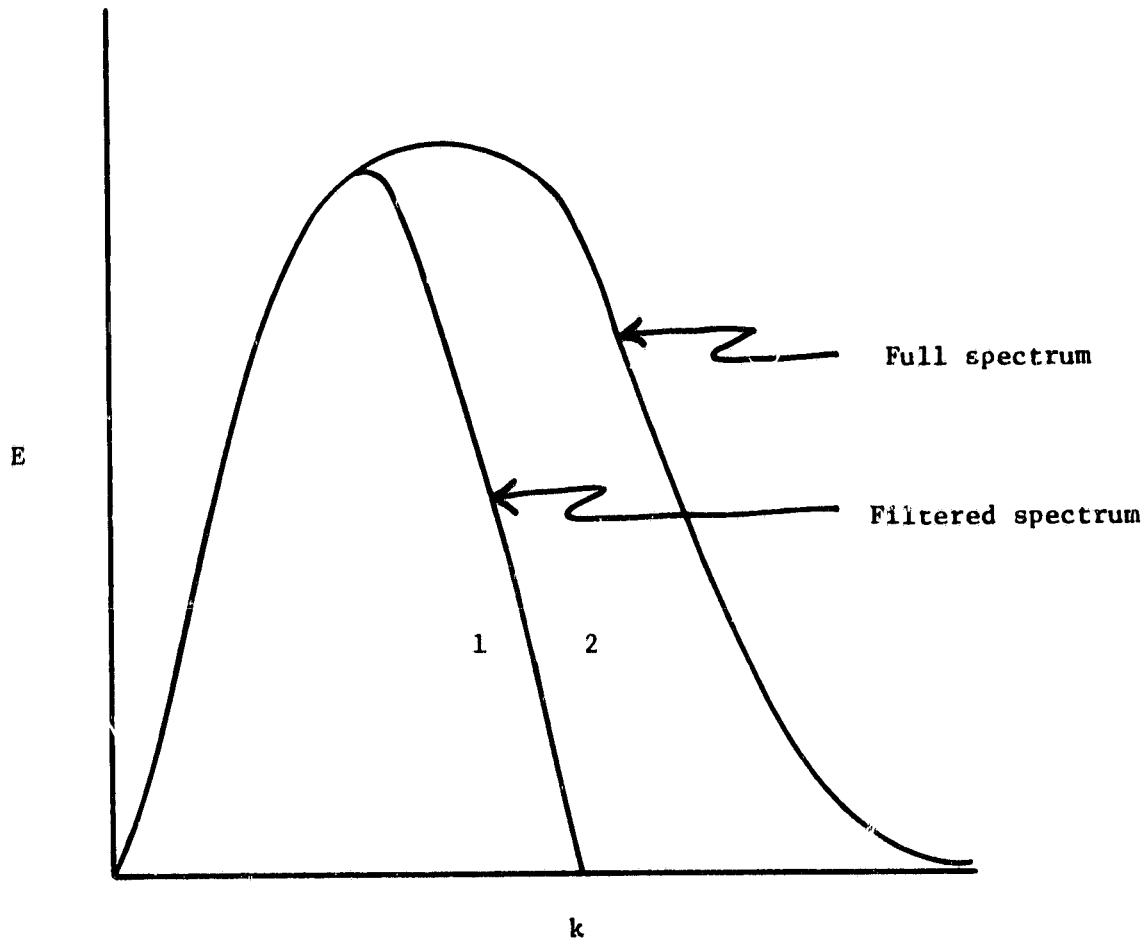

Figure 3.3 A typical turbulence spectrum and the effect of filtering. Region 1 represents the smallest scales of the filtered or resolved component of the field. Region 2 represents the largest scales of the subgrid scale or unresolved component of the field. The scale similarity model relates these.

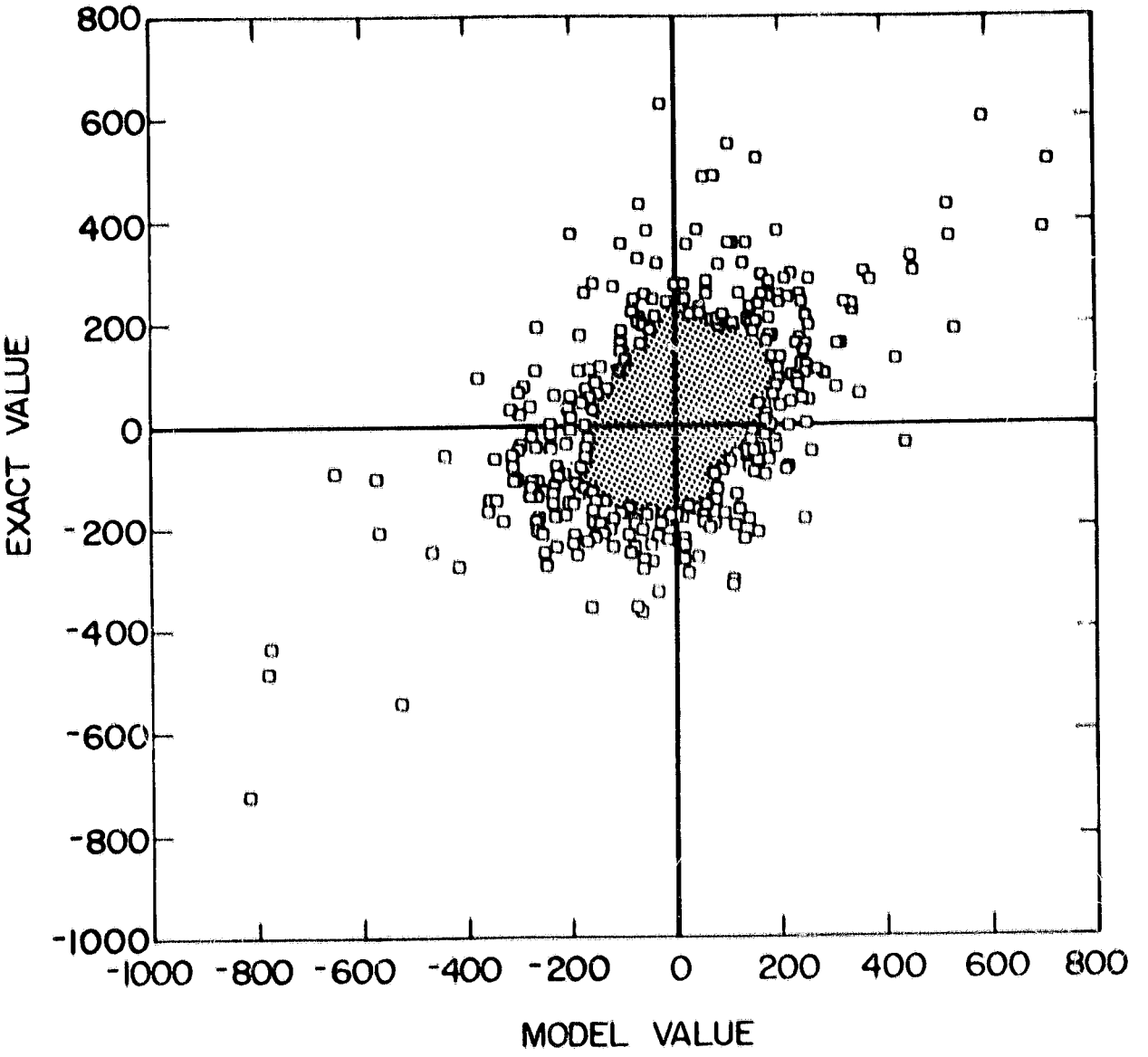

Figure 3.4 Scatter plot of $u_i \partial \tau_{ij} / \partial x_j$ (the dissipation due to the subgrid scale model) for the scale-similarity model in strained turbulence. The correlation is improved relative to the model shown in Figure 3.1 but the model has no average dissipation. From McMillan et al. (1980).

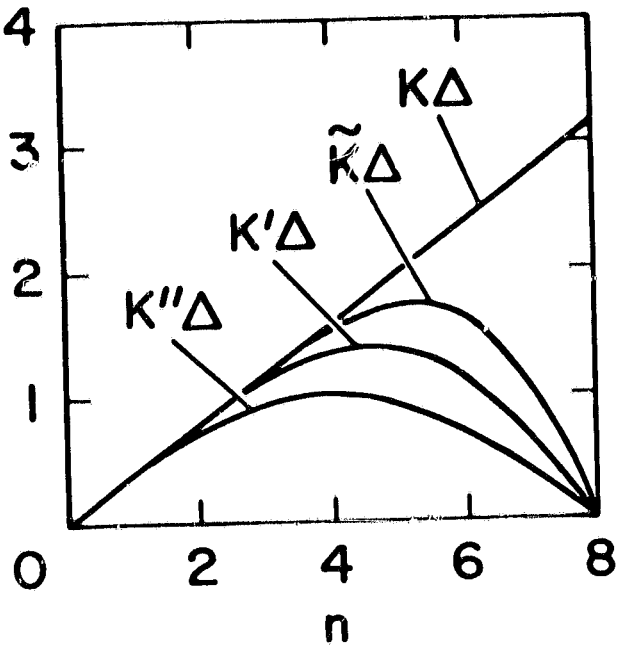

Figure 4.1a The effective wave member for a number of approximations. The methods used are: $k\Delta$, pseudospectral; $k''\Delta$, second order central difference; $k'\Delta$, fourth order central difference; $\tilde{k}\Delta$, compact method.

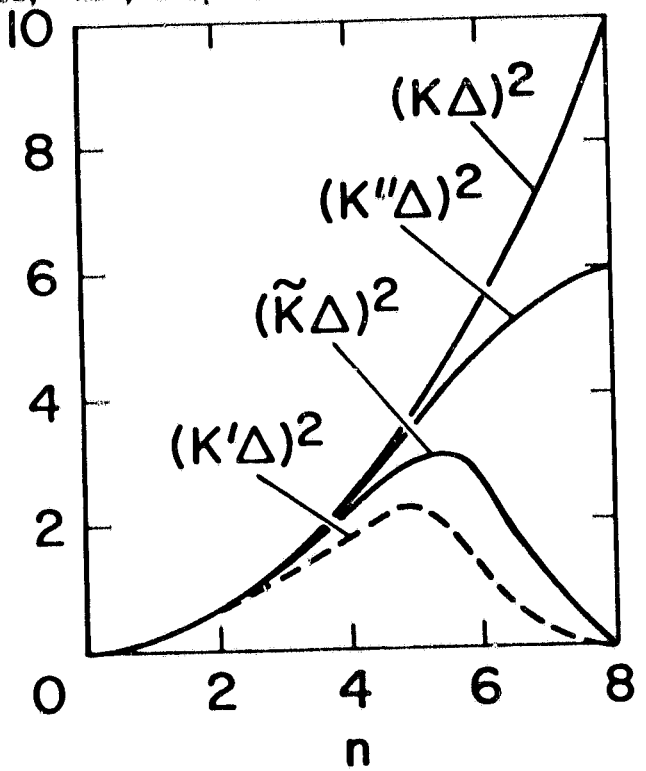

Figure 4.1b The square of the effective wave number in various second derivative approximations. The methods are given in Figure 3.1. From Mansour et al. (1978).

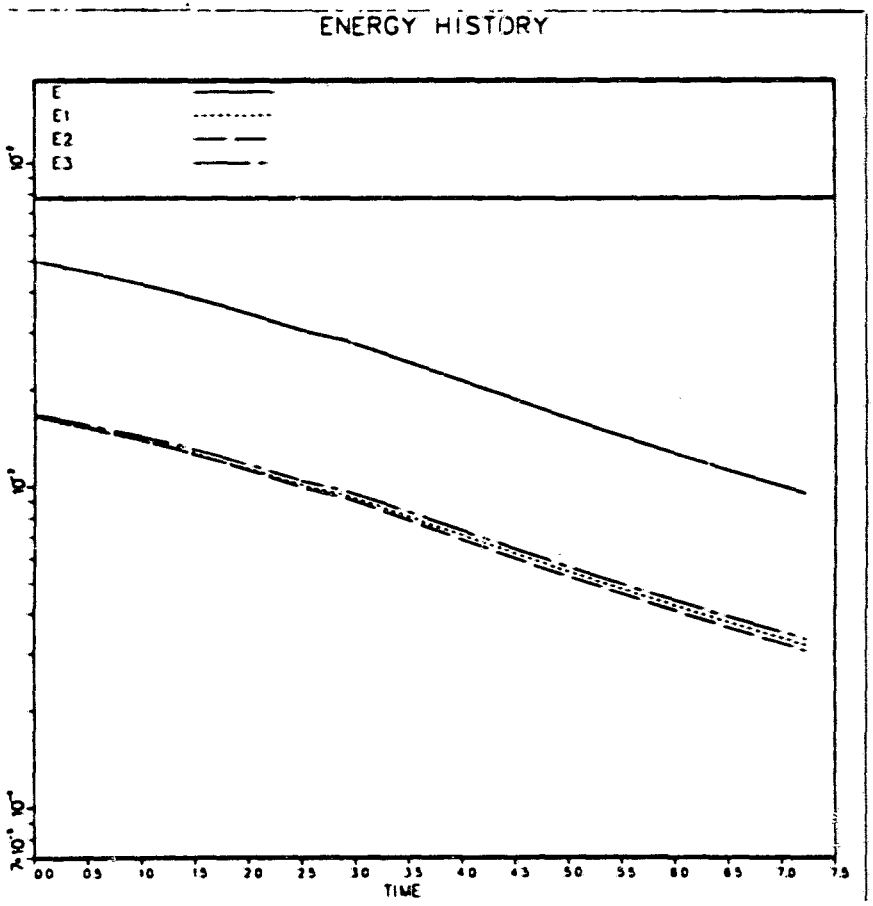

Figure 5.1 The turbulent kinetic energy and its components in a direct simulation of a turbulent flow at $R_\lambda \simeq 40$.

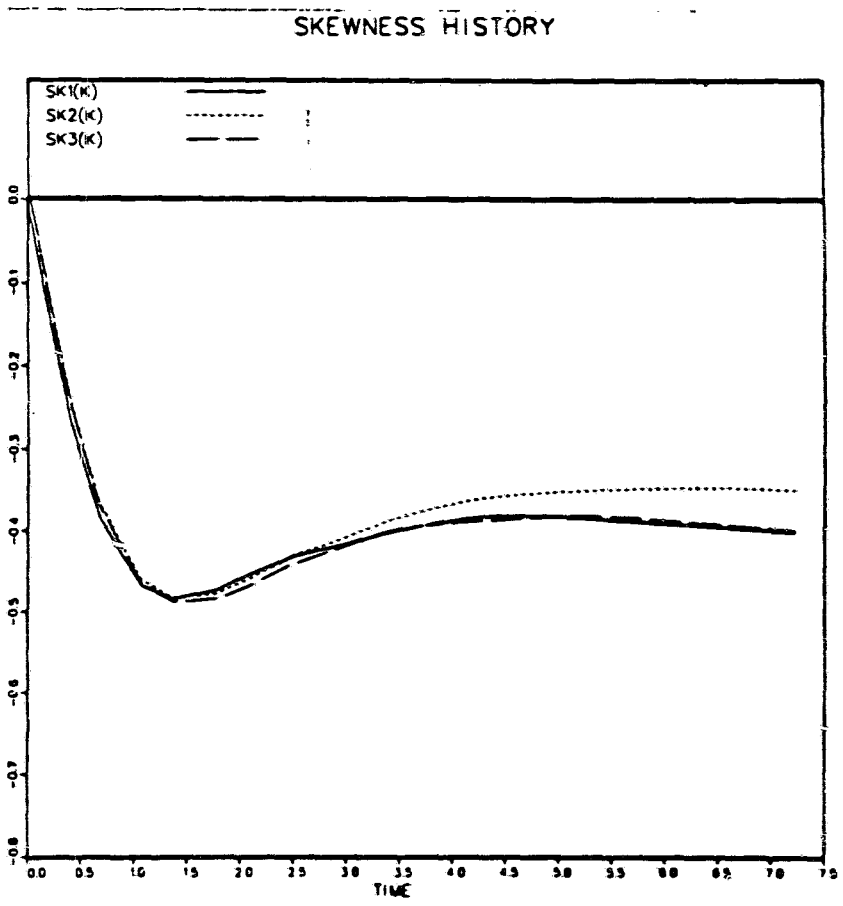

Figure 5.2 The skewness history in the flow of Figure 3.1.

From Feiereisen et al. (1981)

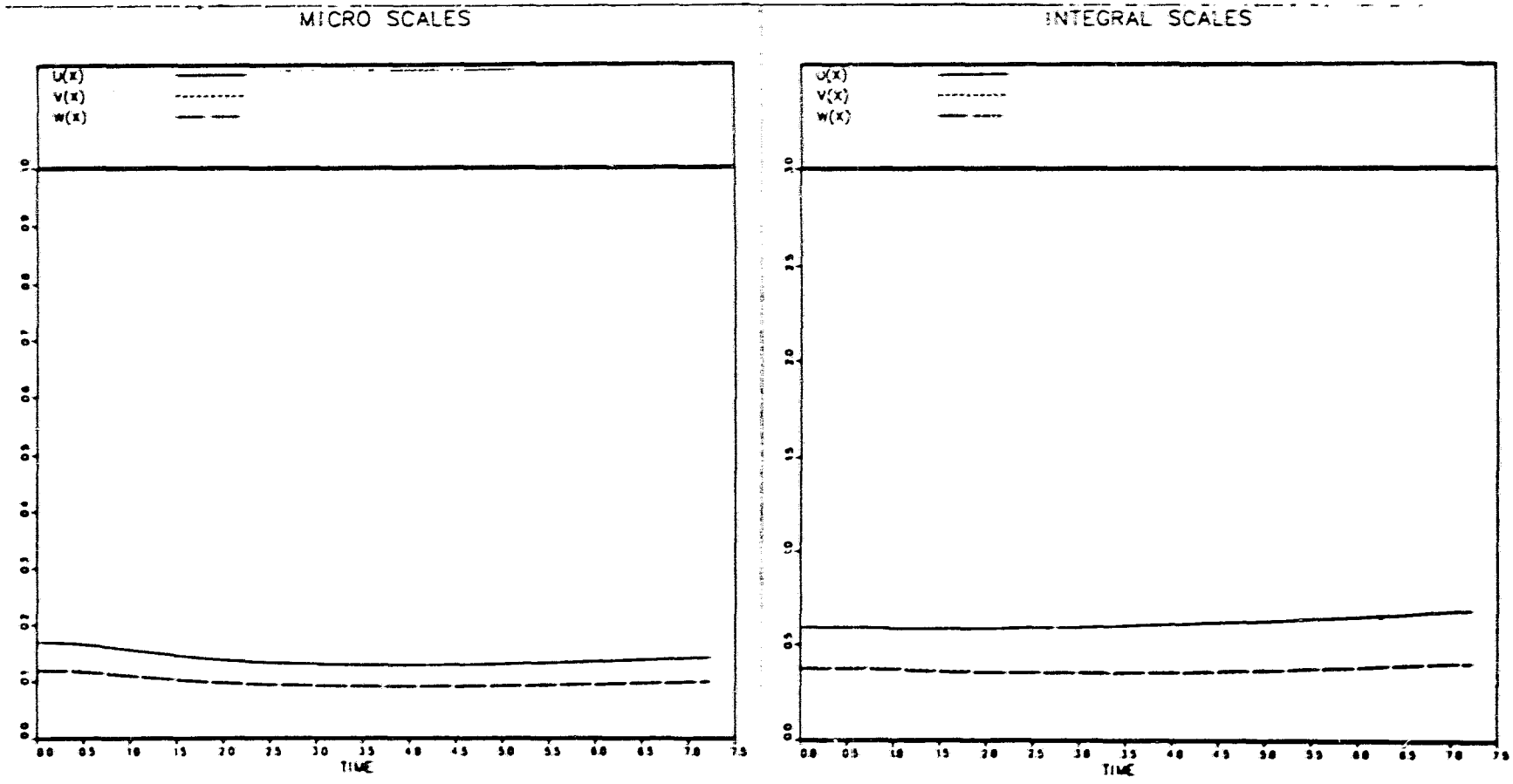

Figure 5.3 The microscales and integral scales in isotropic turbulence; same flow as Figure 3.1 and 3.2. From Feiereisen et al. (1981).

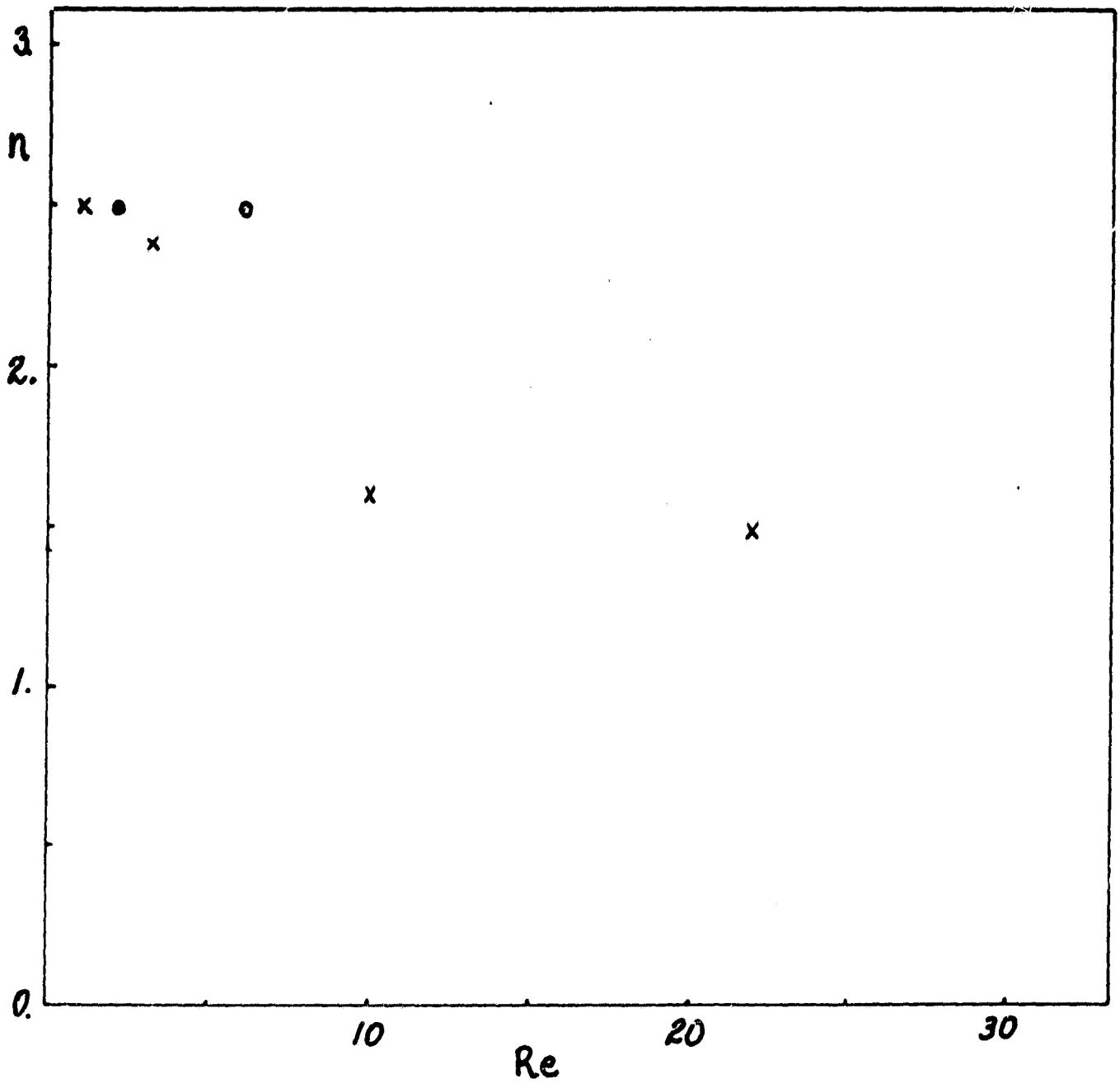

Figure 5.4 The decay index for isotropic turbulence as a function of the Reynolds number. Crosses are computational results; other symbols are experiments. From Shirani et al. (1981).

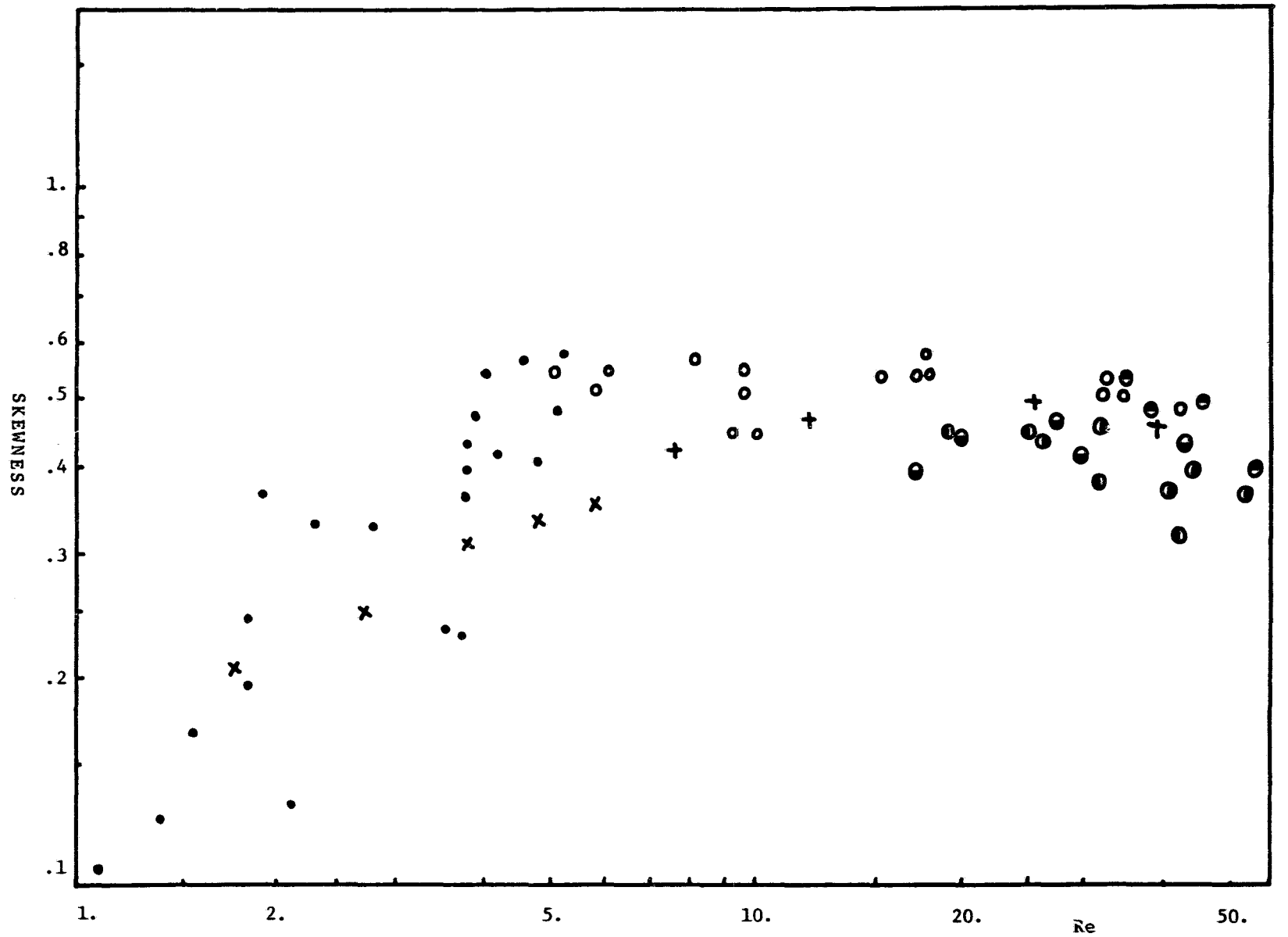

Figure 5.5 The skewness of the velocity derivative as a function of Reynolds number for isotropic turbulence Symbols are: x direct simulations; + large eddy simulations; all other symbols are experimental data. From Shirani et al. (1981).

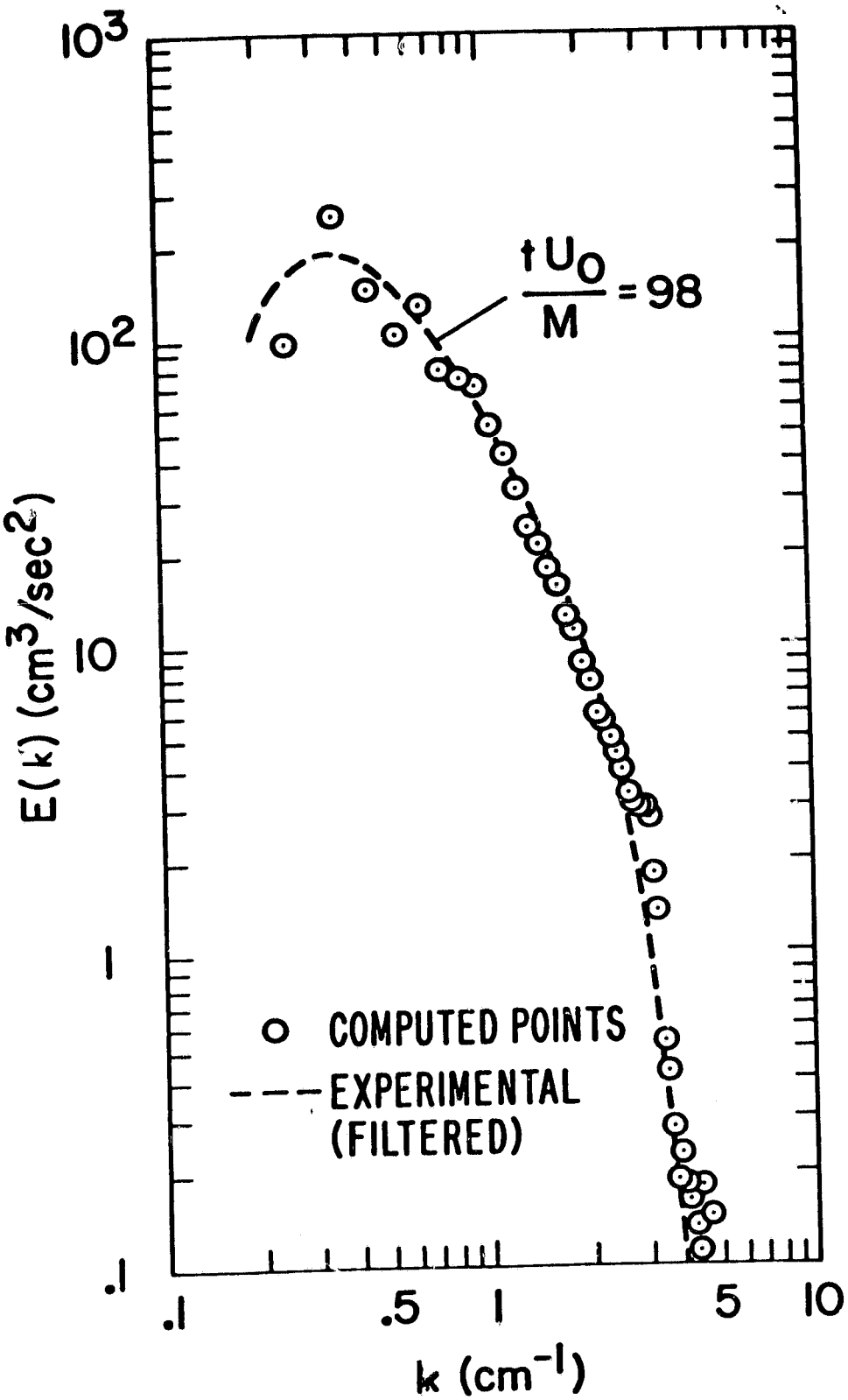

Figure 5.6 The filtered energy spectrum from a typical large eddy simulation. Points are computed results; the line represents the filtered experimental data.

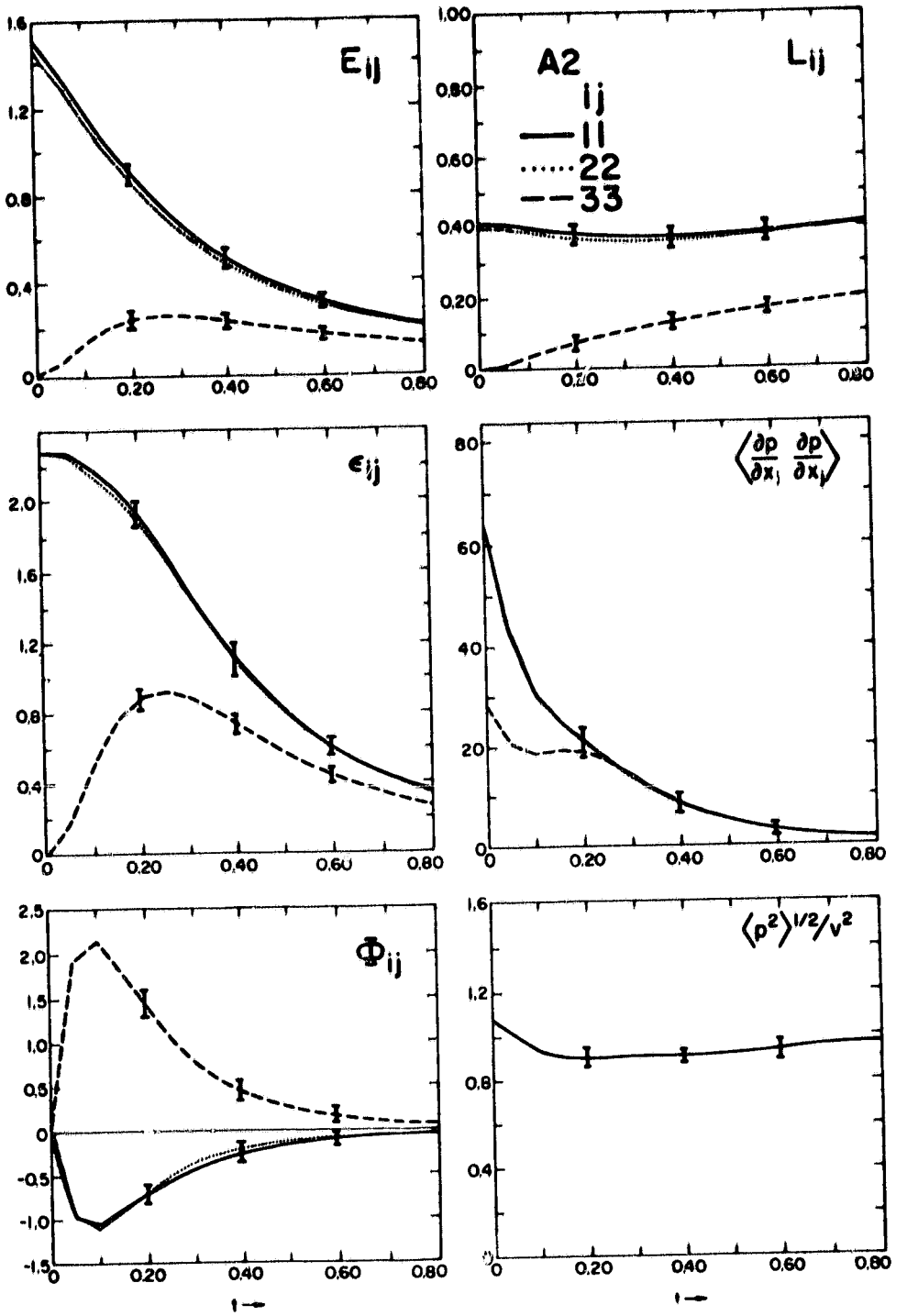

Figure 5.7 A number of quantities on a direct simulation of anisotropic turbulence. The quantities are:

E_{ij} : Reynolds stress tensor

ϵ_{ij} : Dissipation tensor

Φ_{ij} : Pressure strain tensor

L_{ij} : Integral length scales

The fifth is the r.m.s. pressure gradient and the sixth, the r.m.s. pressure fluctuations. From Schumann and Herring (1976).

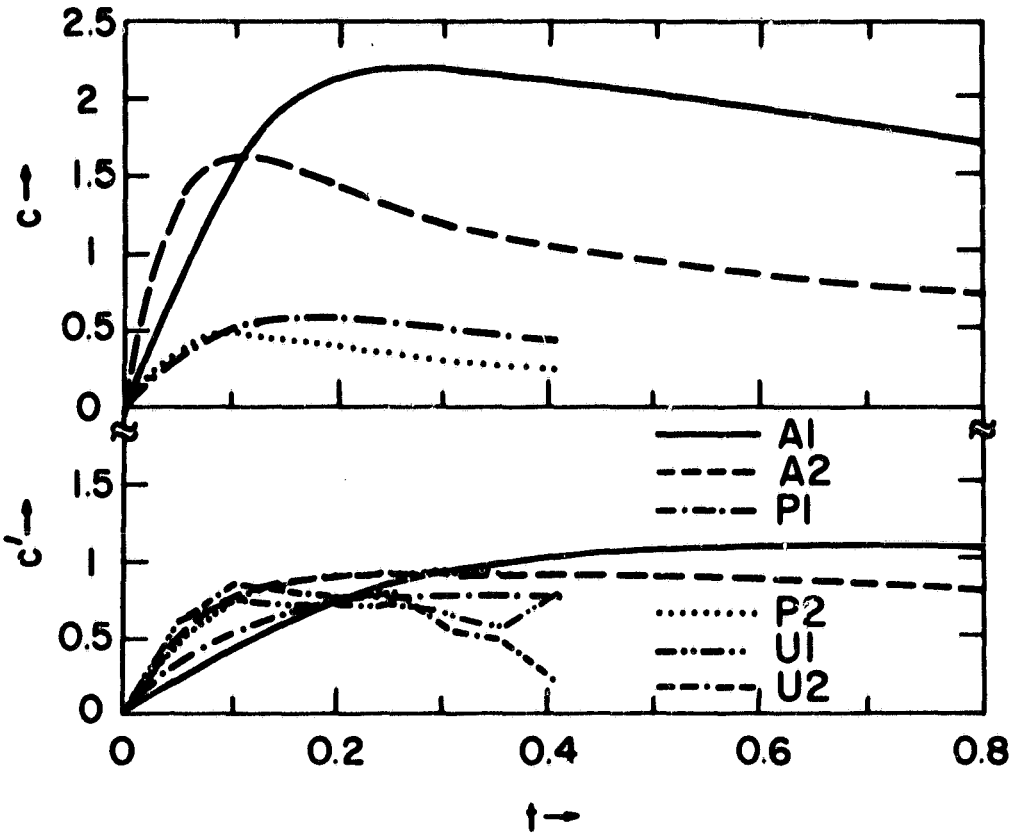

Figure 5.8 Rotta's constants C and C' (see eqs. 5-6, 5-7) versus time for several axisymmetric anisotropic cases. From Schumann and Herring (1976).

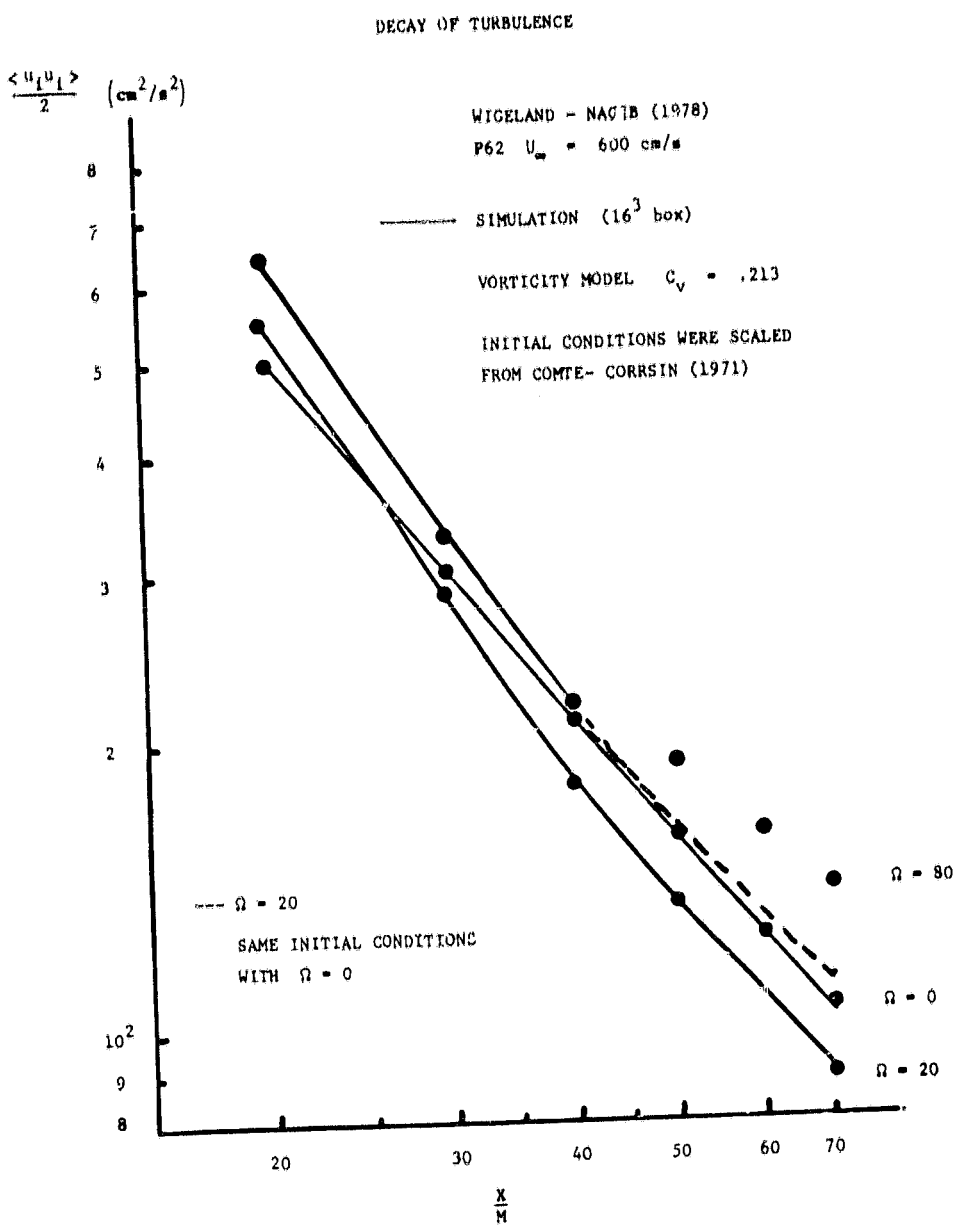

Figure 5.9 The decay of rotating turbulence. Lines are large eddy simulation; points are data. Rotation was present from the start of the calculation. From Bardina et al. (1981).

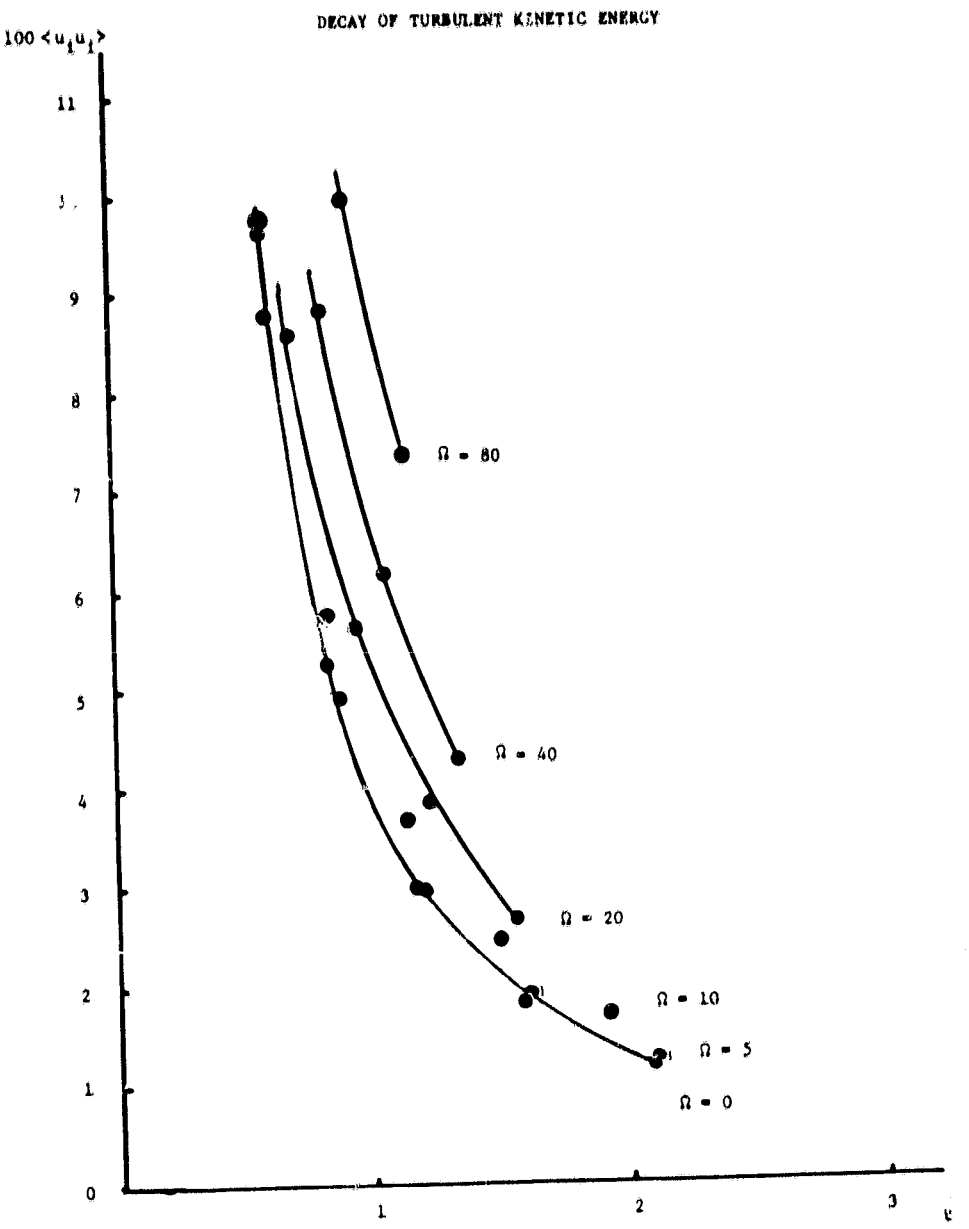

Figure 5.10 Direct simulation of rotating turbulence. The flow was allowed to relax before rotation was "turned on." From Bardina et al. (1981).

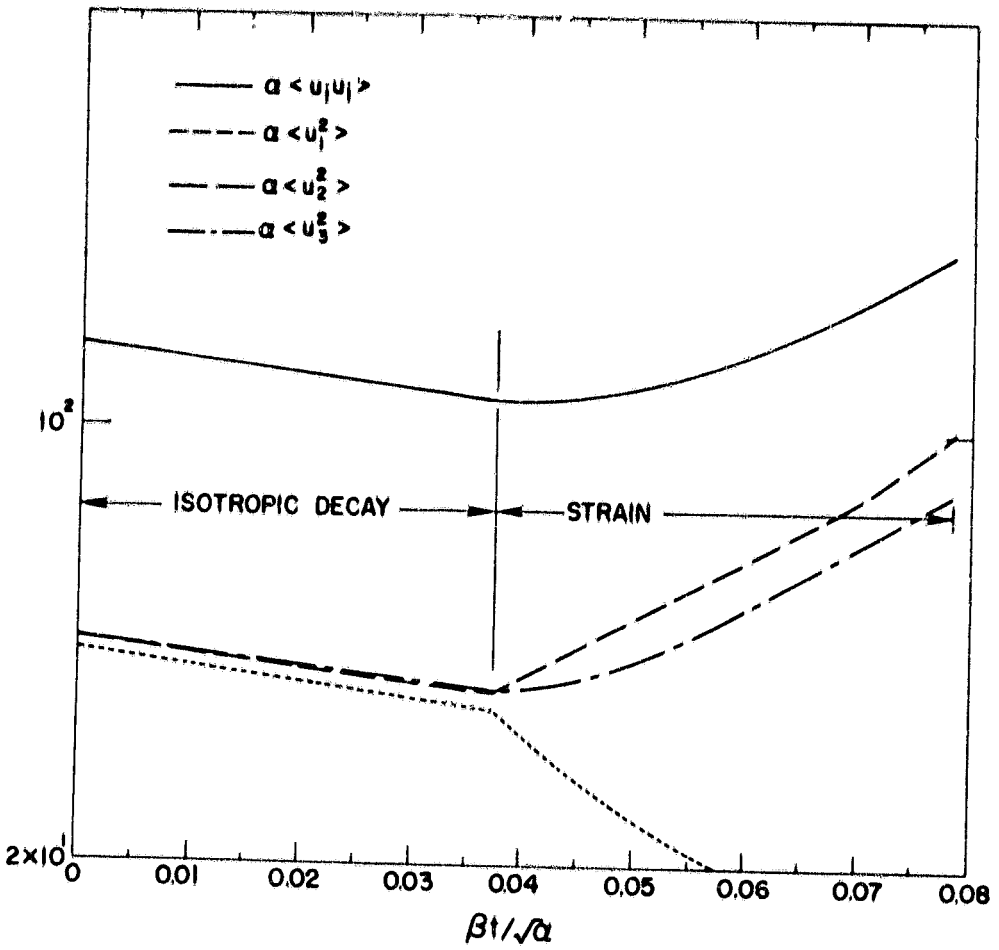

Figure 5.11 The behavior of turbulence undergoing plane strain. From McMillan et al. (1980).

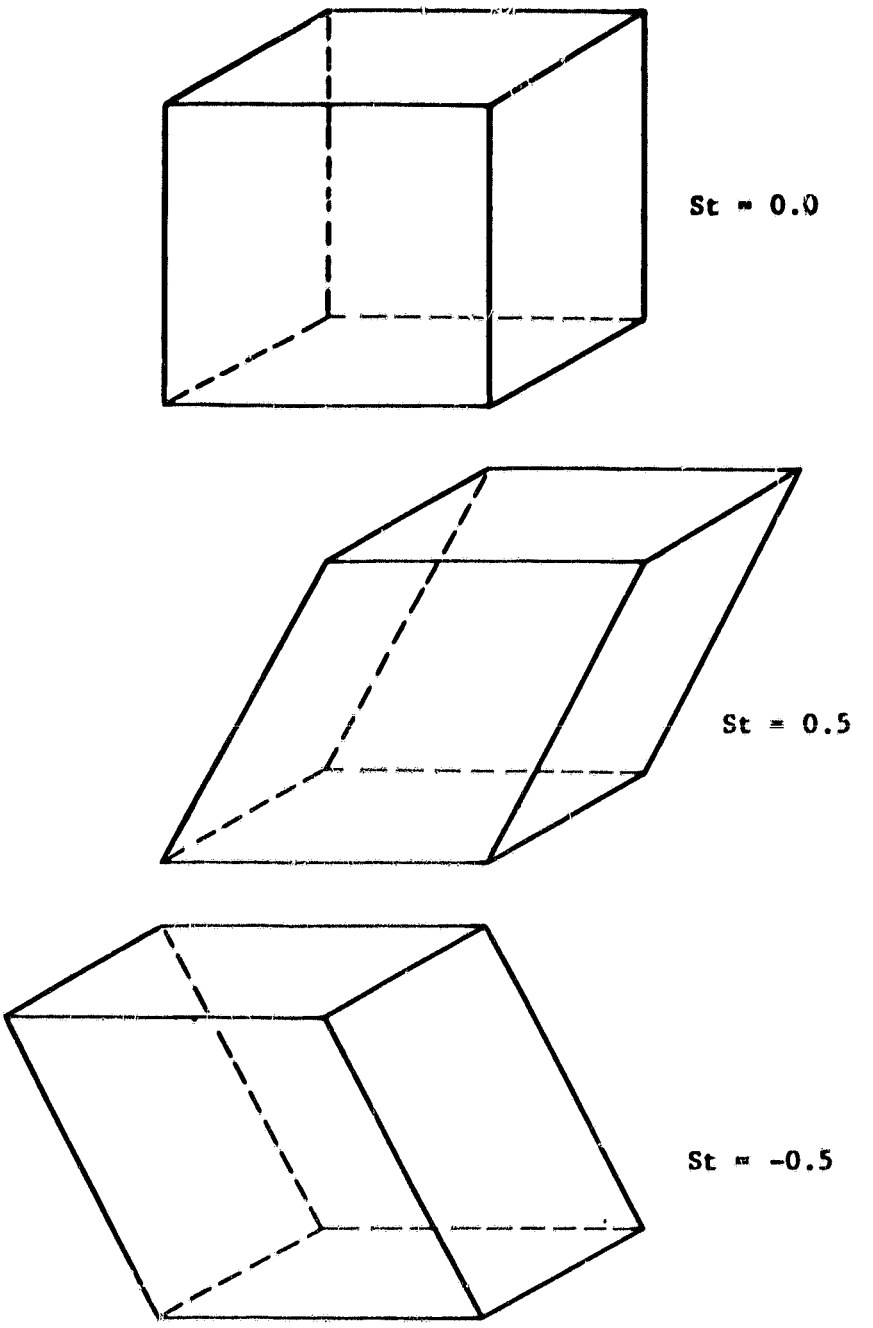

Figure 5.12 The mesh used in sheared turbulence. Flow is started with coordinate system shown on top. When it has sheared to the position of the middle figure, the flow is interpolated on to the grid shown at the bottom. From Feiereisen et al. (1981).

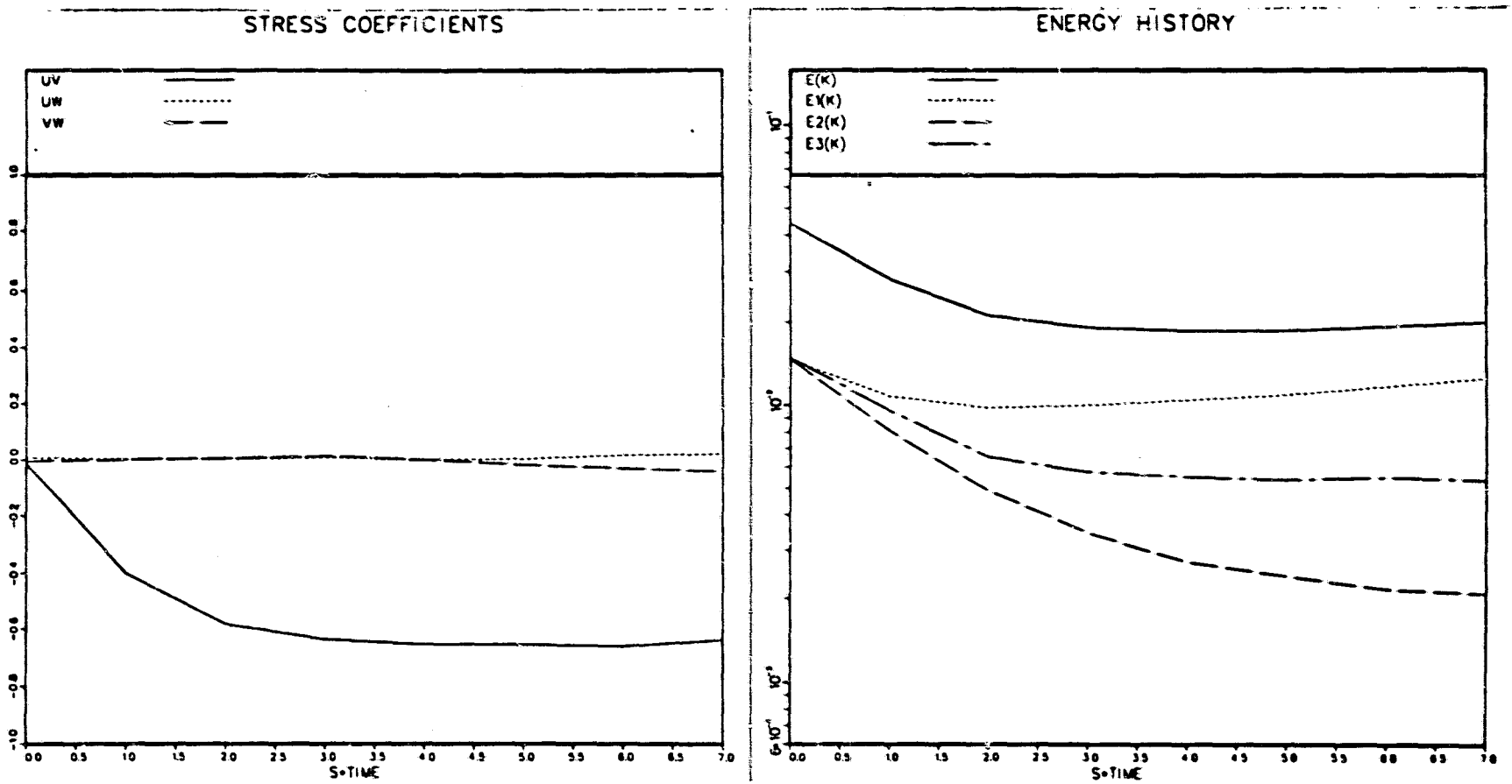

Figure 5.13 The stress coefficients $\langle u_i u_j \rangle / (\langle u_i^2 \rangle \langle u_j^2 \rangle)^{1/2}$ and energy history in sheared turbulence. From Feiereisen et al. (1981).

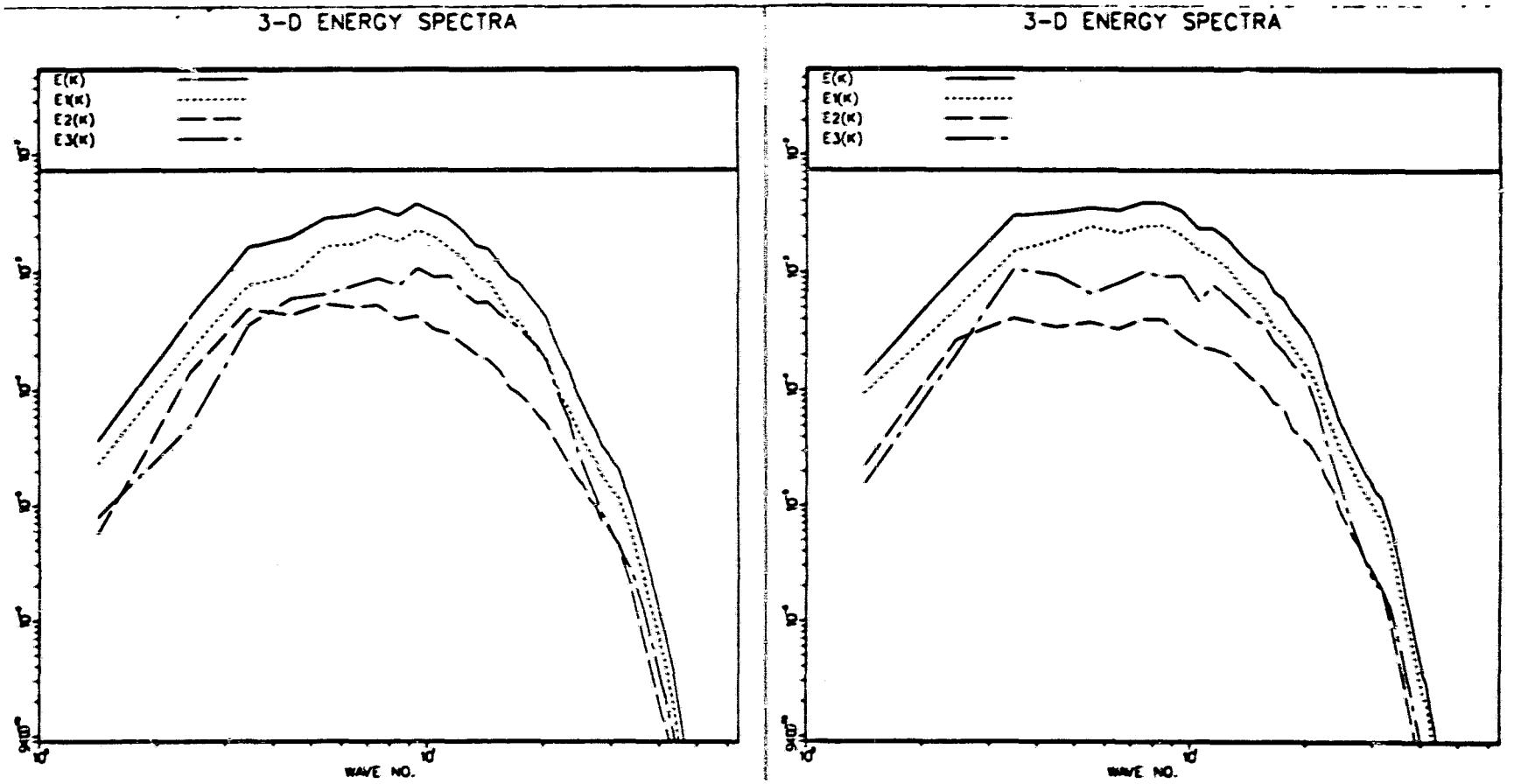

Figure 5.14 The energy spectrum and its components at two different times in sheared turbulence. From Feiereisen et al. (1981).

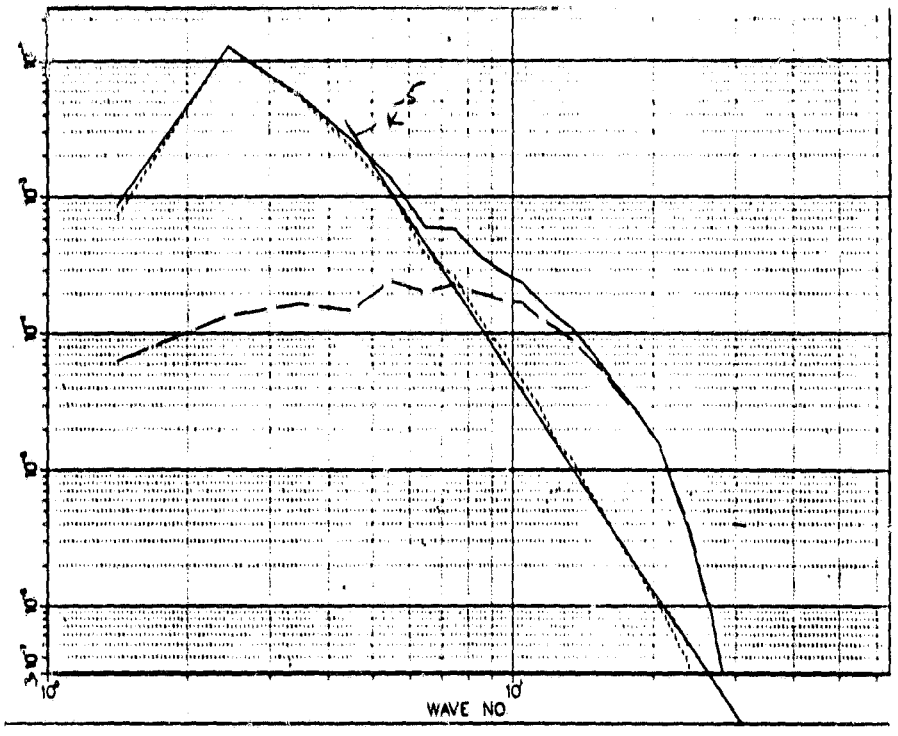

Figure 5.15 The pressure spectrum and its components in sheared turbulence. Dashed line is "rapid" component. Dash-dot line is "Rotta" component. From Shirani et al. (1981).

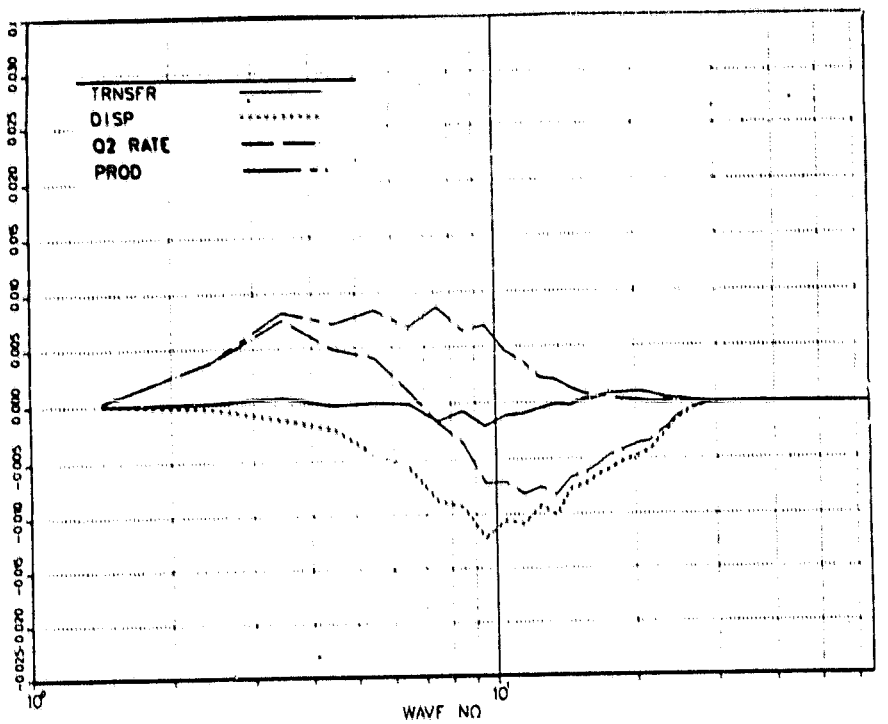

Figure 5.16 The spectra of the various terms that contribute to the change of the 3-D energy spectrum. From Shirani et al. (1981).

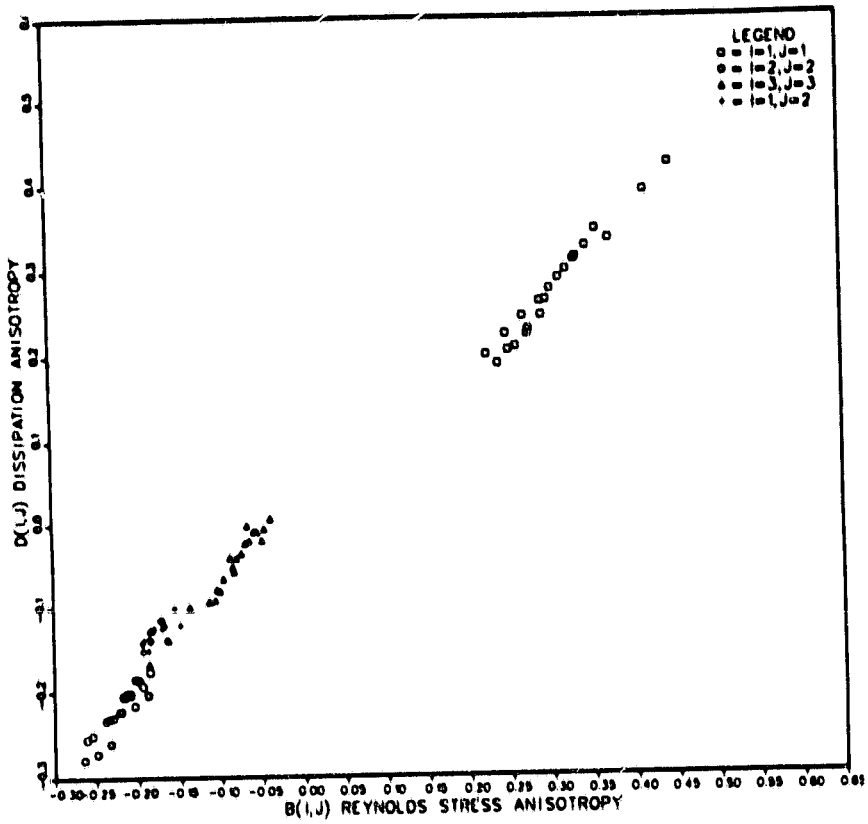

Figure 5.17 The dissipation anisotropy vs the Reynolds stress anisotropy in sheared turbulence. From Feiereisen et al. (1981).

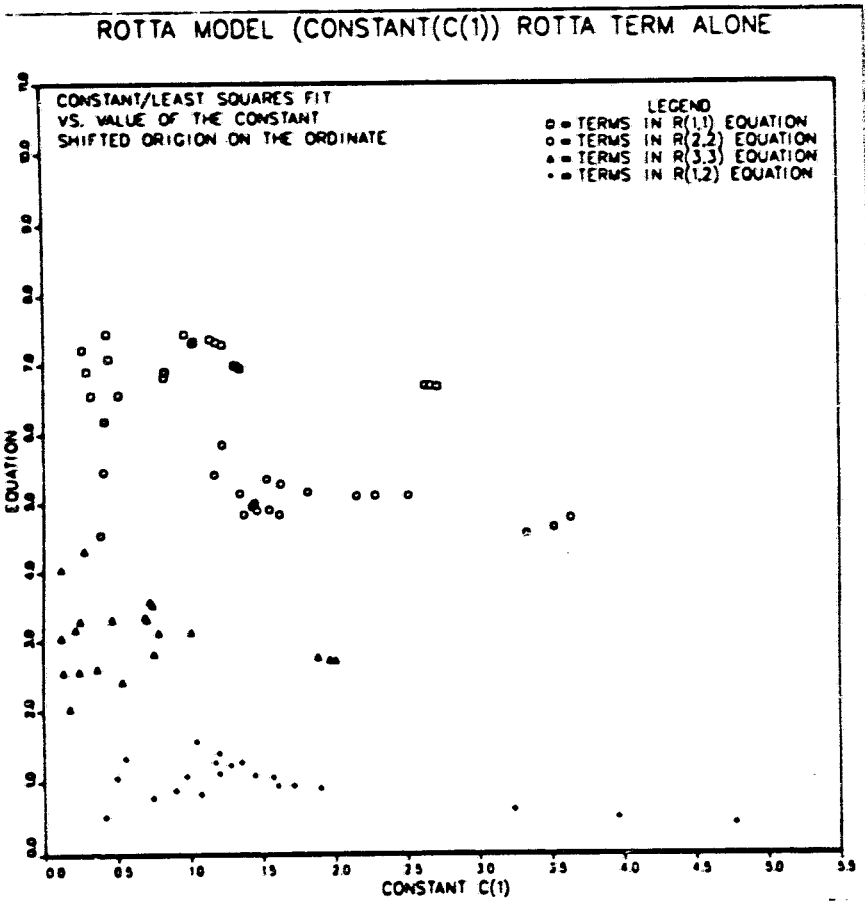

Figure 5.18 The Rotta "constant" C in sheared turbulence. The abscissa is the model constant obtained from the simulations. The ordinate is the ratio of the abscissa to the value obtained from a least squares fit. A perfect fit would give a value of 1.0 for the ordinate; the values for the various components have been shifted for clarity. From Feiereisen et al. (1981).

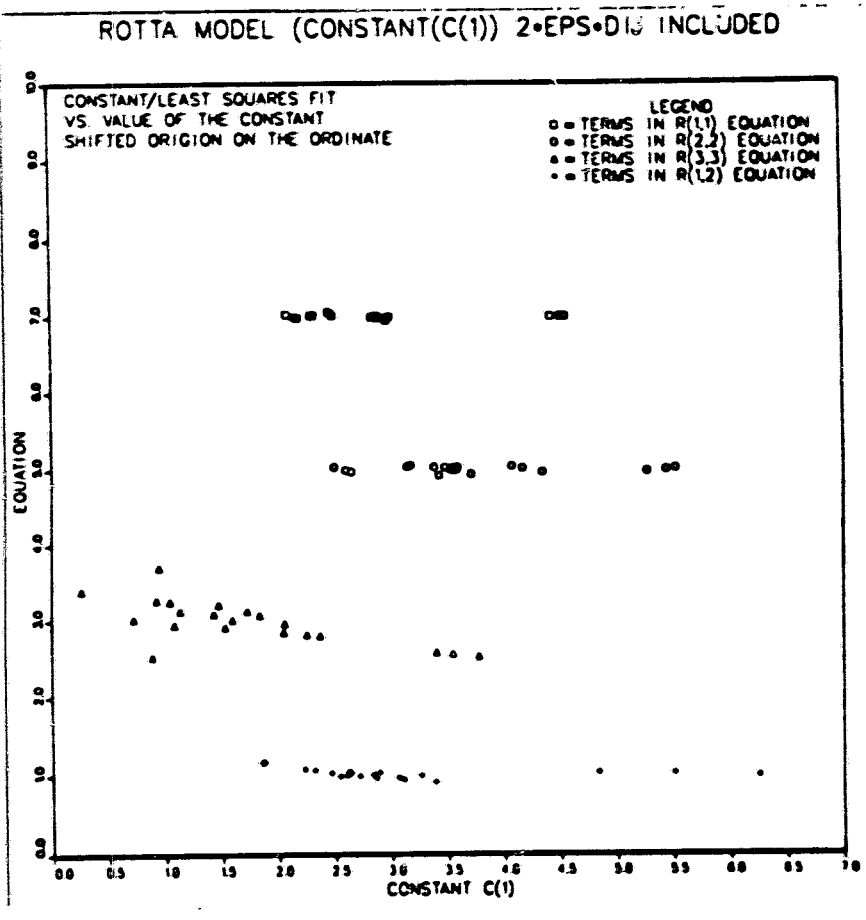

Figure 5.19 The Rotta "constant" when the dissipation anisotropy is included. See Fig. 5.18 for explanation. From Feiereisen et al. (1981).

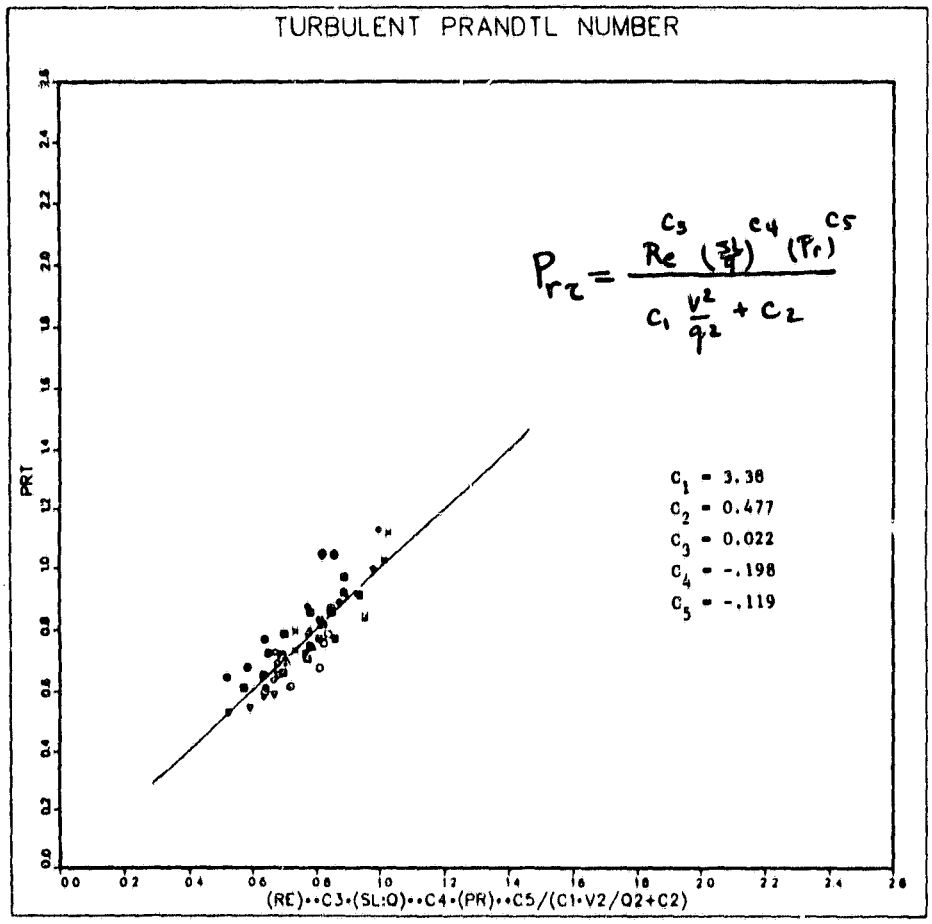

Figure 5.20 A new model for the turbulent Prandtl number. The form is indicated on the figure. From Shirani et al. (1981).

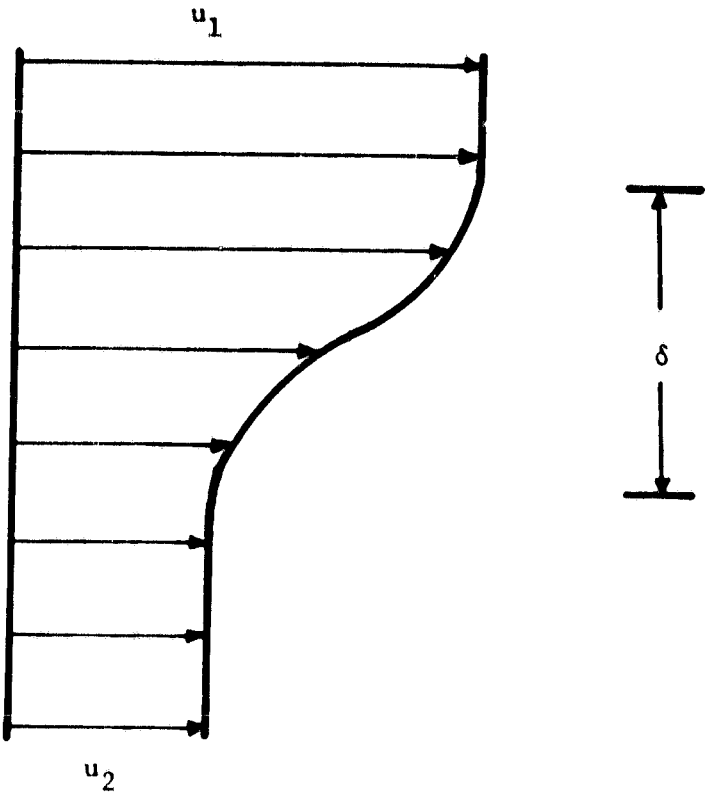

Figure 6.1 A schematic of the mixing layer.

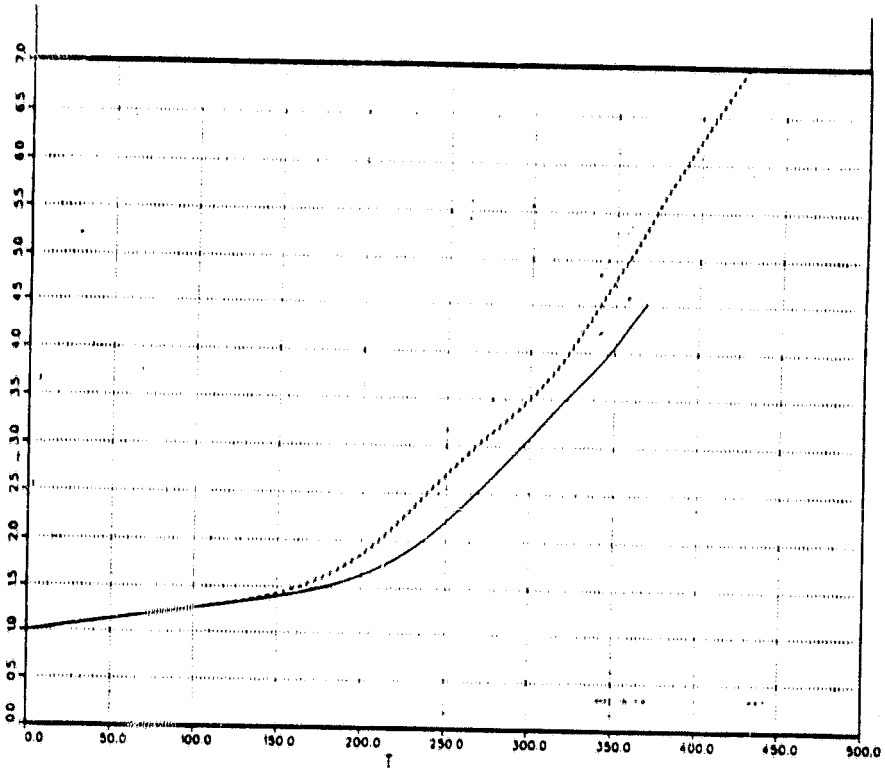

Figure 6.2 Momentum thickness of a developing mixing layer vs time; low initial intensity cases. From Cain et al. (1981).

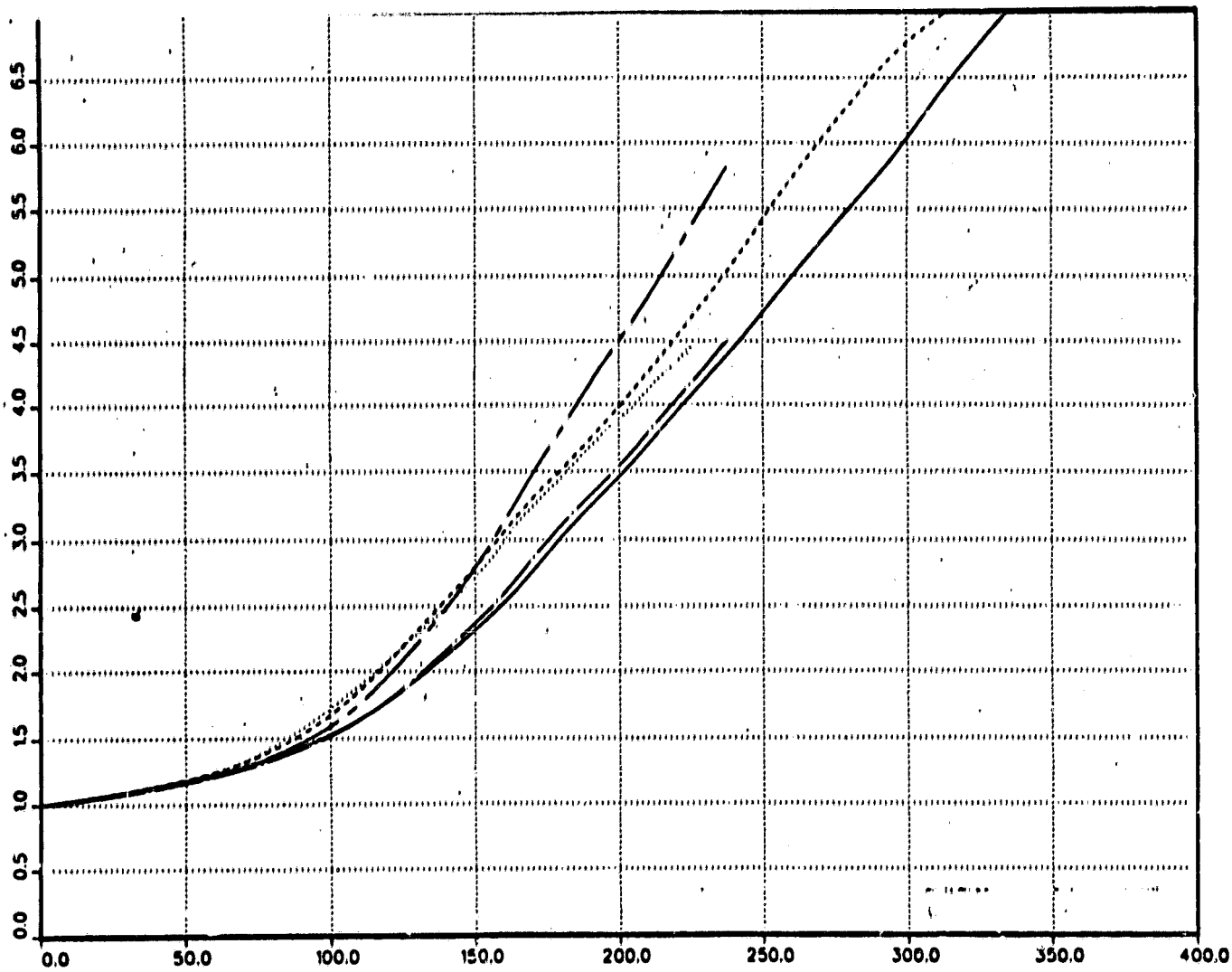

Figure 6.3 Momentum thickness of a mixing layer vs time; medium initial intensity cases. From Cain et al. (1981).

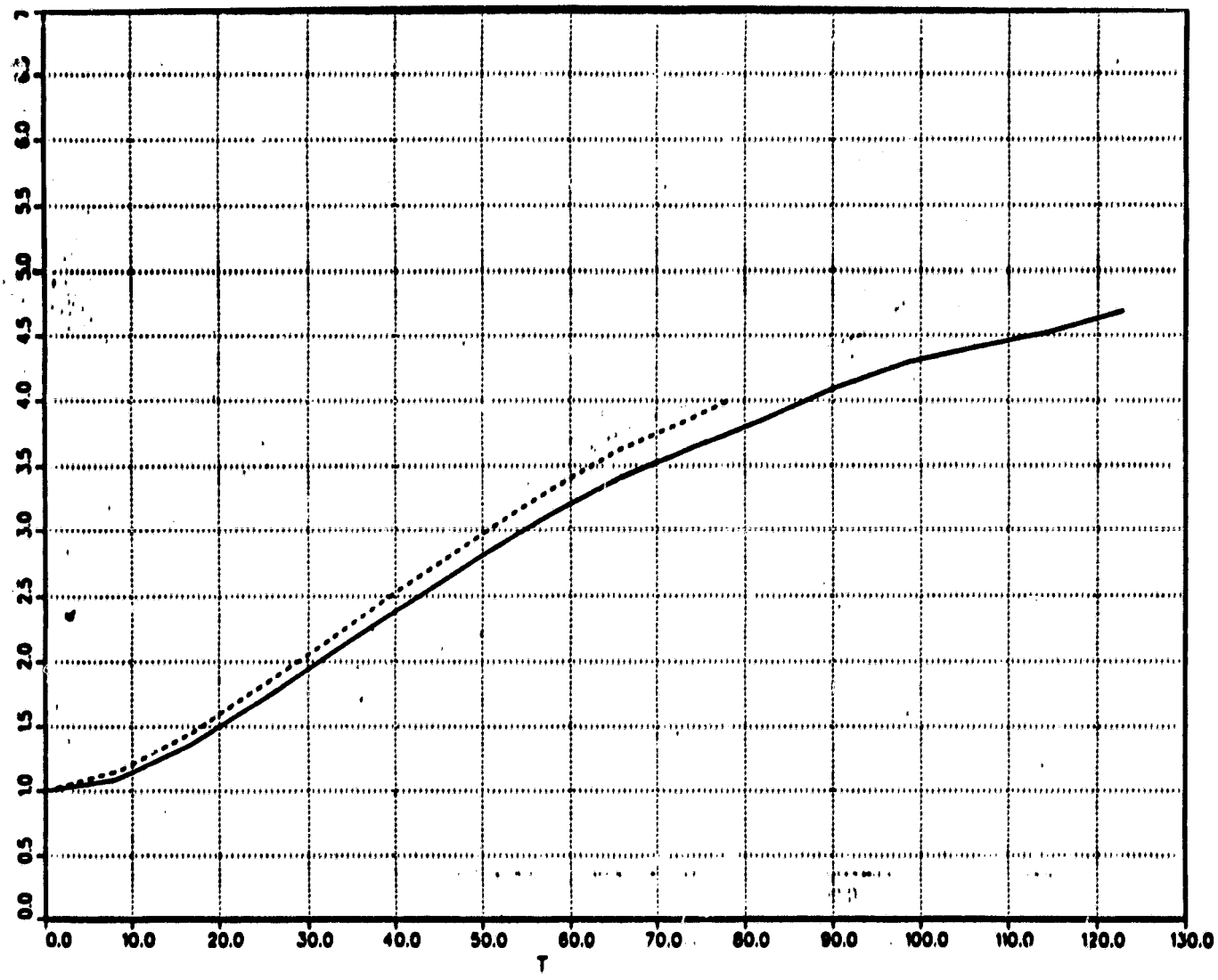

Figure 6.4 Momentum thickness of a mixing layer vs time; high initial intensity cases. From Cain et al. (1981).

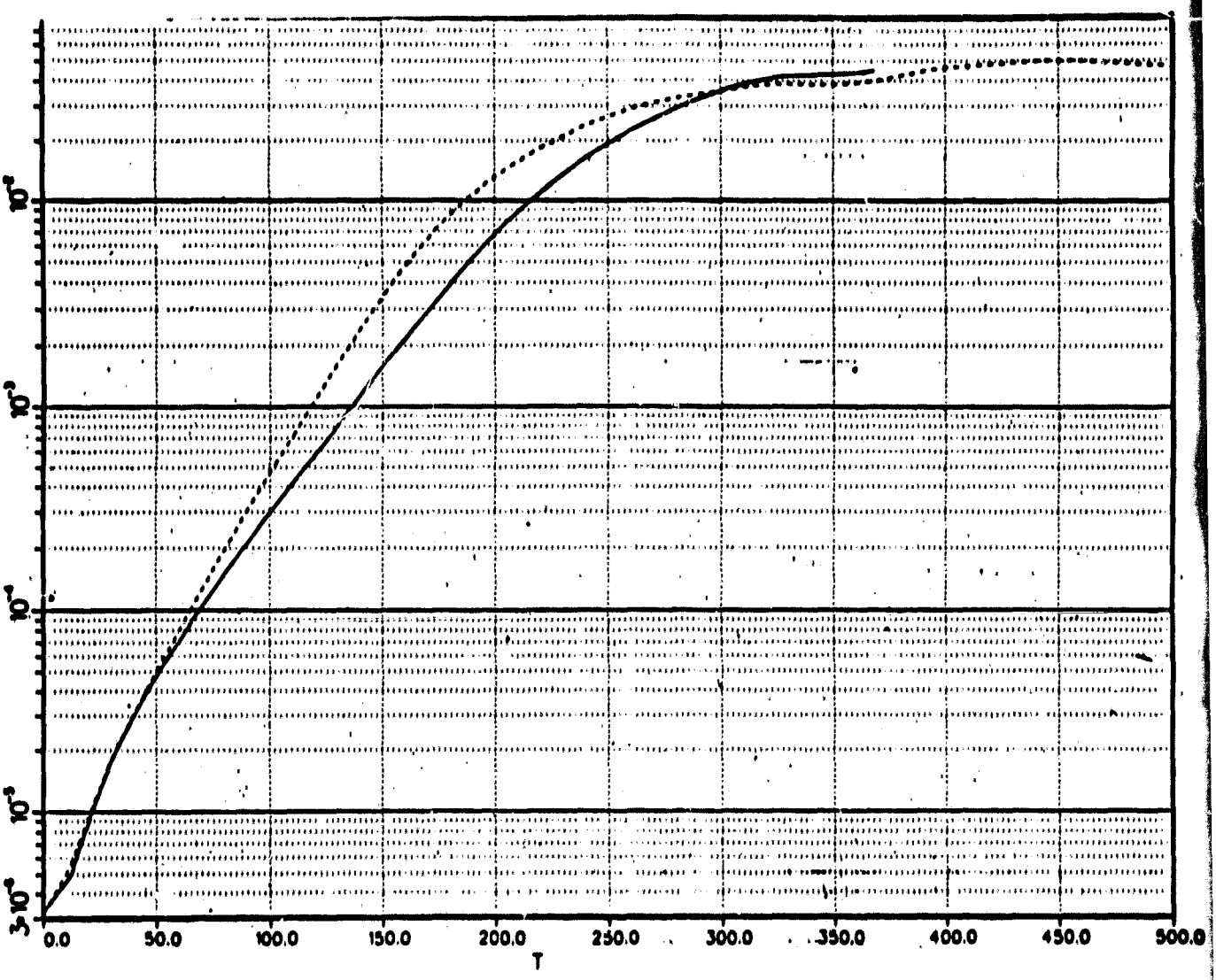

Figure 6.5 Turbulence intensity at center of mixing layer vs time; low intensity cases. From Cain et al. (1981).

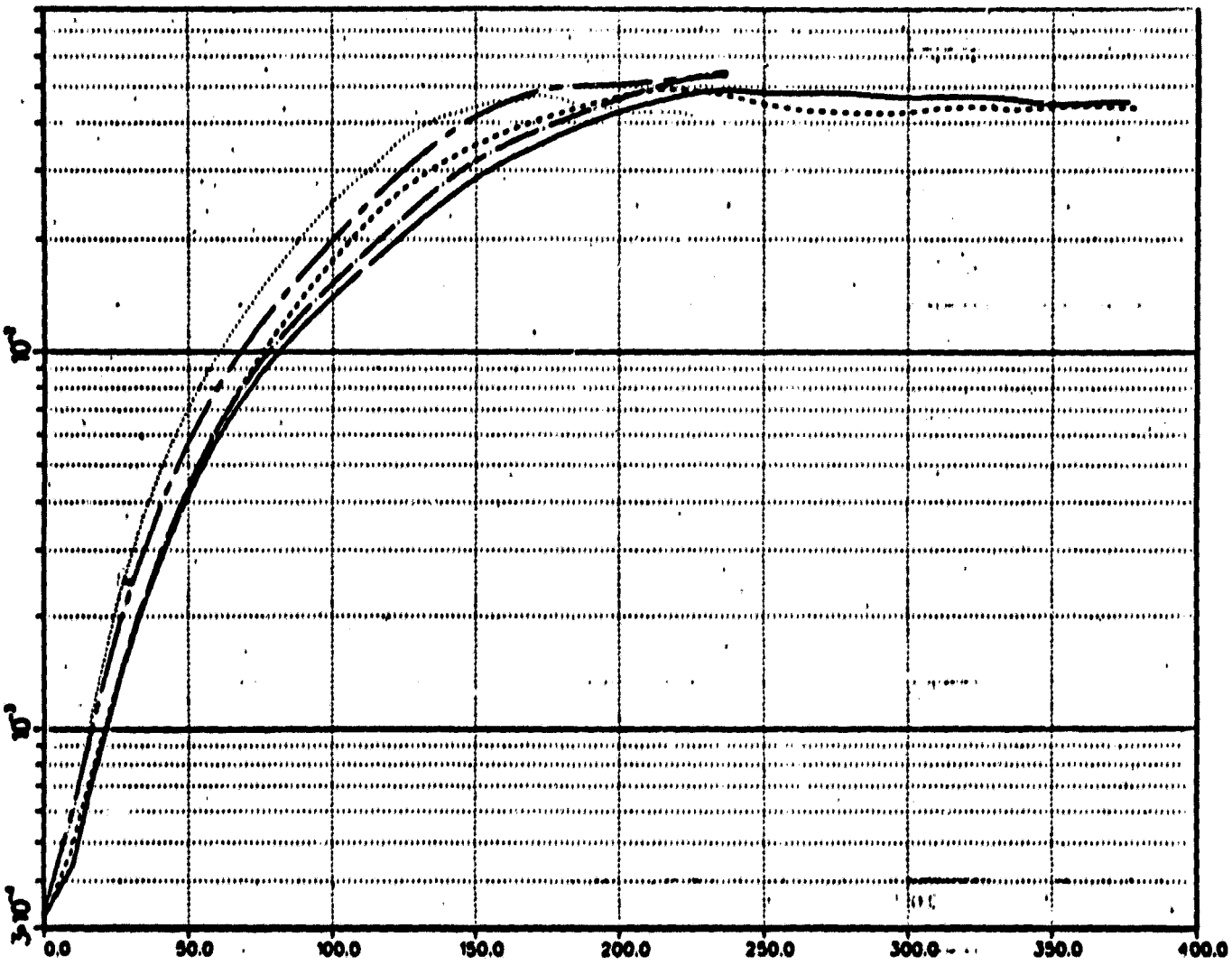

Figure 6.6 Turbulence intensity at center of mixing layer vs time; medium initial intensity cases. From Cain et al. (1981).

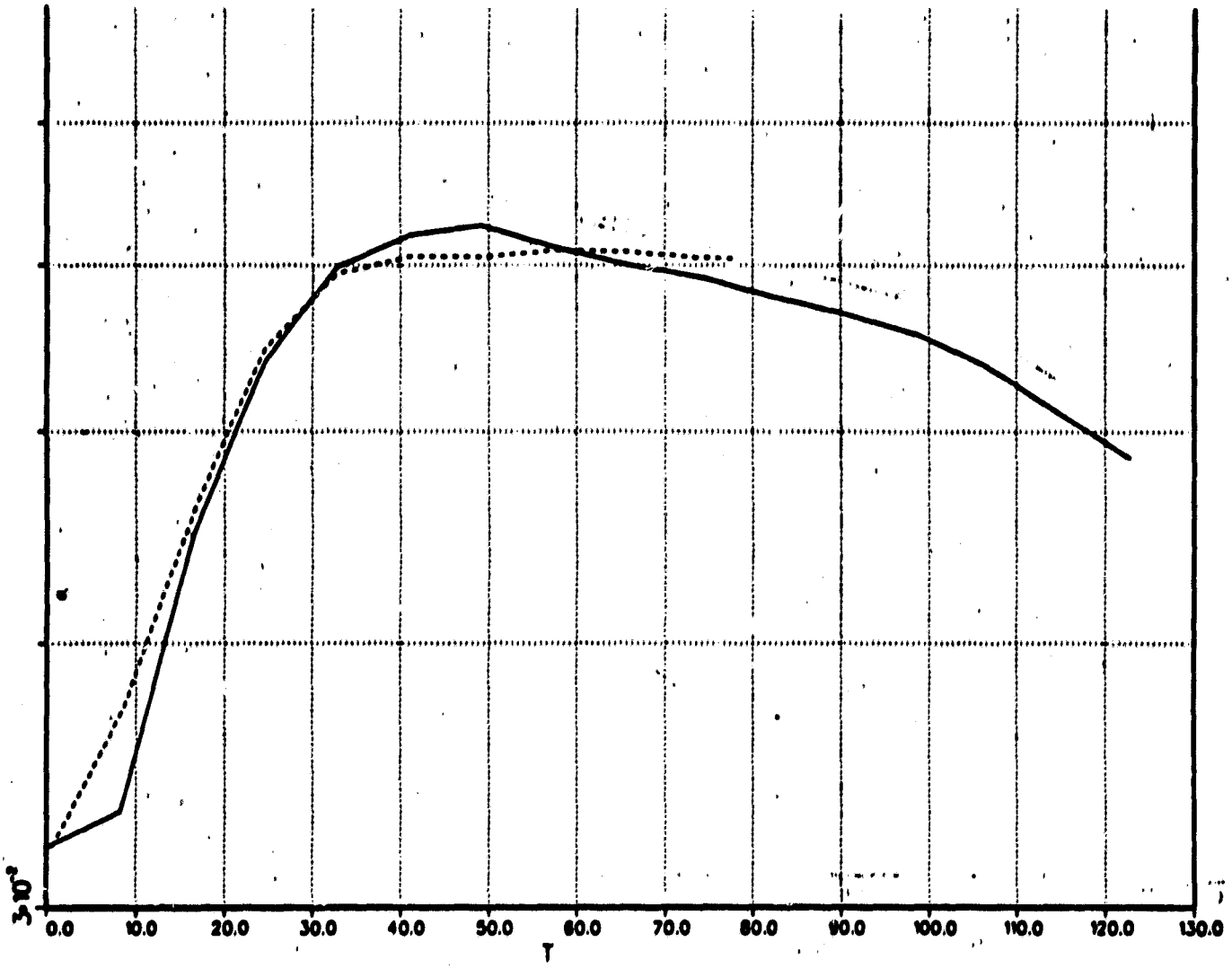

Figure 6.7 Turbulence intensity at center of mixing layer vs time; high initial intensity cases. From Cain et al. (1981).

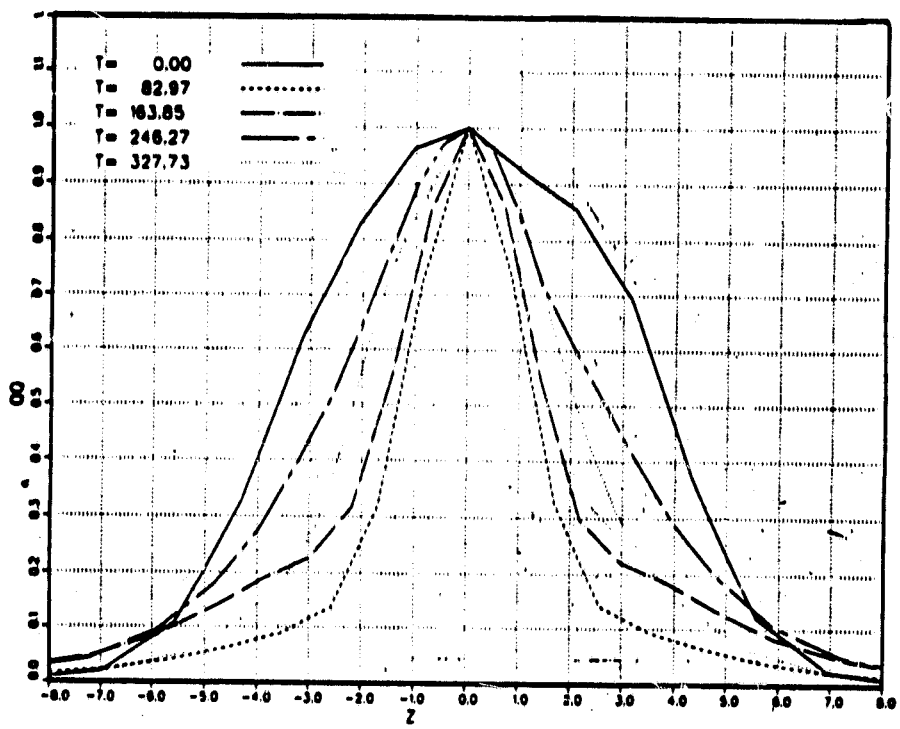

Figure 6.8 Profiles of turbulence intensity vs time; low initial intensity case. From Cain et al. (1981).

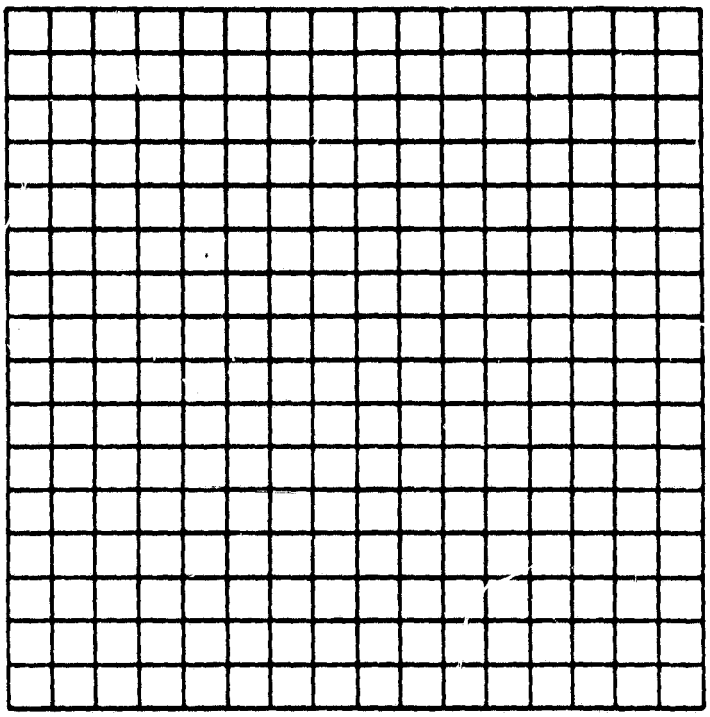

Figure 6.9 "Dye lines" at intiial time in mixing layer. From Cain et al. (1981).

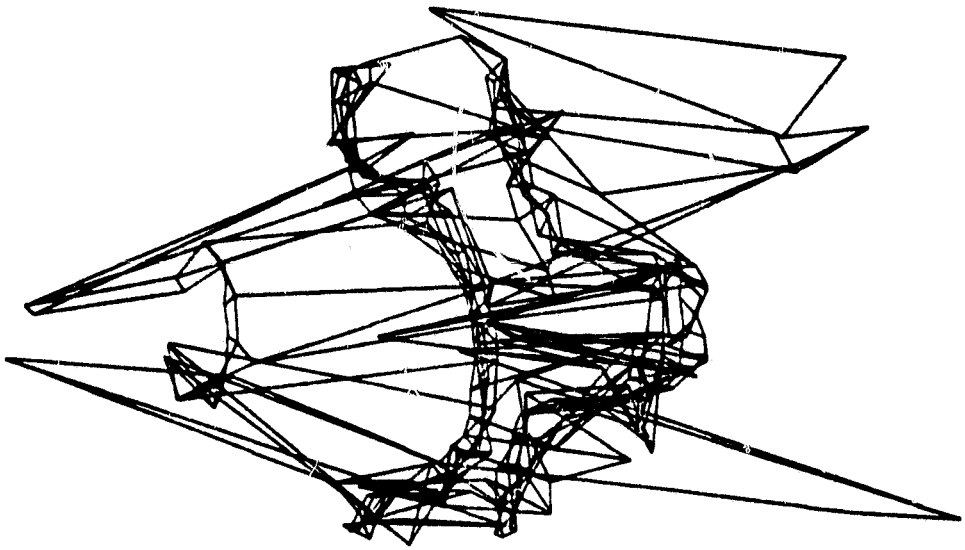

Figure 6.10 "Dye lines" late in mixing layer development; low initial intensity case. From Cain et al. (1981).

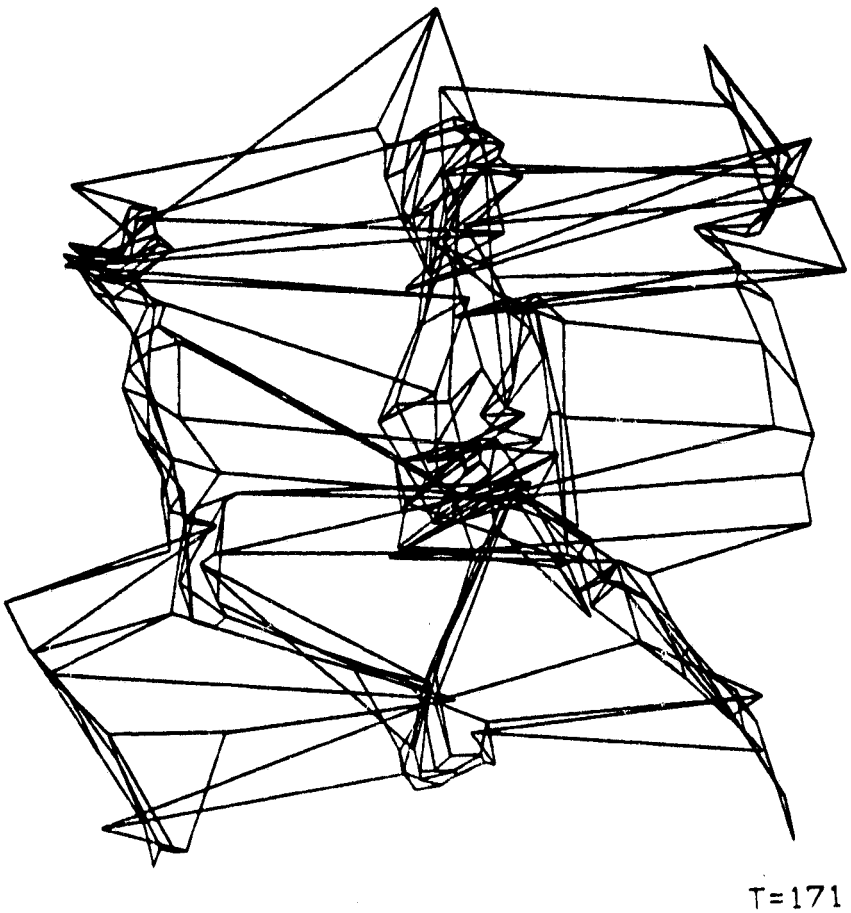

Figure 6.11 "Dye lines" late in mixing layer development; medium initial intensity case (same as Figure 6.10) except for intensity). From Cain et al. (1981).

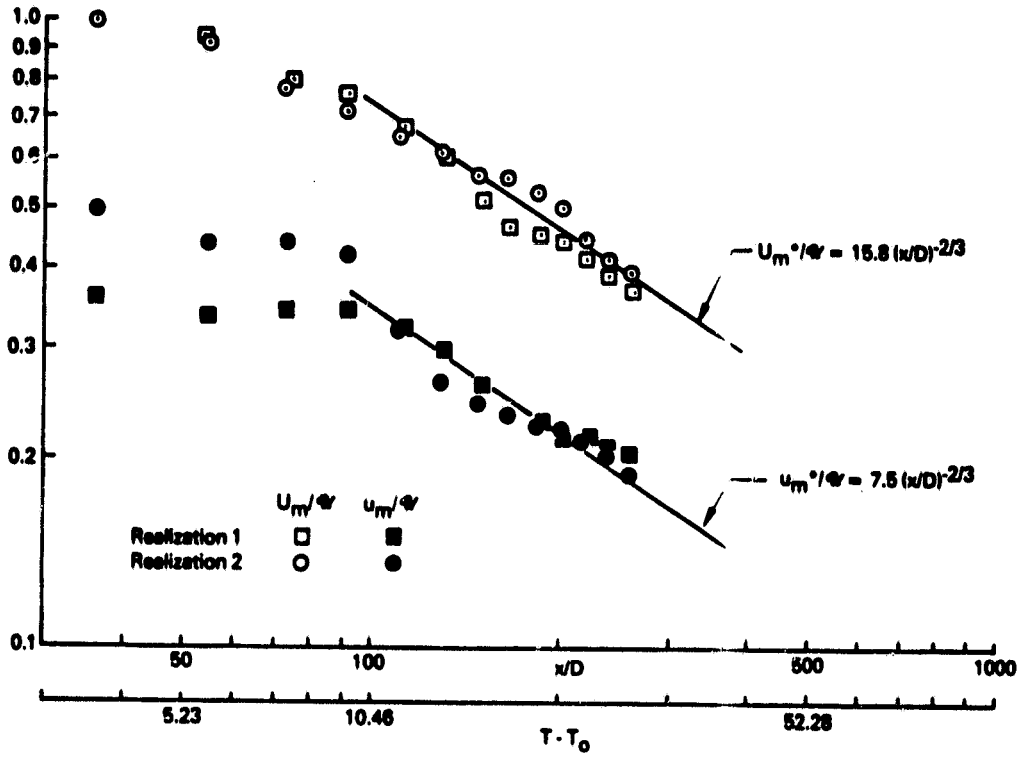

Figure 6.12 Decay of Maximum Mean Velocity (U_m) and Maximum Axial Turbulent Intensity (u_m) in Wake. From Riley and Metcalfe (1978).

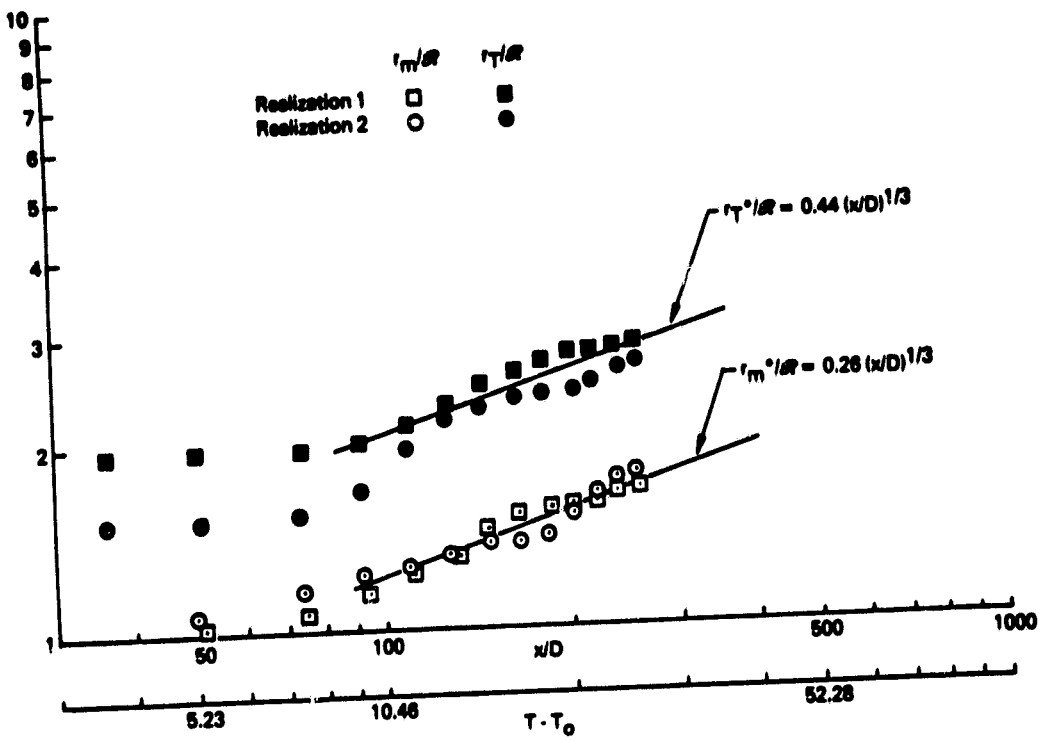

Figure 6.13 Growth of Mean Wake Radius (r_m) and Turbulent Wake Radius (r_T). From Riley and Metcalfe (1978).

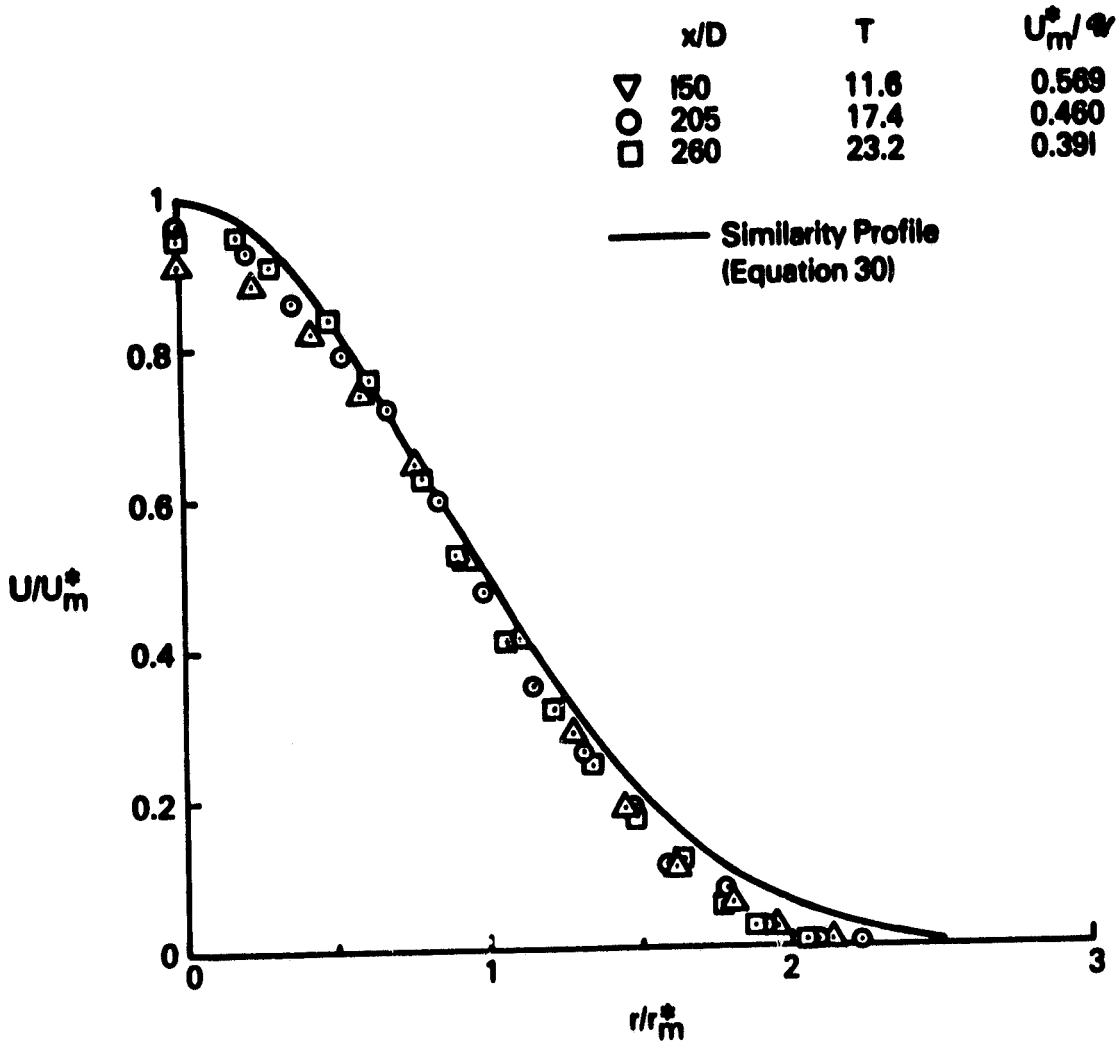

Figure 6.14 Normalized Profile of Axial Mean Velocity in Wake. From Riley and Metcalfe (1978).

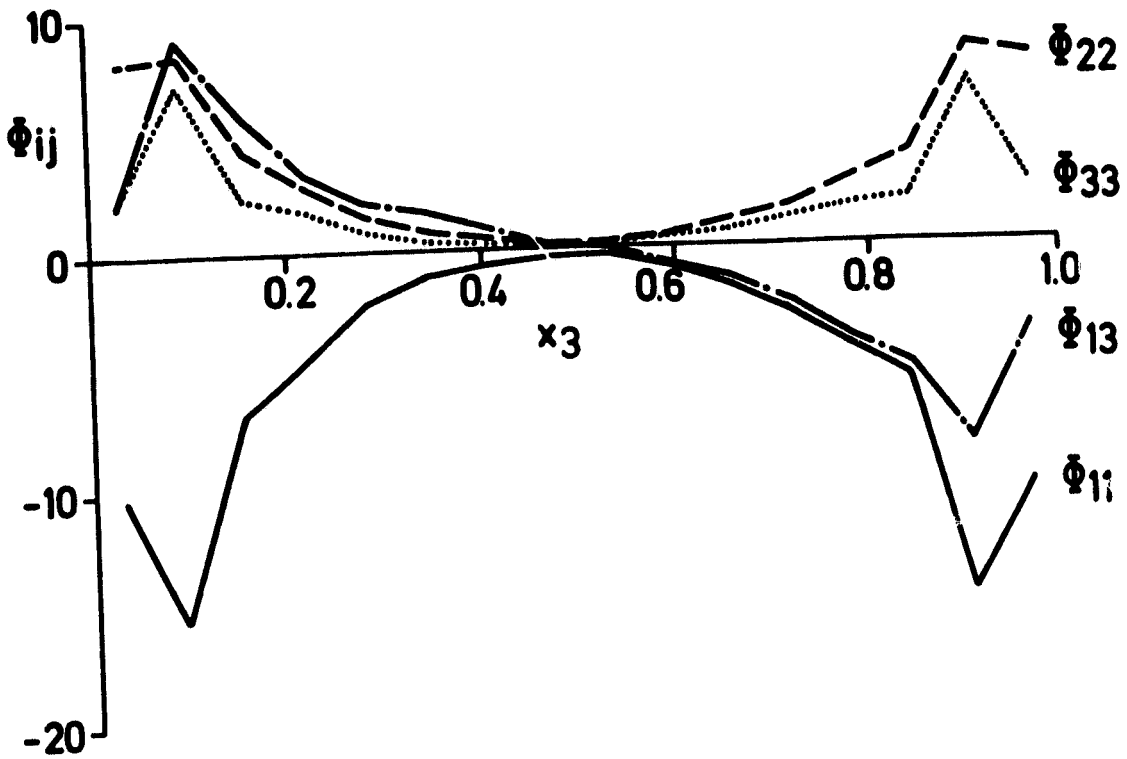

Figure 7.1 The pressure-strain terms as a function of the normal coordinate in a channel flow. From Schumann et al. (1980).

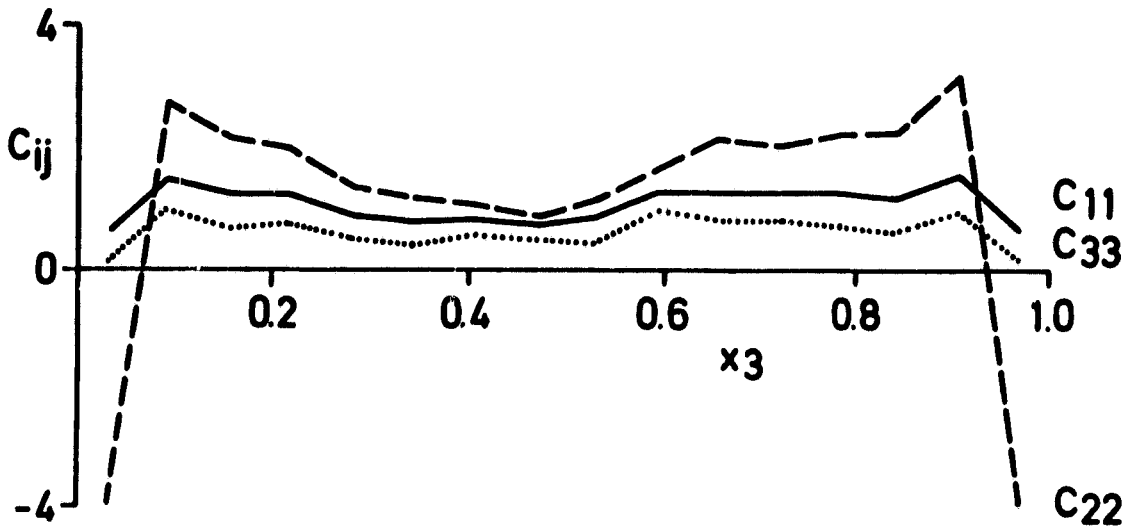

Figure 7.2 The 'constant' in the model of the pressure-strain term as a function of the normal coordinate. From Schumann et al. (1981).

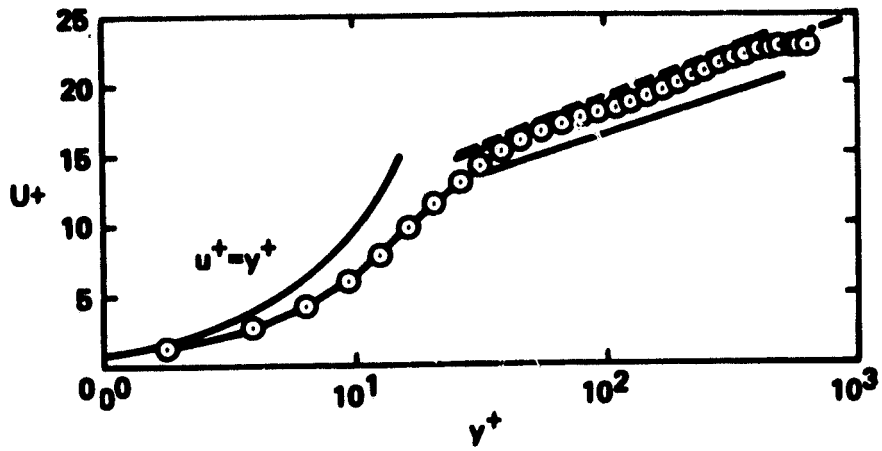

Figure 7.3 The mean in the channel flow compared with three sets of experimental results. From Kim and Moin (1979).

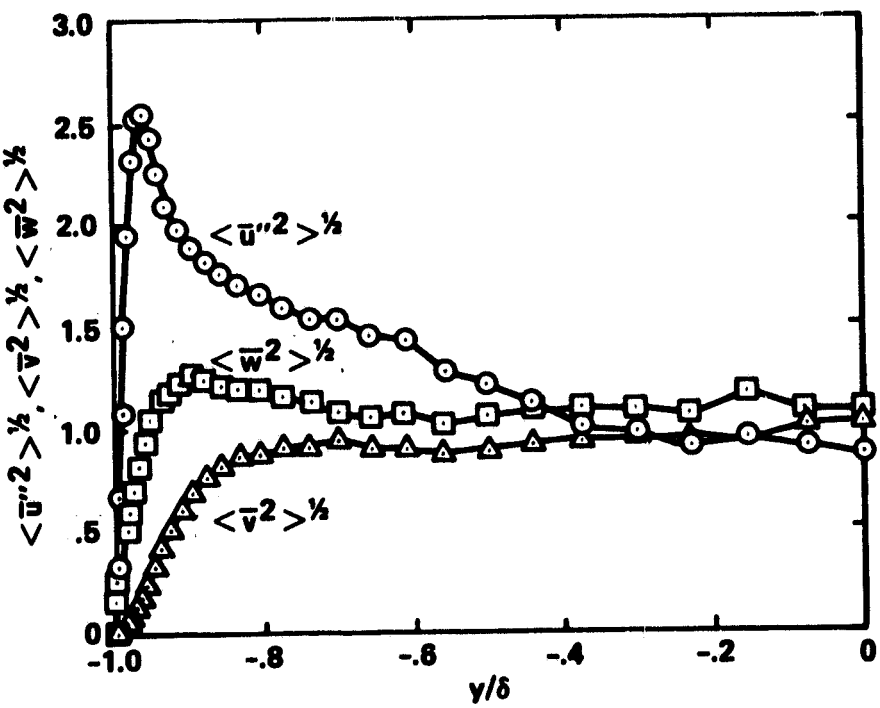

Figure 7.4 Turbulence intensities in channel flow (resolved component only). From Kim and Moin (1979).

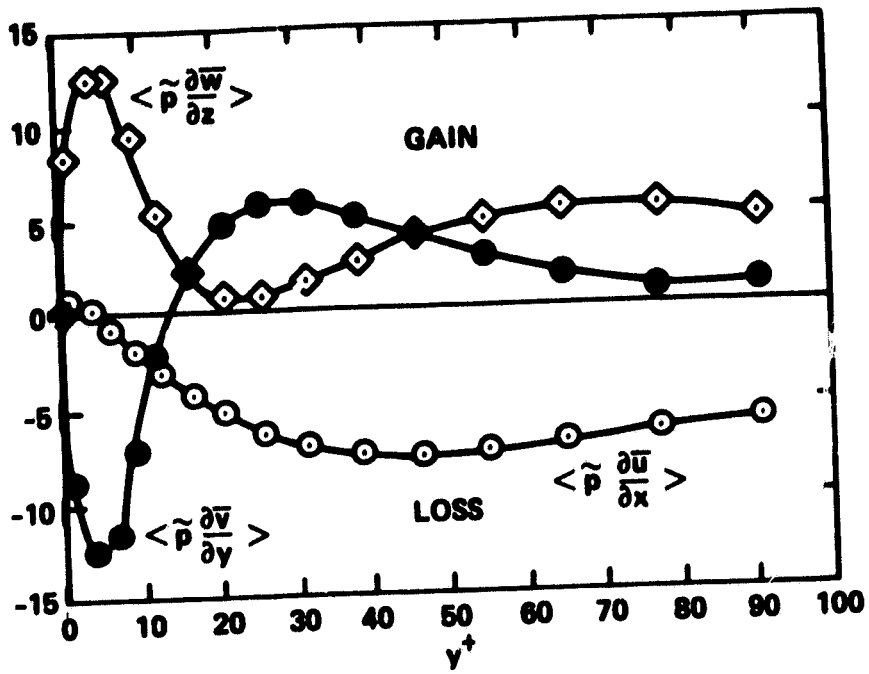

Figure 7.5 The pressure-strain terms in a channel flow. From Kim and Moin (1979).

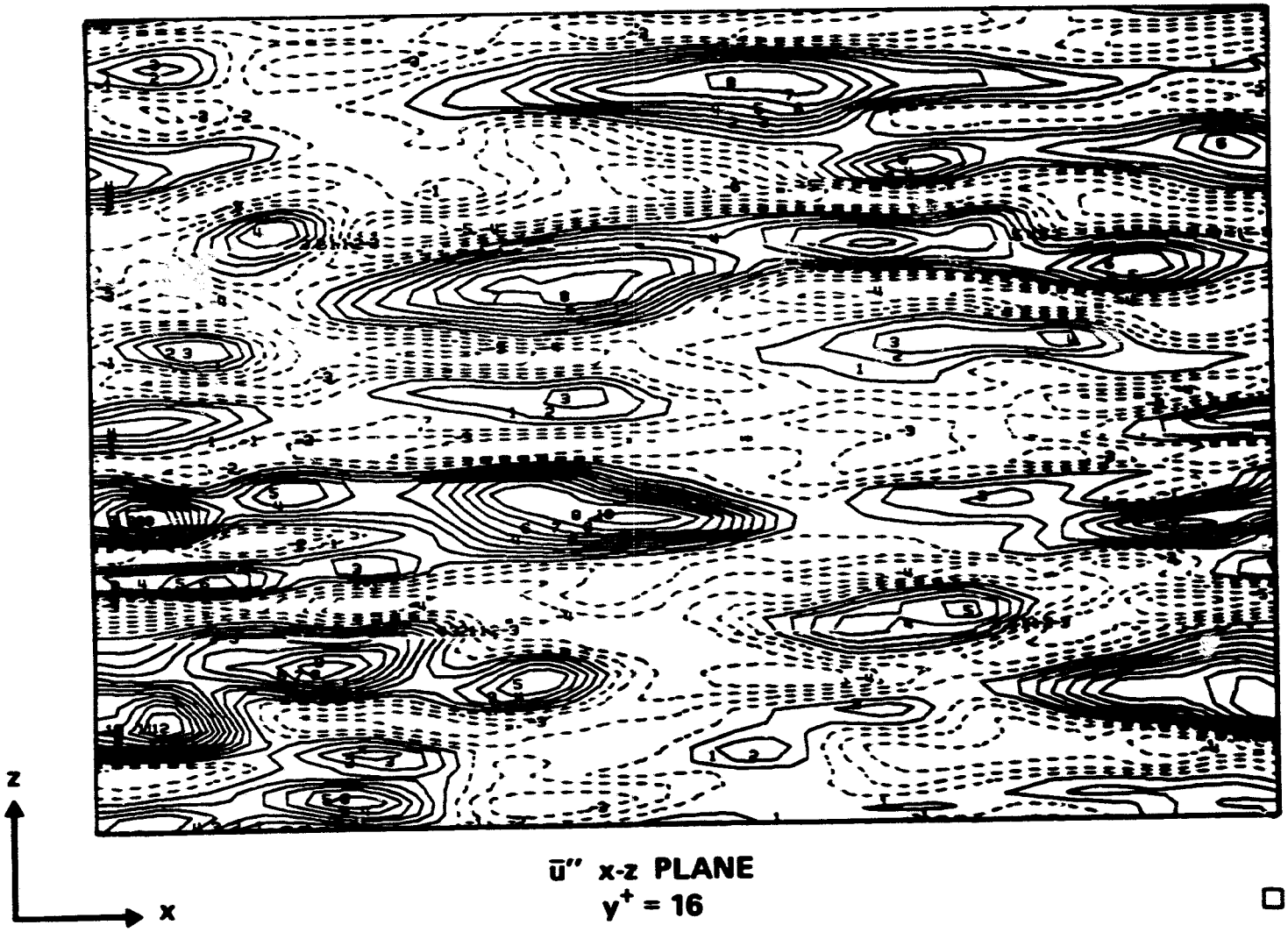

Figure 7.6 Contours of fluctuations of the streamwise velocity near the wall. From Kim and Moin (1979).

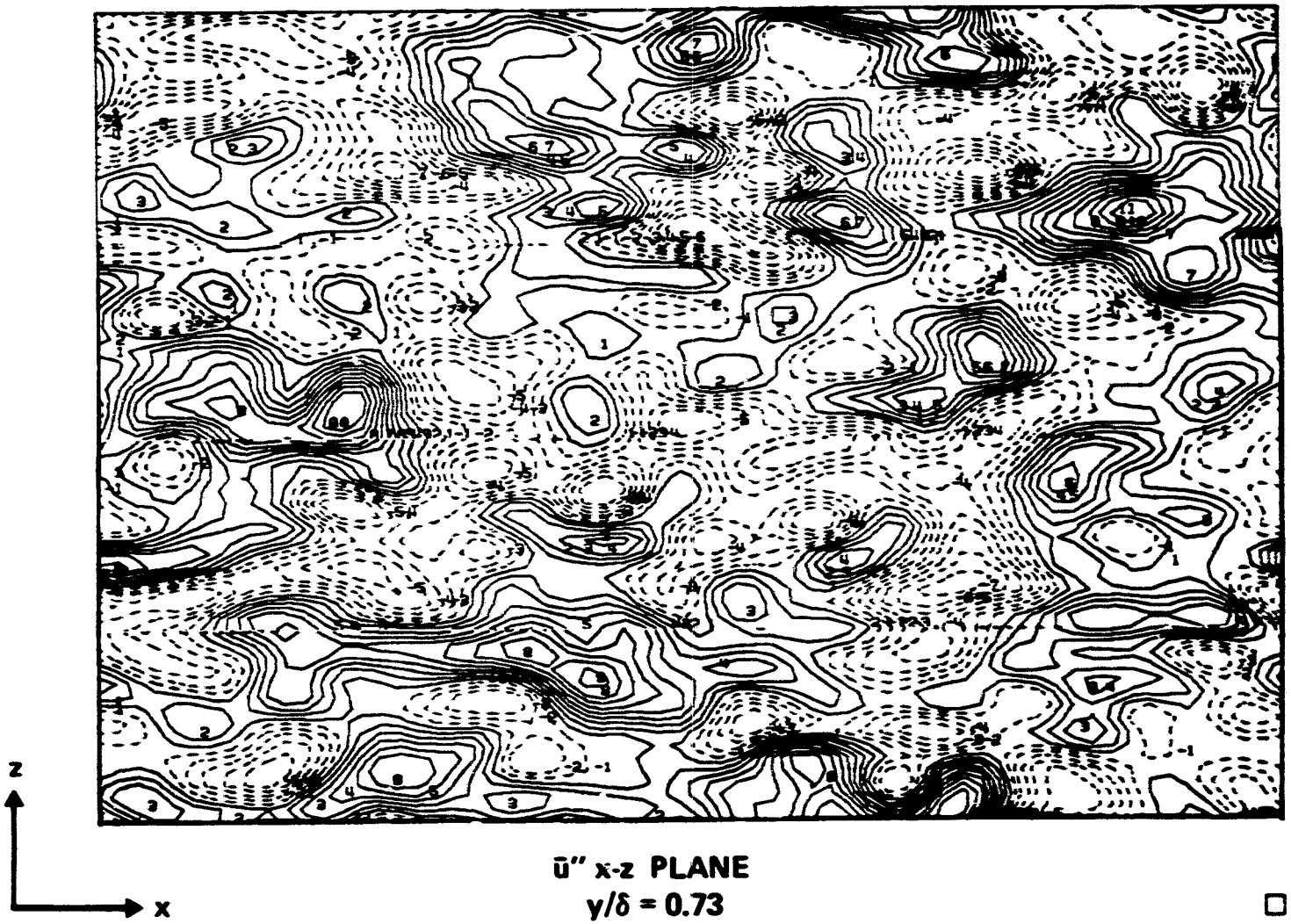

Figure 7.7 Contours of the fluctuations of the streamwise velocity near the center of the channel. From Kim and Moin (1979).

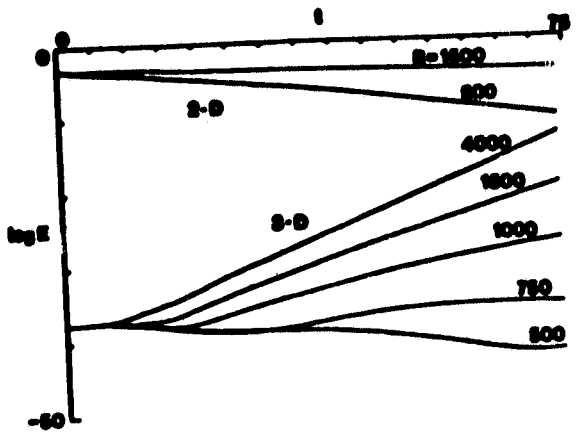

Figure 7.8 Energy of two- and three-dimensional waves in a perturbed laminar channel flow. The 2-D waves decay while the 3-D waves grow. From Orszag and Patera (1981).